UNIVERSITY OF OKLAHOMA

GRADUATE COLLEGE

NMR CONSIDERATIONS IN SHALES AT ELEVATED TEMPERATURE

A THESIS

SUBMITTED TO THE GRADUATE FACULTY

in partial fulfillment of the requirements for the

Degree of

MASTER OF SCIENCE

By

ADITYA CHAKRAVARTY
Norman, Oklahoma
2019

NMR CONSIDERATIONS IN SHALE AT ELEVATED TEMPERATURE

A THESIS APPROVED FOR THE
MEWBOURNE SCHOOL OF PETROLEUM AND GEOLOGICAL ENGINEERING

BY

Dr. Chandra S. Rai, Chair

Dr. Carl H. Sondergeld

Dr. Deepak Devegowda

ACKNOWLEDGEMENTS

I am deeply indebted to my advisors, Dr. Chandra Rai and Dr. Carl Sondergeld for giving me an opportunity to work with them, under their guidance at a world-class, remarkably unique research laboratory, IC^3. They gave me with more freedom, time, resources and most importantly, patience, than I deserve and cared for me and supported me at difficult times. Their level of energy, work ethic and dedication towards their craft has affected me in multitudinous ways. Dr Rai was incredibly patient with me and my research, and always motivated me to stretch my limits. Dr Sondergeld inspired me to read, be prepared, and take risks. They have conveyed so much in so few words.

I take this opportunity to thank Dr. Deepak Devegowda for his continued support and guidance over time. His versatility, leadership and dedication to fitness and well-being has inspired me.

I want to thank Ali Tinni for being a mentor and a friend, and understanding me. His guidance and suggestions were the most formative during my time at IC^3. He inspired me to read and showed me how to work hard and smart. Thank you, Mr. Ali. I acknowledge Son Thai Dang whose valuable inputs shaped this thesis. I resonate with his philosophies and hopefully one day I will match his infectious energy. People like Ali and Son are rare.

I want to thank Mr. Gary Stowe, Mr. Bruce Spears, Mr. Jeremy Jernigen and Ms. Micaela Langevin for their support and care. Special shout-out to Mikki. Shreshth and Abhinav are my pillars of strength. Thank you Japneet for being there. Special thanks to my friends away from home: Pritesh, Saket, Saurabh, and Ashutosh. Last but not the least, Meghana.

I always had the love and unwavering support of my parents, my sister, and the rest of my family. This thesis is dedicated to the memory of my father, Manas Chakravarty, who always showed me the right way. Six years back when I was a clueless, partying college kid in IIT, he suggested that I work on shales.

TABLE OF CONTENTS

LIST OF TABLES

LIST OF FIGURES

ABSTRACT

The process of hydrocarbon production from unconventional resource shales begins with identifying zones in the well which have the most favorable features – in terms of fluid content, fluid flow and rock mechanical properties.

Both in the oilfield and in the laboratory, Nuclear Magnetic Resonance (NMR) based techniques are used to characterize fluids in rock samples. Rock properties like fluid-filled porosity, fluid type, wettability, pore size distribution can be estimated using NMR. By comparing the laboratory results with the field data, the relationship between rock properties and production behavior can be better understood. Routine laboratory NMR measurements are made at room temperature while oilfield NMR tools capture measure data at reservoir temperature (usually over 100°C). The difference in temperature makes the direct comparison of lab and log data risky. While considerable literature exists on probing porous media with NMR at elevated temperature, no reference exists on how temperature impacts NMR measurements in shales.

The present thesis summarizes 2 MHz NMR experiments made on shales and conventional reservoir rock samples at reservoir temperature (110°C) and one atmospheric pressure. Based on our results we outline key considerations in interpretation of 2 MHz NMR measurements in porous media at elevated temperature which include: 1) temperature correction of NMR porosity used for conventional rocks does not apply to shales. 2) mobilization of heavy hydrocarbon and adsorbed water at elevated temperature leads to increase in measured NMR porosity at elevated temperature in shales. 3) A revised equation is proposed to predict the NMR porosity of shales at elevated temperature.

1: INTRODUCTION

1.1 Introduction to relevant concepts of NMR

Nuclear Magnetic Resonance (NMR) refers to the behavior of atomic nuclei in presence of magnetic fields (Coates, 1999). An NMR measurement can be made on any species which an odd number of protons or neutrons or both. Examples include hydrogen (^{1}H), carbon (^{13}C) and sodium (^{23}Na). The interaction of such spinning magnetic nuclei with an external magnetic field produces measurable signals. These signals form the basis of NMR measurements. Our study focusses on NMR of hydrogen nuclei or protons. Owing to the intrinsic magnetism of its nucleus, hydrogen nuclei can be visualized as minute bar magnets (**Figure 1.1**).

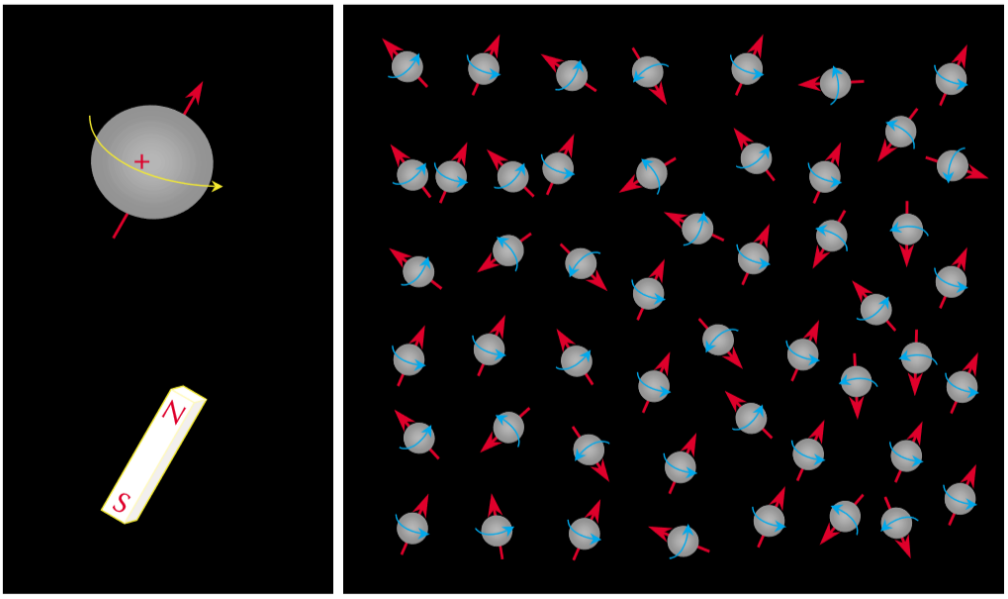

Figure 1.1: A Hydrogen nucleus with an odd number of electrons has an intrinsic magnetic moment and behave as a magnet (Coates, 1999).

In absence of external magnetic field these nuclei would be arranged randomly. In presence of a magnetic field, the field exerts a torque which results in a precessional motion of nucleus (**Figure 1.2**). The precessional frequency is called Larmor frequency (f) and is expressed as:

$$f = \frac{\gamma B_0}{2\pi} \quad \text{.....eq 1.1}$$

Where ϒ is gyromagnetic ratio of nucleus and B_o is the magnetic field. According the laws of quantum mechanics, when an external magnetic field is applied to a proton, the system splits into two energy states. As shown in (**Figure 1.3**), this energy depends on the orientation of the precessional axis of the proton with the direction of applied magnetic field. When this axis is parallel to the field, the energy is lower and higher when the axis is anti-parallel to field. The difference between the number of nuclei in high and low energy states make up the bulk magnetization which is measured by NMR device.

In medical NMR, a linear gradient is used to map hydrogen nucleus population (protons) in three-dimension space. In the oilfield, an NMR tool generates a magnetic field gradient, and the strength of the magnetic field is a function of radial distance from tool surface. This implies that the location investigated by the NMR device depends on the Larmor frequency at which the tool operates. Only the species which are precessing at a frequency close the operating frequency of the NMR tool (resonate with the tool) would be sensitized and contribute to NMR signal.

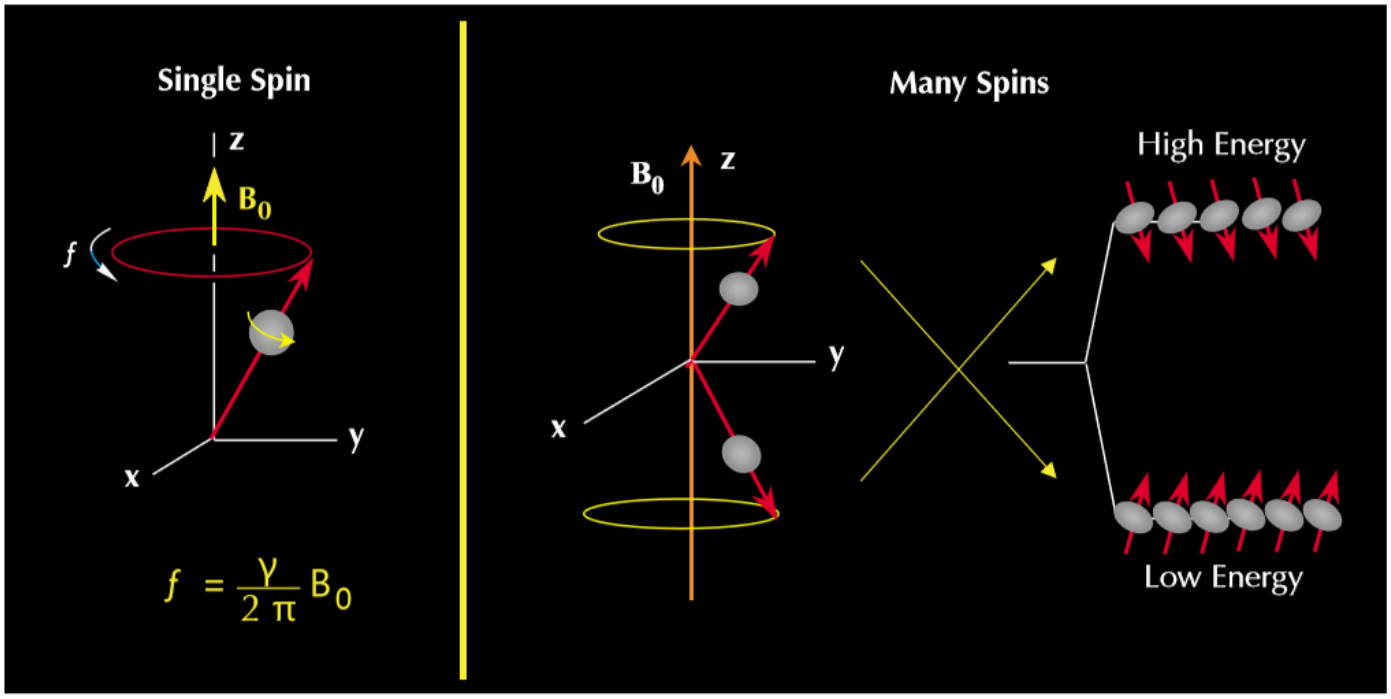

Figure 1.2: An external magnetic field splits the intrinsic magnetic moment into high and low energies owing to quantum mechanical laws (Coates, 1999).

The net magnetization **Mo** can be defined as net magnetization per unit volume. If there are N nuclei present per unit volume, the magnetization is governed by the Curie Law:

$$\boldsymbol{M}_0 = N\frac{\gamma^2 h^2 I(I+1)}{3(4\pi^2)kT}\mathbf{B}_0 \qquad \text{..... eq 1.2}$$

where k= Boltzmann's constant, T=absolute temperature (^{o}K), h=Planck's constant and I= spin quantum number of nucleus. $\mathbf{M_o}$ is the experimental observable and is directly proportional to number of protons and applied magnetic field and inversely proportional to absolute temperature. A schematic of the high and low energy states and bulk magnetization is shown in figure z.

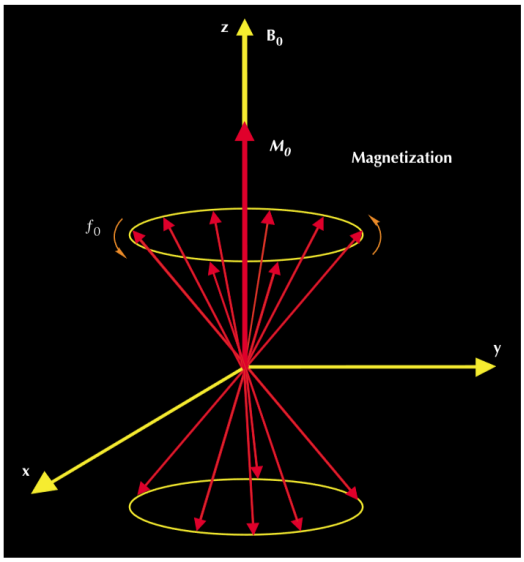

Figure 1.3: The moment parallel to applied magnetic field has low energy and the moments oriented anti-parallel to applied magnetic field have higher energy. (Coates, 1999)

1.2 Laboratory measurement of NMR relaxation in rock pores

The alignment of protons to an external magnetic field is not instantaneous. As shown in **Figure 1.4**, the process of polarization increases with a constant defined as the longitudinal relaxation time (T1).

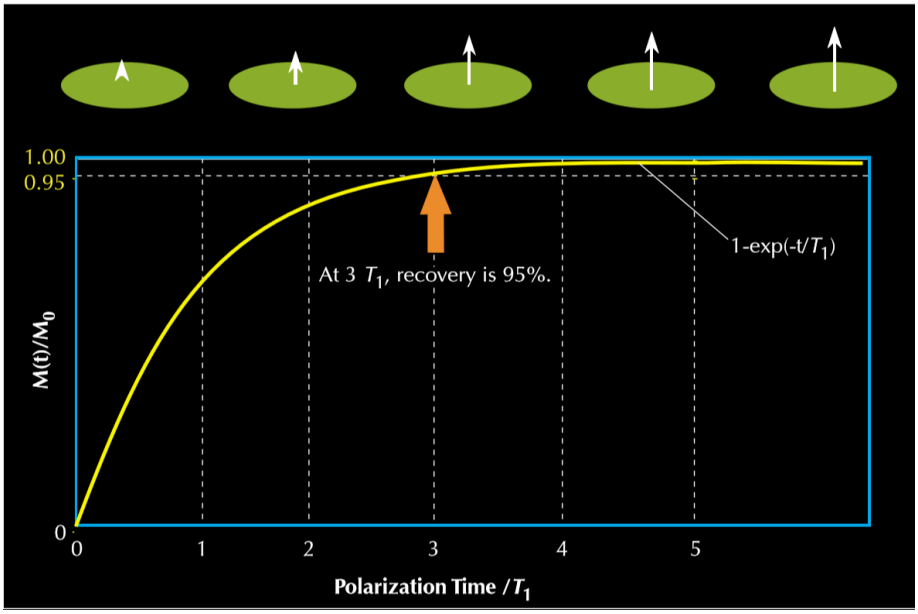

Figure 1.4: The longitudinal relaxation (T1) is a process by which magnetization grows with applied magnetic field. (Coates, 1999)

T1 measurements in the present study were made using an inversion recovery pulse sequence (Green Imaging Technology, 2009). The inversion recovery pulse sequence consists of a 180° radio- frequency pulse (**Figure 1.5**). After delay time (TI) it is followed by a 90° pulse to tip the magnetization in the transverse plane.

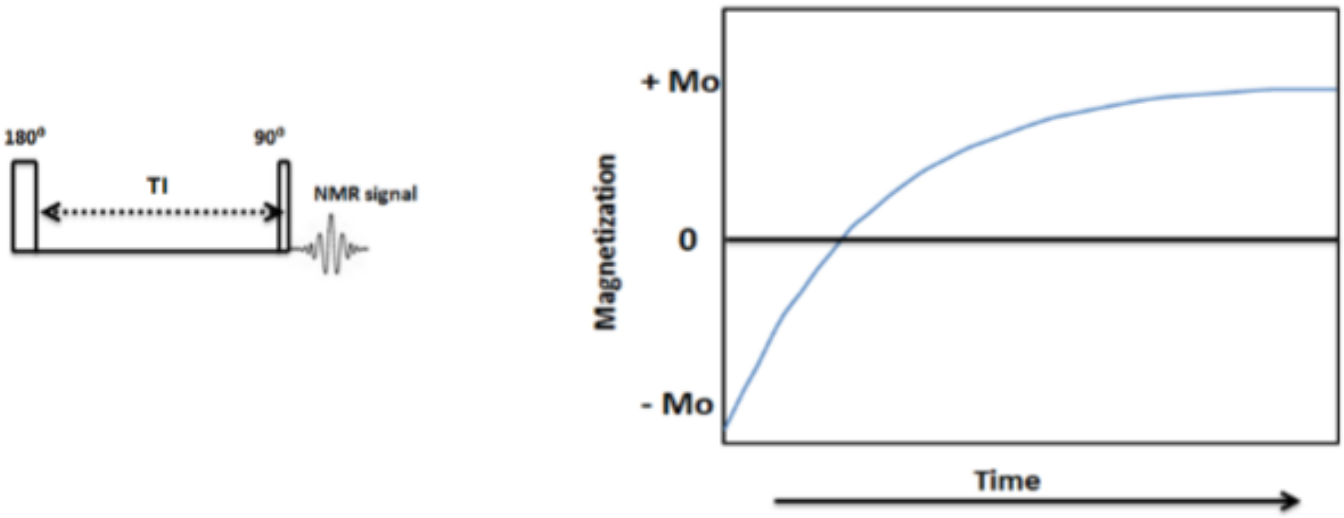

Figure 1.5: **Schematic of the inversion recovery pulse sequence (left panel) to measure longitudinal magnetization (T1). (Right panel) With increasing time (TI), usually taken to be five times T1, the magnetization saturates and the curve reaches an asymptote (Coates,1999).**

In the presence of static magnetic field $\mathbf{B_0}$, a secondary magnetic field $\mathbf{B_1}$ is pulsed such that a torque is applied on the magnetization from the longitudinal (original $\mathbf{B_0}$ axis) onto the transverse plane, which is perpendicular to the longitudinal plane. Such a pulse is defined as a '90° pulse'. The magnetization is said to be 'tipped' on to the transverse plane. As the net magnetization is

due to a collection of nuclei, it now starts to decay as different proton populations begin to lose phase coherency. This is due to the inhomogeneities of magnetic field; different proton populations precess with a different Larmor frequency (Coates et al., 1999). The causes of such inhomogeneities would be discussed in later sections. A receiver coil measures magnetization in the transverse plane records a decaying signal and that is termed as a Free Induction Decay of FID (**Figure 1.6**, left).

-

Figure 1.6 (Left): Free Induction Decay (FID) spectrum shows the magnetization in transverse plane. (Right): A 180° pulse re-phases the spinning nuclei to generate a spin echo at time TE=2τ. (Coates, 1999)

The de-phasing of the transverse magnetization signal is reversed by applying a '180° pulse' of **B1** magnetic field (Figure 1.6, right). As a result of re-focusing of magnetization. The transverse magnetization (T2) is determined using the Carr-Purcell-Meiboom-Gill (CPMG). The CPMG pulse sequence consists of a 90° pulse followed by a sequence of 180° pulses separated by time interval known as inter-echo spacing (TE) (**Figure 1.7**). The mechanical limitations of the

instrument limit the shortest echo spacing (tau, τ=TE/2) to 57 μs. The application of 180° pulses causes the magnetization of the nuclei to re-focus after a time interval of TE and this re-focused magnetization is captured by the same radio frequency coil which transmitted the radio-frequency pulses. Between transmitting and receiving back the radio signals the receiver is inactive for a time known as the 'receiver dead time' (~40 microsecond, in our case) to eliminate the electro-mechanical effects of signal transmission or ringing effects (Coates et al., 1999). The receiver dead time imposes a limit on the minimum inter-echo spacing possible in the NMR spectrometer.

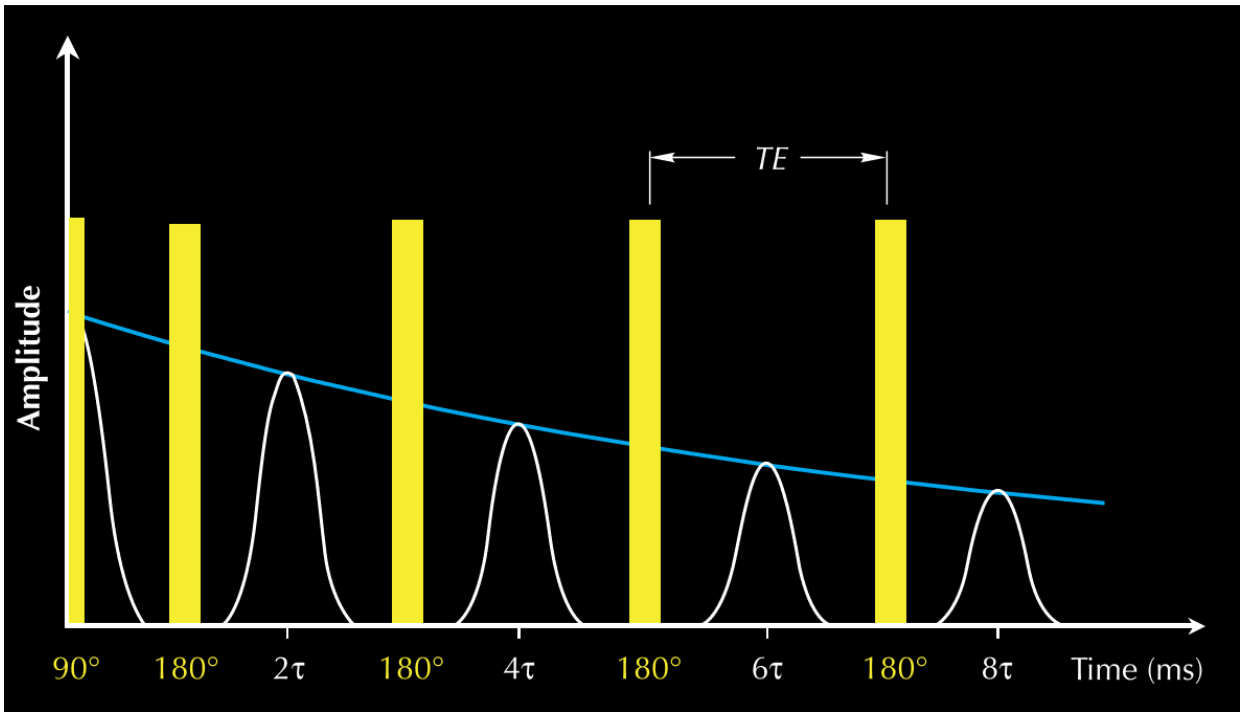

Figure 1.7: **Schematic representation of the Carr-Purcell-Meiboom-Gill (CPMG) pulse sequence used to obtain transverse magnetization (T2) spectra. The raw data in a T2 measurement, the decay curve (shown by blue line), which is inverted using a multi-exponential scheme to generate T2 distribution. (Coates, 1999)**

1.3 NMR relaxation mechanisms in rock

For fluids confined in pore volume of rock, three relaxation processes occur independently and simultaneously (Coates, 1999). They are:

1. Bulk relaxation: impacts T1 and T2 relaxation.
2. Surface relaxation: also impacts T1 and T2 relaxation
3. Diffusion in presence magnetic field gradient: impacts T2 relaxation

In presence of magnetic gradient, the molecular diffusion would cause additional de-phasing. This happens because a nucleus moving into a region where magnetic strength is different will precess with a different frequency. Since these relaxation processes happen in parallel, the transverse (T2) and longitudinal (T1) relaxation times are expressed as:

$$\frac{1}{T_1} = \frac{1}{T_{1\text{bulk}}} + \frac{1}{T_{1\text{surface}}} \quad \text{..... eq 1.3}$$

$$\frac{1}{T_2} = \frac{1}{T_{2\text{bulk}}} + \frac{1}{T_{2\text{surface}}} + \frac{1}{T_{2\text{diffusion}}} \quad \text{..... eq 1.4}$$

$$\frac{1}{T_{1\text{surface}}} = \rho_1 \left(\frac{S}{V} \right)_{\text{pore}} \quad \text{..... eq 1.5}$$

$$\frac{1}{T_{2\text{surface}}} = \rho_2 \left(\frac{S}{V} \right)_{\text{pore}} \quad \text{.....eq 1.6}$$

$$\frac{1}{T_{2diffusion}} = \frac{D(\gamma GTE)^2}{12} \quad \text{..... eq 1.7}$$

where ρ_1 = surface relaxivity of T1, ρ_2 = surface relaxivity of T2, S/V_{pore} = surface to volume ratio, D = molecular diffusion coefficient, G= gradient (G/cm), TE = inter echo spacing using in CPMG experiment, Υ = gyromagnetic ratio of proton.

Reservoir rocks usually show a distribution of pore sizes. For conventional rocks, the theory is based on the premise that a single fluid is filling the pore space. This implies that the transverse magnetization decays not with one time constant, but a summation of magnetizations caused in pores of different sizes. The transverse magnetization is affected by surface relaxation. Smaller pores have higher S/V ratios, meaning relaxation due to surface effects dominate and this results in higher relaxation rate and lower relaxation time compared to larger pores which have a smaller S/V ratio. (**Figure 1.8, top**) shows the multi-exponential decay character of a rock containing a distribution of pore sizes. This decay is fitted into a multi-exponential scheme to generate a T2 distribution (**Figure 1.8, bottom**).

Figure 1.8 (top): A distribution of pore sizes results in a multi-exponential decay of the magnetization signal. This signal is inverted to obtain a T2 distribution (bottom). (Coates, 1999)

1.4 Fluid cutoffs in conventional rocks based on NMR T2 relaxation time

In conventional rocks, the distinction between free and bound water can be done through NMR. It is one of the most widely used applications of NMR in oilfield (Coates, 1999). To carry out this analysis, the spectra of a sample completely saturated with a liquid is obtained. Then the rock is drained using a centrifuge or a porous plate technique to a desired saturation. The remaining fluid content in rock is then quantified using NMR. The free and bound fluid volumes

are estimated from the cumulative NMR porosity plot (**Figure 1.9**). In the absence of laboratory data, default values of T2 cutoff of 33 ms is used for sandstones and 92 ms for carbonate rocks.

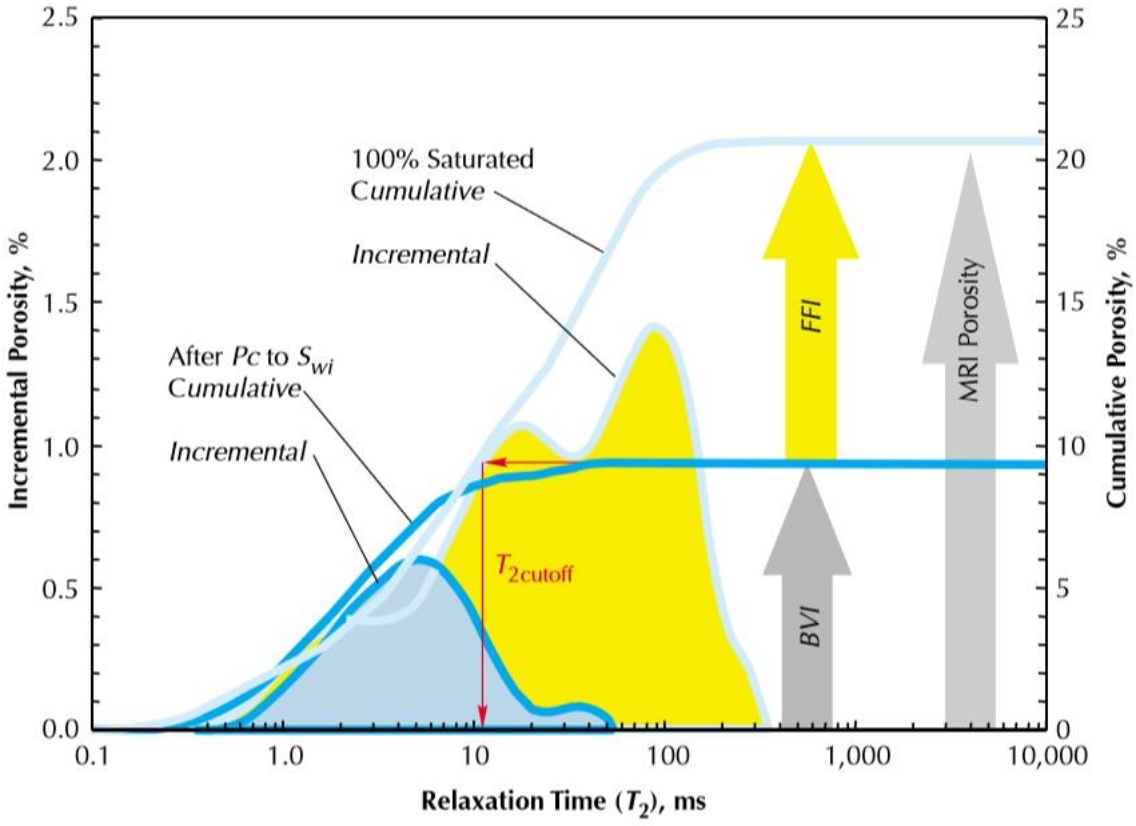

Figure 1.9: Estimation of free (FFI) and bound (BVI) fluid volumes from NMR data (Coates, 1999). Measurements consist of NMR at 100%saturation and NMR after removing free water with a centrifuge or porous plate technique.

1.5 From conventional rocks to shales

The pore system in shale rocks is different from conventional rocks like sandstone and limestone. Sandstone like Berea sandstone are comprised dominantly of quartz grains with presence of diagenetic cement and minor amounts of clays. The average pore diameter is of the order of 100 μm. On the other hand, shales are formed from compaction of fine-grained

sediments, often along with organic matter. This process of deposition results in a pore system in shale in which pores are hosted by both mineral grains and organic matter. Also, since framework grains are much smaller compared to sandstones, the size of pores are much smaller than those found in sandstones. The average pore diameter of pore found in shale is of the order of ~0.1 μm (**Figure 1.10**). Shale may contain significant amounts of clays. The presence of clays and small pore dimensions means that there is significant area available in the pore space for fluids like water and hydrocarbon to be adsorbed. As the proton containing fluids reside in these pores, and since NMR response of fluids is deeply connected to surface properties, the complex characteristics of pore systems in shale complicate NMR interpretation.

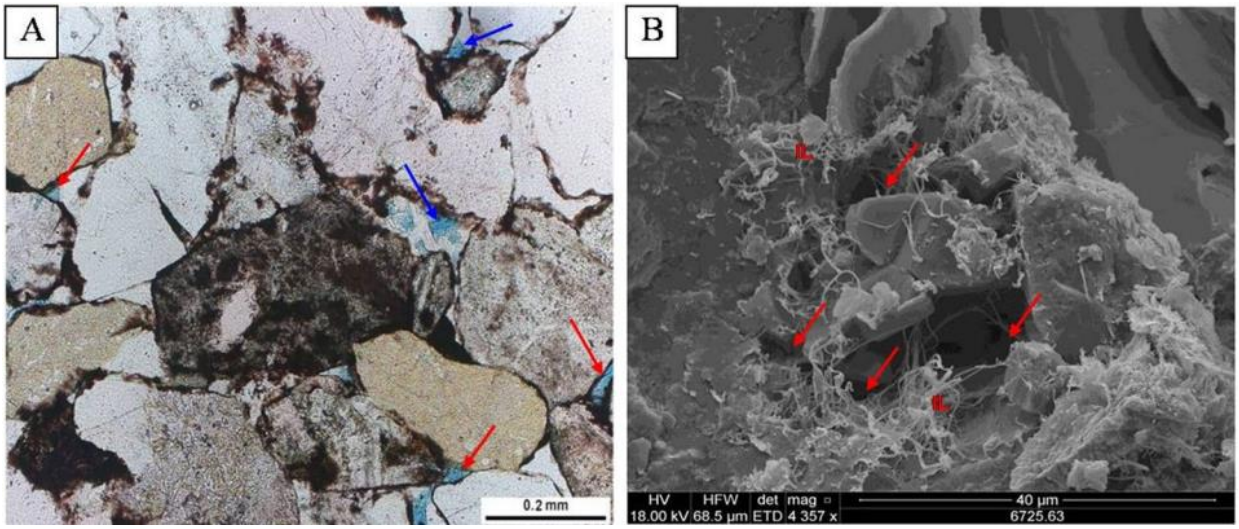

Figure 1.10: (left) pore system of Berea sandstone and (right) pore system of shale (Lai et al., 2018). The pores are indicated by red arrows. Sandstone pore sizes are of order ~0.2 mm whereas shale pore sizes of the order ~0.1 μm.

Unlike conventional rocks, owing to highly heterogenous nature of grain surfaces, shales have highly heterogenous wettability. Mineral surface can be water-wet, oil-wet or mixed-wet. The presence of significant amounts of clays complicates the problem. **Figure 1.11** shows

presence of heavy hydrocarbon (asphaltenes) deposited on surface of shale sample. Presence of asphaltene deposits indicates oil-wet mineral surfaces. Heavy hydrocarbon species are solid at ambient room temperature and hence undetected by 2 MHz NMR at 35°C.

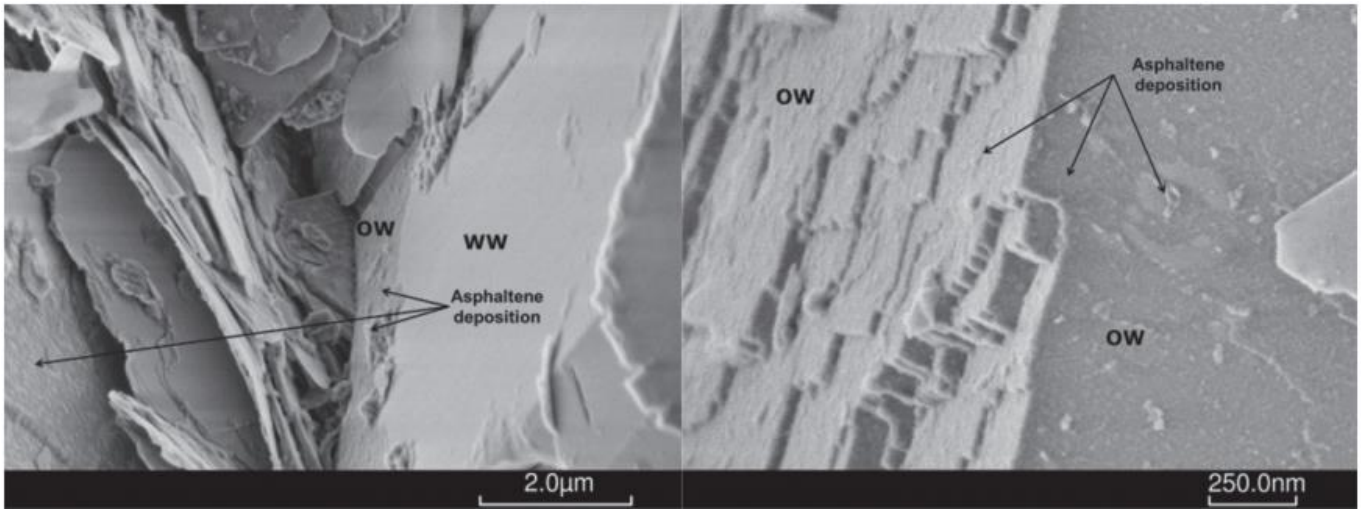

Figure 1.11: SEM photograph of quartz (left) and carbonate (left) mineral grains showing presence of asphaltenes (Lessenger et al., 2016). Heavy hydrocarbon species are solid at ambient room temperature but liquid at reservoir temperatures.

The presence of significant amounts of clays in shale complicates the problem of NMR interpretation. The presence of clays impacts fluid flow and storage properties significantly. The pore size in clays are very small, of the order of ~ 2 nm (Curtis, 2013). It is conceivable that confinement in such small pore sizes impacts the molecular motion and hence the relaxation of fluid species. Owing to very high surface areas, they can have considerable impact on the surface interaction dominated NMR spectra.

Clays and other water wet/mix wet minerals like quartz and feldspar can have a significant amount of water absorbed physically on their surfaces. **Figure 1.12** shows the presence of deposits of heavy hydrocarbon on clays in shales

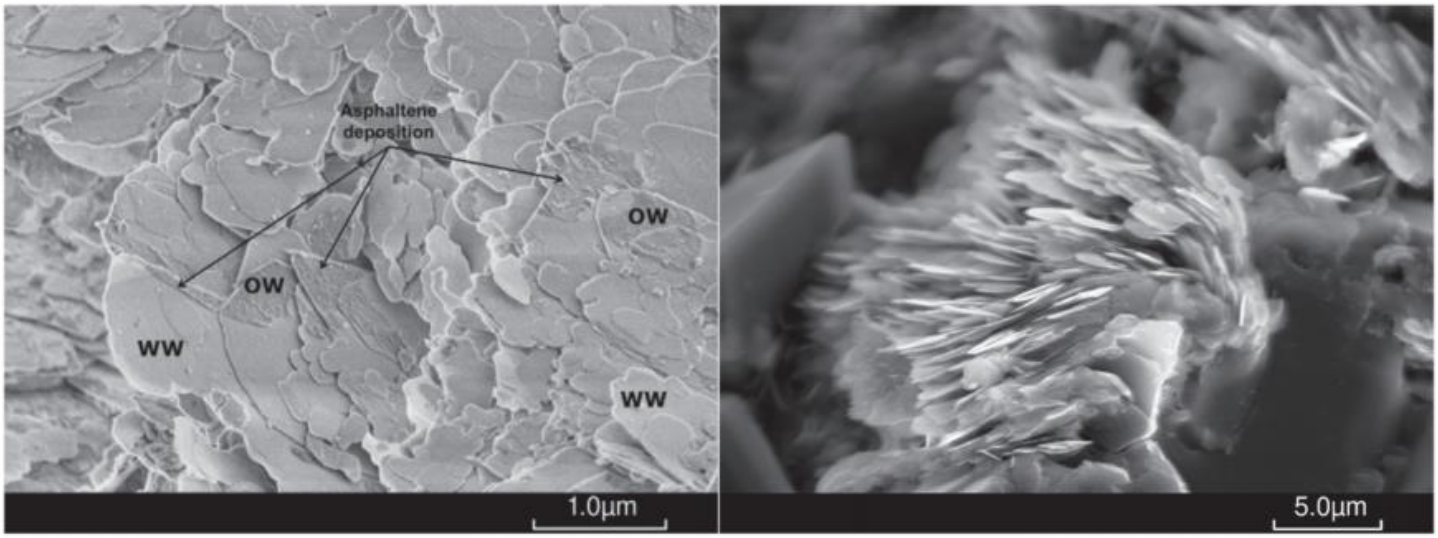

Figure 1.12: SEM photograph of chlorite (left) showing presence of asphaltene deposits, the regions are marked at OW (Lessenger et al., 2016). Regions where asphaltenes are absent are marked at WW (water wet). Platy illite (right) is also mix wet and shows presence of both oil and water.

Overall, it is evident that there are fluid species present within the pore system of shale which can alter the NMR response, if temperature is changed. With an increase in temperature, species like heavy hydrocarbon and adsorbed water on mineral surfaces are likely to be mobilized. If species were solid state before, the high relaxation rates would cause extremely low T2 times and hence such species are undetected by NMR. With mobilization, the relaxation rates reduce and T2 times increase, therefore it is expected that some of these fast-relaxing species would enter into the detection window of NMR at elevated temperature.

1.6 NMR applications for unconventional resource shale

In a rock with uniform wettability the NMR T2 response can be idealized as shown in **Figure 1.13.** In contrast with the conventional rocks like sandstone, the pore system in shale rocks is comprised of oil-wet pores (presumably hydrocarbon hosted pores), water-wet pores (mineral-hosted pores) and mixed-wet pores (pores at the interface of oil and water wet pores) (Curtis et al., 2013). The fluid wetting the surface will relax quicker compared to the bulk fluid, so the presence of surfaces of varying wettability results in a multi-modal NMR T2 signature. The scanning electron microscope picture of an Eagle Ford shale **Figure 1.13 (right)** sample clearly shows the presence of pores hosted in minerals, organic matter as well as at the interfaces of minerals and organic matter. This implies presence of pore systems of multiple wettability in shales.

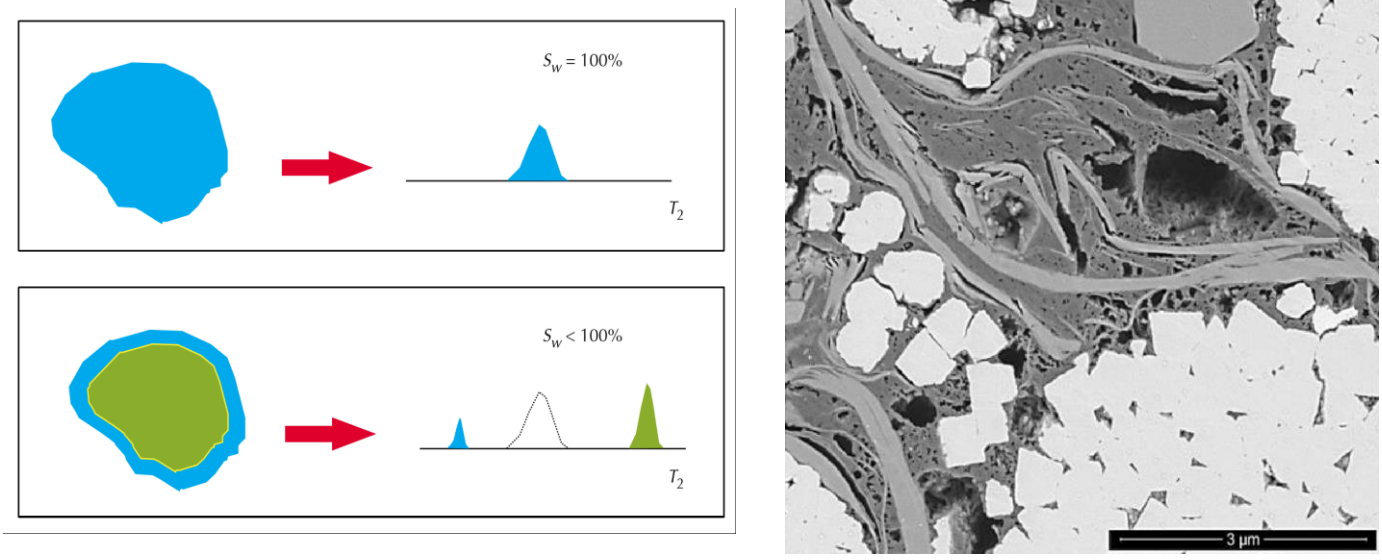

Figure 1.13: (Left panel) NMR T2 response in a pore of uniform wettability (Coates, 1999). The upper row shows the case when only wetting phase is present, the lower row shows the liquid in contact with surface relaxes quicker due to surface relaxation contribution while the liquid not in contact behaves like bulk fluid. (Right panel): Pore system in Eagle Ford shale (Curtis et al., 2013). Light grey areas represent mineral grains and dark grey areas

represent organic rich matrix, these pore systems have different wettability. It is evident that same fluid in shale rock can be hosted in systems of varying surface relaxations, as it depends on the wettability of pore surface.

This complicates the conventional interpretation of T2 spectra in shale. In one of the earliest NMR studies on shale, Martinez (2000) showed the NMR T2 spectra of samples from several shale plays. A comparison between the relaxation rates shows that shales have much shorter relaxation times compared to conventional sandstones or limestones (**Figure 1.14**). This behavior can be attributed to 1) the orders-of-magnitude smaller size of shale hosted pores in comparison to conventional rocks, and 2) surface interaction of fluids with the rock surface. Several attempts have been made to quantify the wettability of shales using NMR (Odusina et al., 2011 and Sulucarnian et al., 2012).

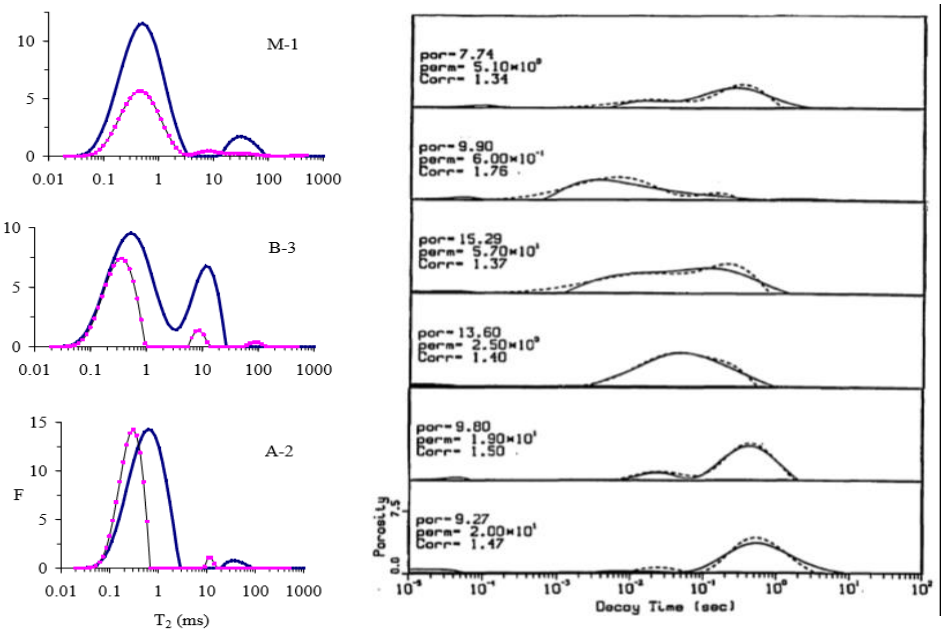

Figure 1.14: **NMR T2 spectra of dry (pink) and water saturated (blue) shale samples (Martinez, 2000) (left panel). In comparison, conventional rocks like sandstone have much**

longer T2 times (right panel). Shown here are NMR T2 spectra of kerosene-saturated sandstone samples (Straley, 1995). The relaxation times are in the range of 100-1000 ms range while in shales the dominant peak is near 1 ms.

1.6 NMR spectra interpretation in shale

Owing to difference in pore characteristics of between shale and conventional rock, the interpretation of T2 spectra for shales is different from the interpretive framework of conventional rocks like sandstone. **Figure 1.15** shows the position of different fluid species confined in shales and sandstone. The locations of free fluid, capillary and clay bound are shifted towards much shorter T2 times.

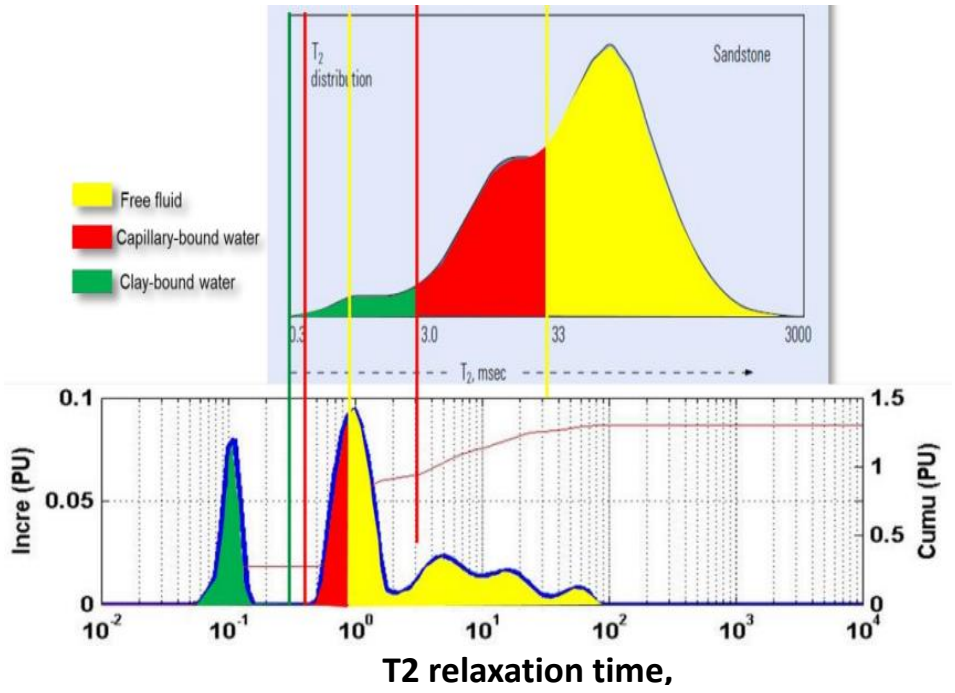

Figure 1.15: Speciation of different pore fluids in shale and sandstone based on their T2 relaxation times (Simpson et al., 2018).

The contrast in the wettability of different pore systems present in shales has been applied to quantify the porosity associated with each system, using NMR. Using 70 wt % $MnCl_2$ solution imbibition, Gannaway (2014) showed the partition of 2 MHz NMR T2 spectra into the different pore systems (**Figure 1.16**).

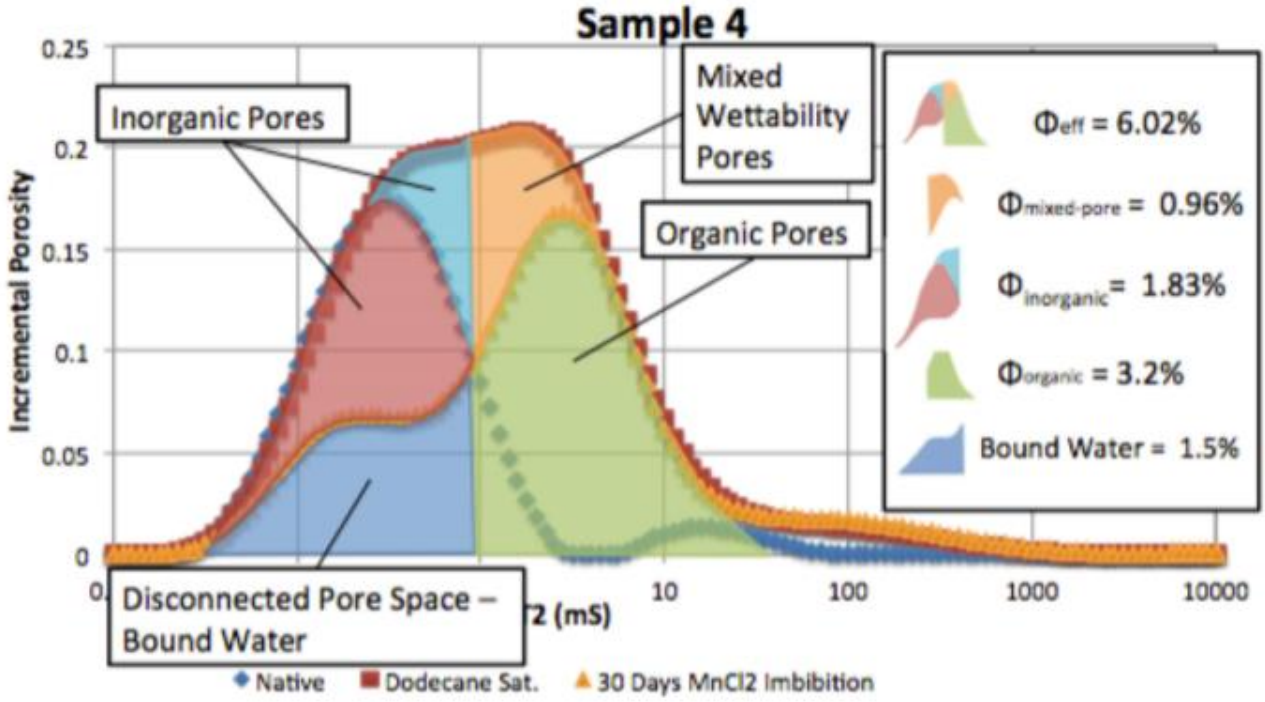

Figure 1.16: **Partition of NMR T2 spectrum of a Barnett shale sample based on $MnCl_2$ solution imbibition. Note that these are not simplistic cut-offs; they are volumes represented by Gaussian curves after inverting the T2 decay data. (Gannaway, 2014).**

Two-dimensional NMR T1-T2 correlation maps are routinely used to identify fluids in shale (Minh et al., 2012, Singer et al., 2013, Kausik et al., 2016, Romero-Sarmiento et al., 2016). Based on the T2 relaxation times and T1/T2 ratio, the viscosity and the confining environment of fluid in the pore systems can be inferred. This enables the differentiation of organic and inorganic porosity systems (**Figure 1.17**).

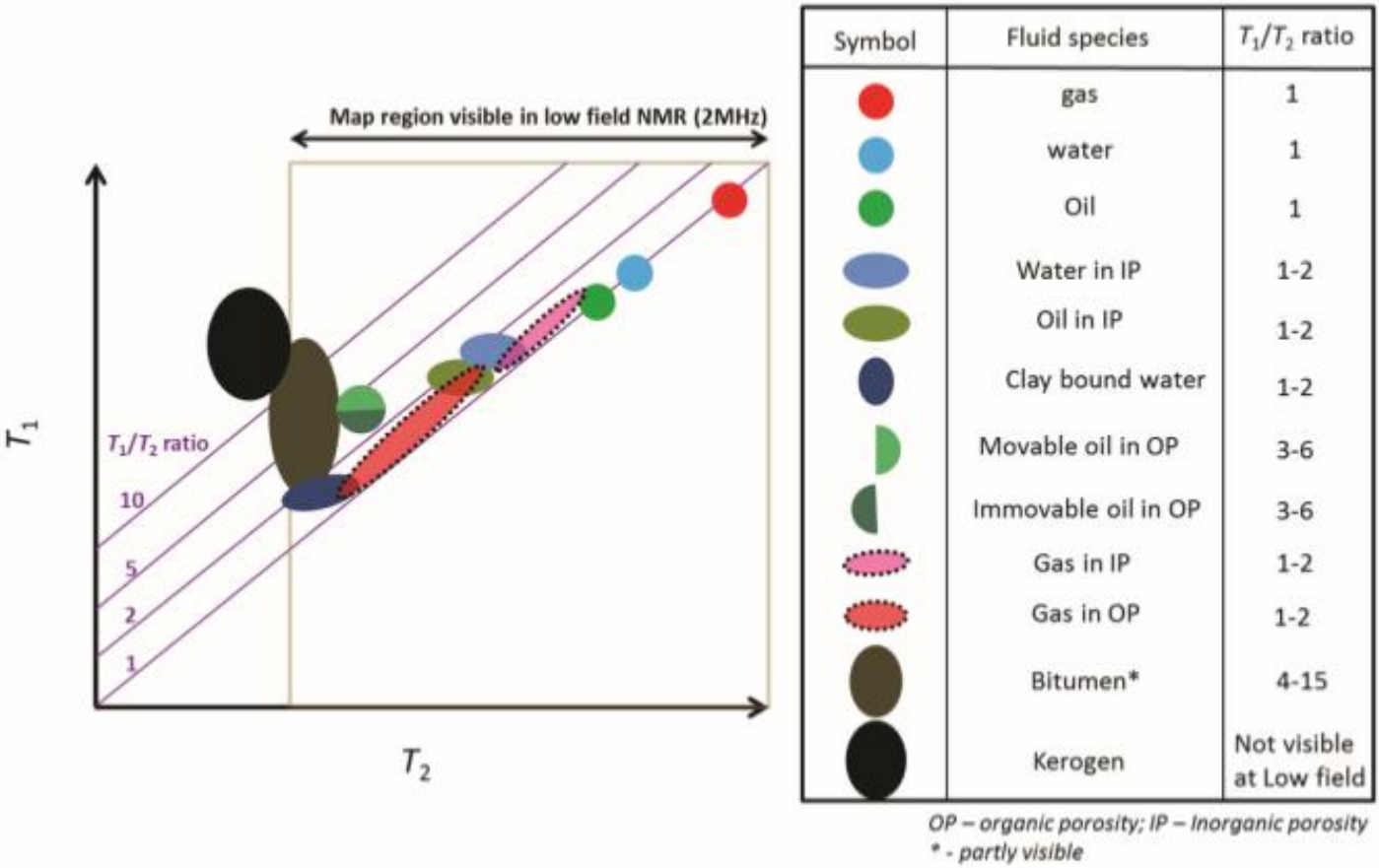

Figure 1.17: **Fluid typing based on T1-T2 NMR data in shale (Kausik et al., 2016).**

1.7 NMR measurements in porous media at elevated temperature

Elevated temperature NMR experiments on porous media have focused on the effect of temperature on the surface relaxivity (Latour at al., 1993; Godefroy et al., 2001). Both research groups studied brine and oil saturated sandstones and limestones. Godefroy (2001) also studied silica gels saturated with brine and oil. Latour et al. (1993) showed that the change in the spectra as a function of temperature of the samples was negligible (**Figure 1.18**).

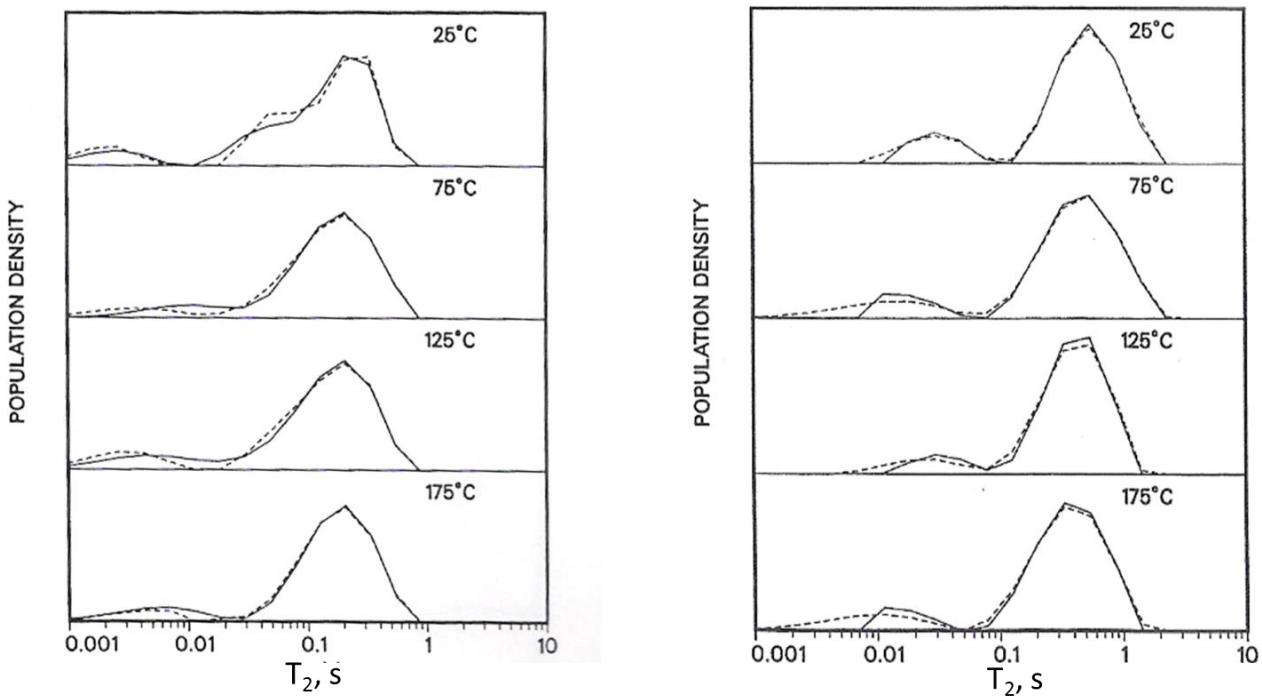

Figure 1.18: **NMR T2 spectra of sandstone and limestone saturated with oil (Latour et al., 1993). The temperature ranged from 25°C to 175°C. Negligible changes in spectra are observed. Dashed lines indicate repeat measurements.**

Godefroy et al. (2001) showed that the surface relaxivity could be modeled using an Arrhenius-type equation and that the surface relaxivity could either increase, decrease or remain constant depending on fluid and surface interactions (**Figure 1.19**). In case of oil the surface relaxivity decreased with temperature which results in longer relaxation times at higher temperature. In water saturated sandstone the surface relaxivity increased, leading to shorter relaxation times at higher temperature. The effect of temperature on surface relaxivity is described by:

$$\rho(T)=\rho(T_0)*(\Delta E/RT) \quad \text{.....eq 1.8}$$

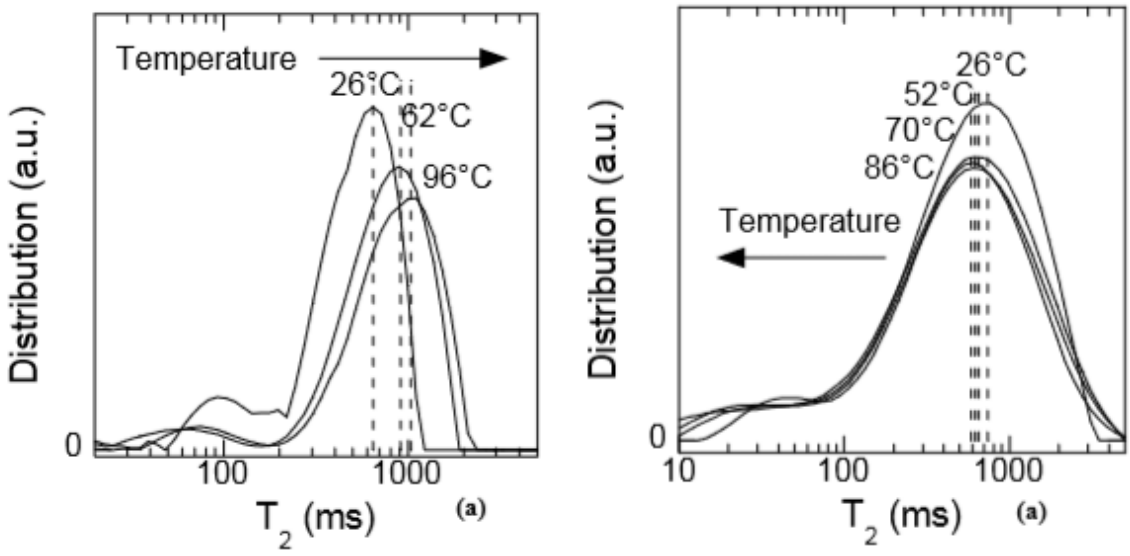

Figure 1.19: **NMR T2 spectra of oil saturated sandstone (left) and water saturated sandstone (right) with varying temperature (Godefroy et al., 2001). For different fluid types, the shift of T2 spectra with temperature is different.**

The increase in temperature will lead to increased thermal motion of the nuclei in the pore systems. If a constant wettability is assumed across the pore system, due to increased thermal motions the rate of diffusion of nuclei across different pore spaces is increased and the T2 spectrum tends to change from a binomial distribution towards a unimodal distribution (**Figure 1.20)**. This phenomenon has been termed as 'diffusional coupling' (Anand et al., 2008).

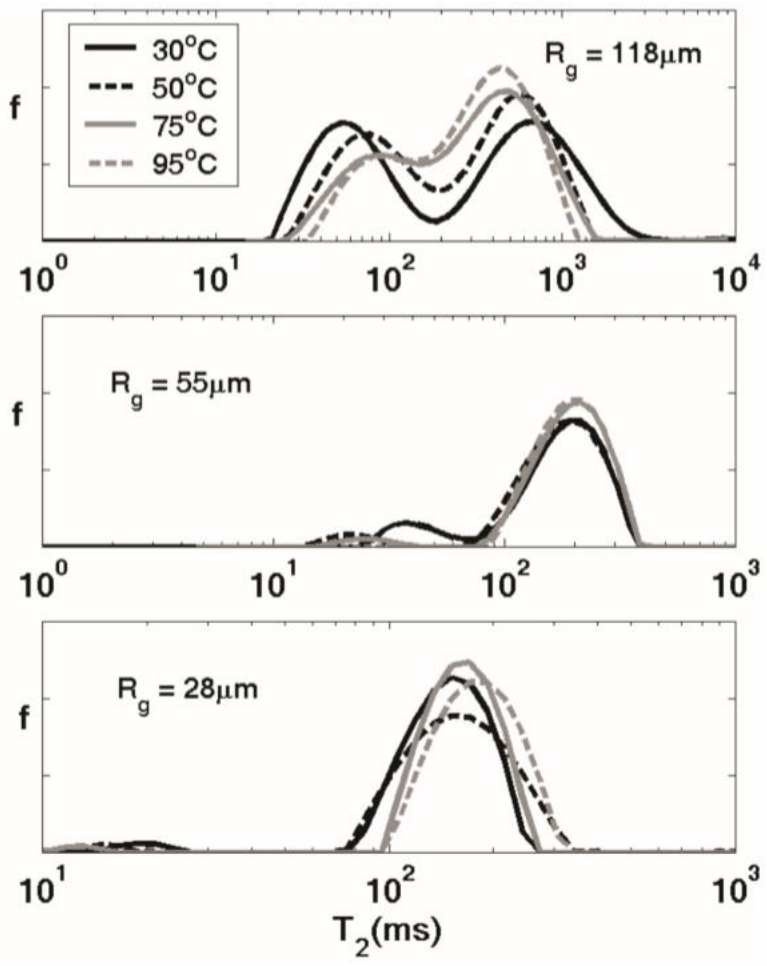

Figure 1.20: **Effect of temperature on the NMR T2 distribution of water saturated silica gel (Anand et al., 2008). As the temperature increases the spectra change character from bimodal to unimodal distribution. Rg is the grain radius.**

1.8 Temperature correction for elevated temperature NMR measurements in porous media

To get an accurate estimate of fluid content in porous media at elevated temperatures, a correction for the temperature is required for the NMR signal. Temperature impacts both

magnetization and relaxation rate in an NMR experiment. The magnetization at temperature T can be expressed mathematically as equation 1.2 (Barakat at al., 2018):

$$M\left(t_{\mathrm{E}}, t_{\mathrm{R}}, T\right) = M_0(T) \exp\left(-\frac{t_{\mathrm{E}}}{T_2(T)}\right)\left[1 - \exp\left(-\frac{t_{\mathrm{R}}}{T_1(T)}\right)\right] \quad \text{(eq 1.9)}$$

Where $M_0(T)$ is the magnetization at equilibrium, t_E is the echo time and t_R is the repeat time or the time between successive CPMG cycles. T_1 and T_2 indicate longitudinal and transverse relaxation, respectively. The equilibrium magnetization M_0 is inversely dependent on the absolute temperature as described by equation 1.3:

$$M_0(T) = \frac{N\mu\hbar\gamma B_0}{2kT} \quad \text{(eq 1.10)}$$

Wherein B_0 is the applied magnetic field, N is number of spin-bearing nuclei, $\hbar$ is Plank's constant, k is the Boltzmann constant, Υ is gyromagnetic ratio, μ is the magnetic moment and T is temperature absolute. To quantify the effect of temperature on the magnetization we can differentiate the logarithm of magnetization with respect to temperature. If the repetition time t_R is chosen to be significantly longer than T_1 (which is the case in our study), the effect of temperature on the overall magnetization can be expressed as shown in equation 1.4 (Barakat et al., 2018).

$$\frac{\partial ln M\left(t_{\mathrm{E}}, t_{\mathrm{R}}, T\right)}{\partial T} \approx \frac{\partial ln M_0}{\partial T} + \frac{t_{\mathrm{E}}}{T_2^2(T)} \frac{\partial T_2(T)}{\partial T} \quad \text{(eq 1.11)}$$

Equation 1.4 shows that the temperature correction in porous media at elevated temperature is a function of both magnetization and relaxation. The magnetization correction is an inverse-temperature relationship whereas in the case of relaxation correction, both the echo time (t_E) as

well as the T_2 distribution ($T_2(T)$) affect the correction. In the oilfield however, it is routine to apply only the magnetization correction (inverse-temperature relationship) to the measured NMR data of fluid saturated rocks (Coman and Tietjen, 2017).

1.9 NMR measurements on hydrocarbon at elevated temperature

Bulk crude oils, mud filtrates and bitumen (heavy hydrocarbon) have been studied for their temperature dependence using NMR (Chen et al., 2004). The dependence of T1 and T2 on the viscosity of a fluid is governed by the Blooembergen-Purcell-Pound (BPP) model and is shown in **Figure 1.21**. The viscosity of oils decreases with increase in temperature. Crude oils show a linear relationship between the log mean T2 and ratio of absolute temperature/viscosity.

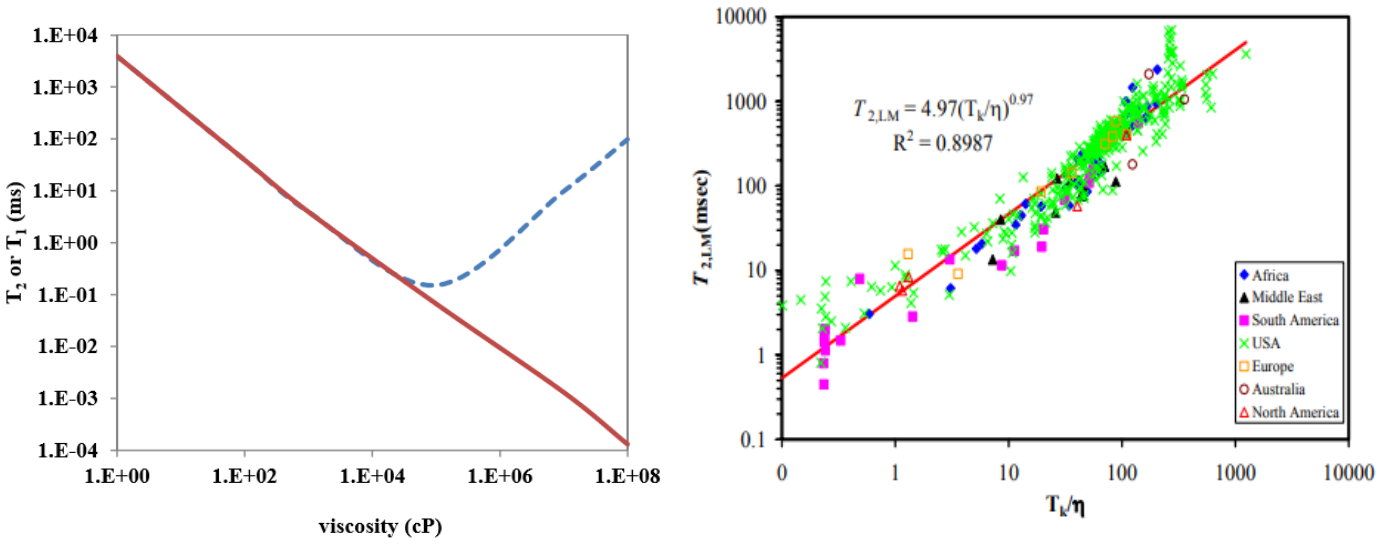

Figure 1.21: **(Left panel) Relationship between T1 and T2 with molecular size or viscosity based on the BPP model. (Right panel) Relationship between log mean of T2 relaxation time (T2LM) and temperature/viscosity ratio from a variety of reservoir oils, T_k=temperature (Kelvin) (Chen et al., 2004).**

Heavy hydrocarbon confined in porous media has also been studied. Tinni et al. (2014) and Sondergeld et al. (2016) studied the NMR response of Berea sandstone saturated with paraffin wax. At 35˚C the wax is solid and appears as a high T1/T2 ratio (~200) peak near 0.1 ms, while at 70˚C the wax has a lower viscosity and exhibits lower T1/T2 ratio (**Figure 1.22**).

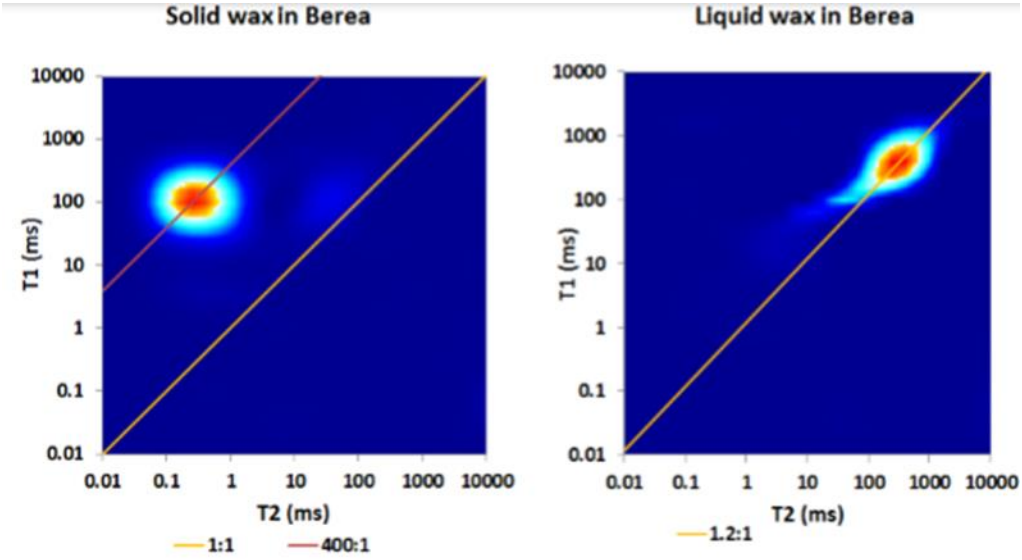

Figure 1.22: **T1-T2 map of paraffin wax saturated Berea sandstone at 35˚C (left panel) and 70˚C (right panel) (Tinni et al., 2014).**

The organization of oligosaccharide coatings on cereal grains has been studied using variable temperature NMR (Ying et al., 2011). The coating of hydrocarbon on the grain walls can be considered analogous to the hydrocarbon coatings on surface of shale rocks. It is observed that the ratio of mobile to immobile nuclei populations increases with increase in temperature (**Figure 1.23**). As temperature increases, more nuclei enter the detection window of NMR due to increased relaxation time as a result of decreased viscosity.

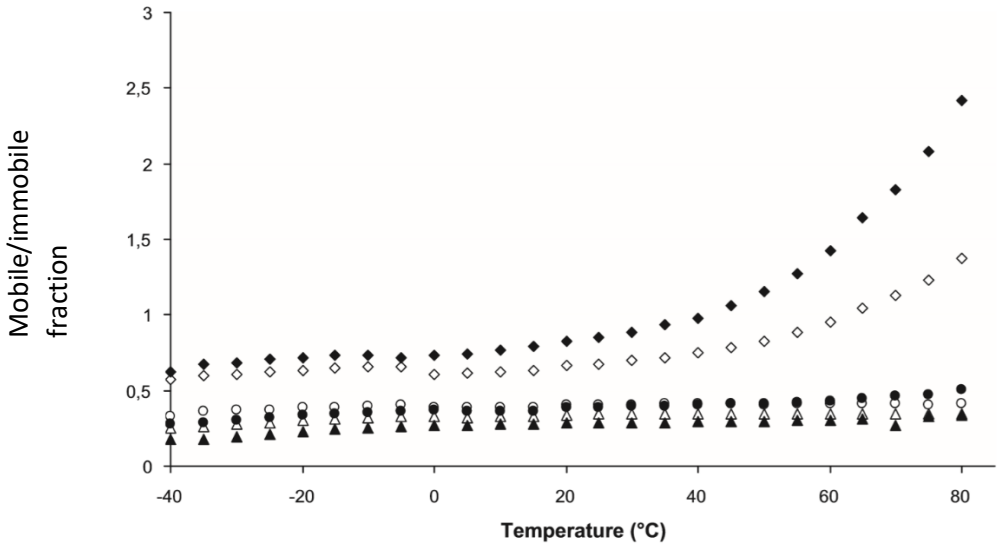

Figure 1.23: **Ratio of mobile to immobile fraction of polymer coatings on cereal grains, as a function of temperature (Ying et al., 2011). Filled and open shapes denote different types of polymers and different shapes represent varying degrees fluid content. This result shows the mobilization of surface of adsorbed hydrocarbon as temperature increases.**

1.10 Elevated temperature NMR measurements on shale

Scant data exists on elevated temperature NMR measurements in shales. Rylander et al., (2013) studied the temperature dependence of NMR T2 response of Eagle Ford shale samples as a part of workflow to integrate core and log response in unconventional reservoirs (**Figure 1.24**). An increase in T2 relaxation time with increasing temperature is observed in the T2 spectrum. They observed is a slight increase of the NMR porosity at 100˚C. Based on their findings, they proposed revised effective porosity cut-offs for free and bound fluid volume for shale at elevated temperatures. At higher temperature, since the T2 spectra shifts towards longer T2 times (**Figure 1.24, right**), the T2 cut-off for effective porosity increases, (**Figure 1.24, left**)

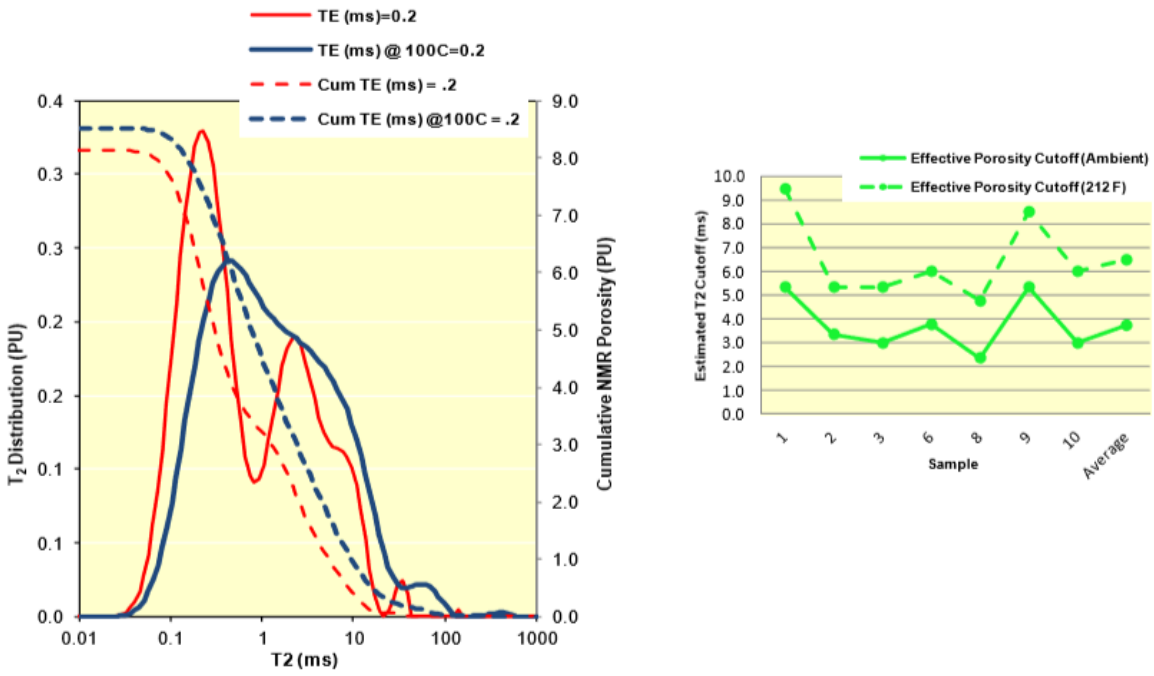

Figure 1.24: **(Left panel) NMR T2 spectra for an 'as-received' Eagle Ford shale sample at ambient temperature (red curve) and at 100˚C (blue curve). The cumulative porosity is indicated by the dashed curves. (Right panel) Effective porosity cutoff obtained for samples based on elevated temperature T2 spectra (Rylander et al., 2013).**

Kausik et al., 2018 used high-field (400 MHz) NMR to study the effect of temperature on the T1-T2 maps of shale and other nanoporous media (**Figure 1.25**). This work focused on the relaxation time spectra as function of temperature. Their results indicate that the relaxation time dependence is proportional to viscosity over temperature for bulk light oil. The relaxation times show a much weaker dependence under confinement. The kerogen and bound water show no dependence of relaxation time on temperature. No analysis was made however, on the effect of temperature on magnitude of measured NMR porosity.

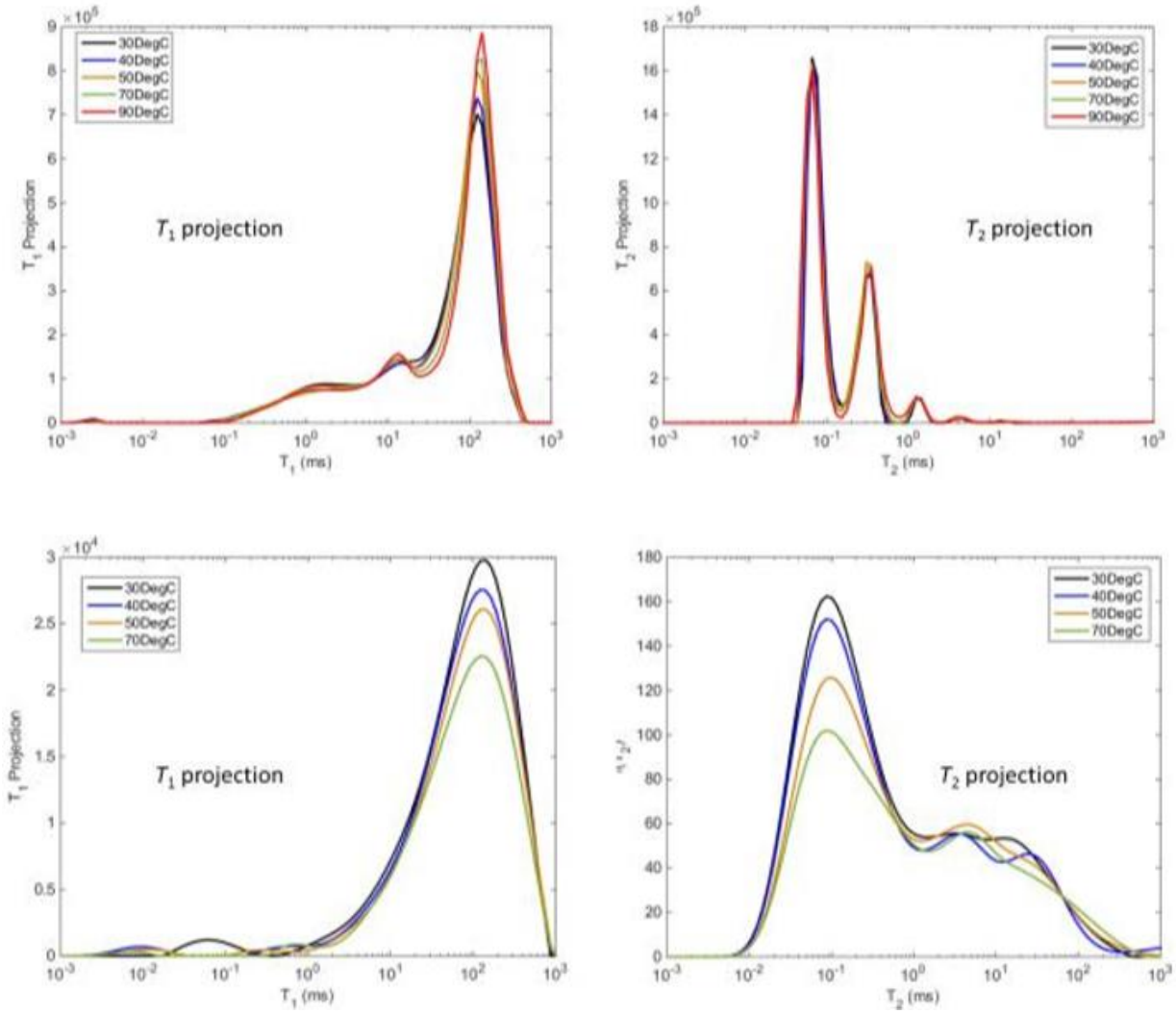

Figure 1.25: High field (400 MHz) T1 and T2 spectra of upper Bakken (upper panels) and middle Bakken (lower panels) shale samples as a function of temperature (Kausik et al., 2018). Note that these are very small samples (dimensions: 3 mm X 12 mm).

Veselinovic et al., 2017 studied the effect of temperature on the low-field (2 MHz) NMR T1-T2 spectra of 'as-received' shale samples. They used T1-T2 based fluid typing based on scheme shown by Kausik et al. (2016) to study the fate of different fluids in shale. Their observations reveal a peculiar behavior of shale rocks (**Figure 1.26**). Between 35°C and 110°C, samples show an increase while two samples show a decrease of measured NMR porosity with temperature. Between 35°C and 65°C, all but two samples either have constant porosity or show an increase of porosity.

This is a remarkable difference from the NMR behavior of conventional rocks. If no additional nuclei are being introduced into the system, the measured porosity should decrease as predicted by the Curie law of magnetization (Coman and Tietjen, 2017). The fact that the porosity either increases with temperature or remains constant indicates that additional nuclei are being introduced into the NMR detection window. To the best of author's knowledge, no experimental investigation has been carried out to explain the anomalous measured NMR porosity of shales at elevated temperature.

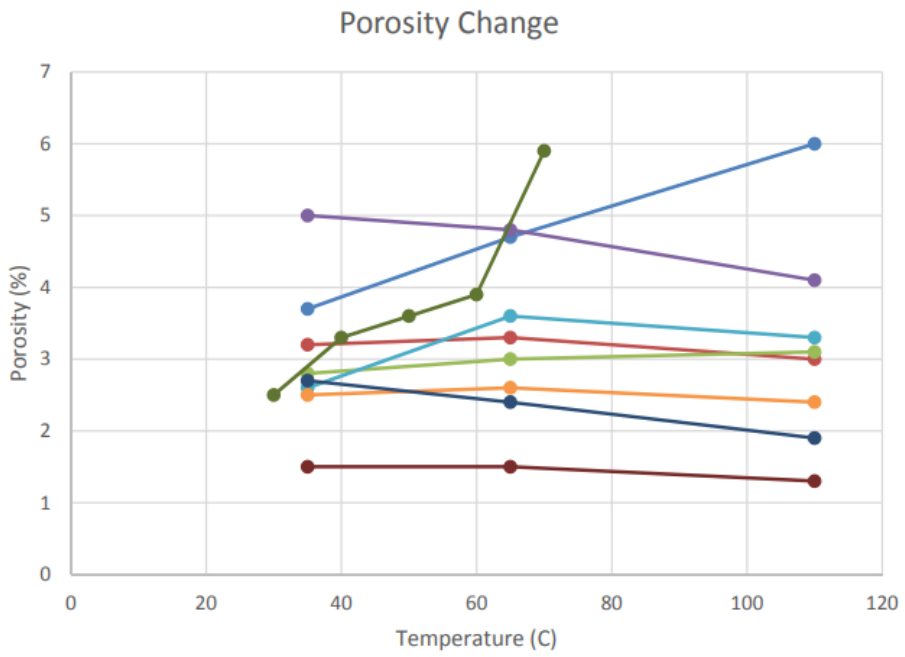

Figure 1.26: **Effect of temperature on NMR T2 porosity of 'as-received' shale samples (Veselinovic et al., 2017). 2 samples show an increase in porosity and 2 samples show a decrease. 4 samples show no change in measured porosity with temperature. Current form of correction predicts that porosity decreases with increase in temperature.**

1.11 Motivation of this thesis

Despite the breadth of literature on NMR studies on porous media at elevated temperature, information on the effect of temperature on the measured NMR behavior of shale rocks and its controlling parameters is missing. This thesis attempts to address:

1. Effect of temperature on measured NMR porosity in shales.

2. Effect of pore fluid on NMR response of shales at elevated temperature.

2: Description of experimental procedures and samples

2.1 Fourier transform infrared (FTIR) spectroscopy for quantitative mineralogy

Fourier transform infrared (FTIR) spectroscopy is a method of vibrational spectroscopy in which infrared (IR) energy level photons interact with the molecules. When a polychromatic light interacts with molecules, the bond absorbs the photon at the frequency of the bond vibration due to resonance and the frequency is a characteristic of the molecule. The nature of these characteristic frequencies allows one to fingerprint different minerals based on their infrared vibrational spectrum. The incident light can either be transmitted through the sample or reflected off the sample surface. We have used potassium bromide (KBr) pellet transmission FTIR method (Griffiths and De Haseth, 2007) in the mid infrared range (400cm^{-1} to 4000 cm^{-1}). The raw data from the FTIR instrument is the interferogram, which is inverted using Fast Fourier transform methods to generate a transmittance spectrum. A Nicolet® 6700 FTIR instrument was used in my study. (**Figure 2.1**).

Figure 2.1: **Thermo Nicolet 6700 FTIR spectrometer.**

The amplitude at a frequency in the FTIR spectrum is related to concentration, path length and absorptivity of each constituent (Beer's law) can be expressed as:

$$A_i(\tilde{\nu}) = a_i(\tilde{\nu})bc_i \quad \text{.....(eq 2.1)}$$

Wherein $A_i(\tilde{v})$ is the absorption of constituent i at wavenumber $\tilde{v}$, $a_i(\tilde{v})$ is the absorptivity constituent i at wavenumber $\tilde{v}$, b is the path length and c_i is the concentration of species i. The application of Beer's law for quantification requires a library of FTIR spectra of known compositional standards (Sondergeld and Rai, 1993; and Ballard, 2007). The library used in the present study contains sixteen minerals. Among them, the FTIR spectra of a sample of six minerals :quartz, calcite, illite, anhydrite, smectite and kaolinite are shown in **Figure 2.2**.

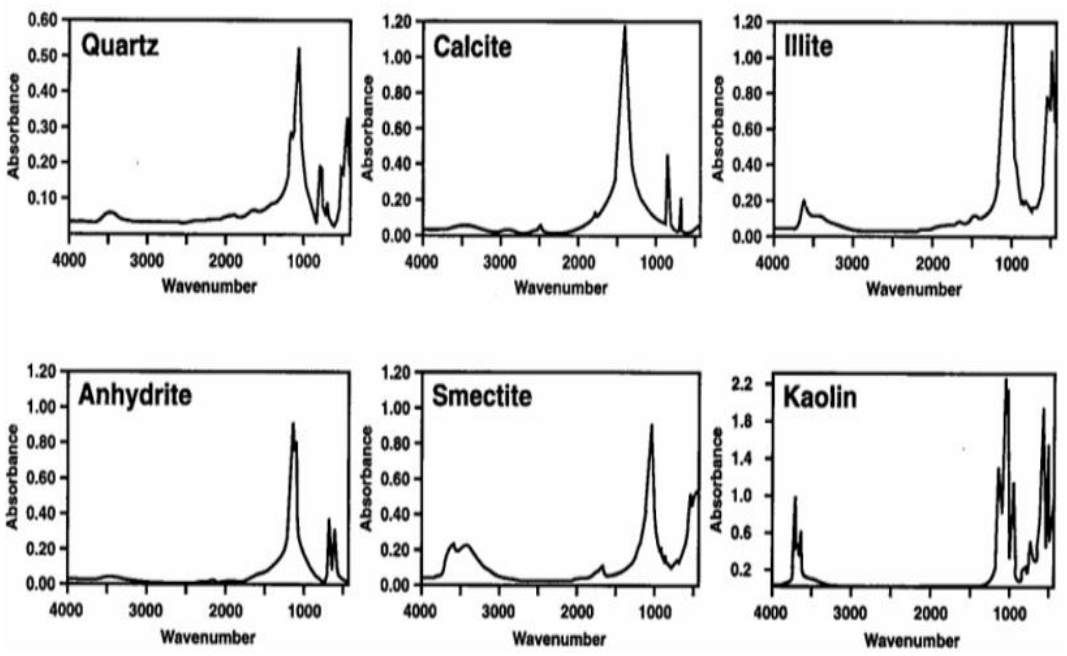

Figure 2.2: Characteristic FTIR spectra of known minerals found in sedimentary rocks (Sondergeld and Rai, 1993).

Before the measurement, 0.3 g of desiccated KBr powder is pressed under vacuum and 10-ton to make a 1 mm thick disk. The disk is used at the reference for the transmission measurement. KBr is particularly suited for this experiment because it does not have its molecular bond vibrational frequencies in the mid infrared ($400cm^{-1}$ to $4000\ cm^{-1}$) range. The measurement of pure KBr disc gives the background spectrum. In the next step, 0.0005 g of extremely finely ground sample is mixed with 0.2995 g of KBr powder and pelletized to create disk from which transmission spectra is obtained. The weights are chosen such that the infrared absorbance relationship with the concentration falls in the linear range, and Beer's law is applicable. It is necessary to remove the organic matter from the crushed rock sample because organic matter have some characteristic FTIR frequencies which overlap with that of clays (Dang et al., 2013). The samples in this study were ashed in a low temperature plasma asher and dried at 100°C for at least 12 hours to remove moisture prior to FTIR measurement.

2.2 Total Organic Carbon (TOC) measurement

The Total Organic Carbon (TOC) content of rock samples was measured with a LECO® CS844 instrument. The sample is heated to 1200°C and the infrared signal from the combustion products is used to quantify the TOC content of the sample. To remove the inorganic carbon from the sample, the powdered sample (weight: 0.1± 0.01g) is treated with 10 wt % hydrochloric acid and agitated and subsequently with deionized water. Prior to the measurement the sample is dried at 100°C for one hour.

2.3 Core sample cleaning using Soxhlet extraction method

The samples were cleaned by Soxhlet extraction method (**Figure 2.3**). The solvent was a mixture of toluene and methanol in 80:20 volume ratio.

Figure 2.3: **Soxhlet extraction apparatus located inside fume hood.**

2.4 Source Rock Analysis (SRA)

Source Rock Analysis (SRA) refers to the method of programmed anhydrous pyrolysis of samples in an inert atmosphere. As the sample is heated at controlled rate, the combustion products are quantified with a Flame Ionization detector (Tissot and Welte, 1984). During the measurement, moveable hydrocarbon present in the sample are volatilized at moderate temperature and are represented in **Figure 2.4** as peak S1. At higher temperature, the kerogen is pyrolyzed which is recorded as the S2 peak. The kerogen content is an indicator of hydrocarbon generation capacity of the source rock. Subsequently, the release of trapped CO_2 reflected in the S3 peak in the pyrogram. We used the HAWK® instrument from Wildcat Technology for our tests.

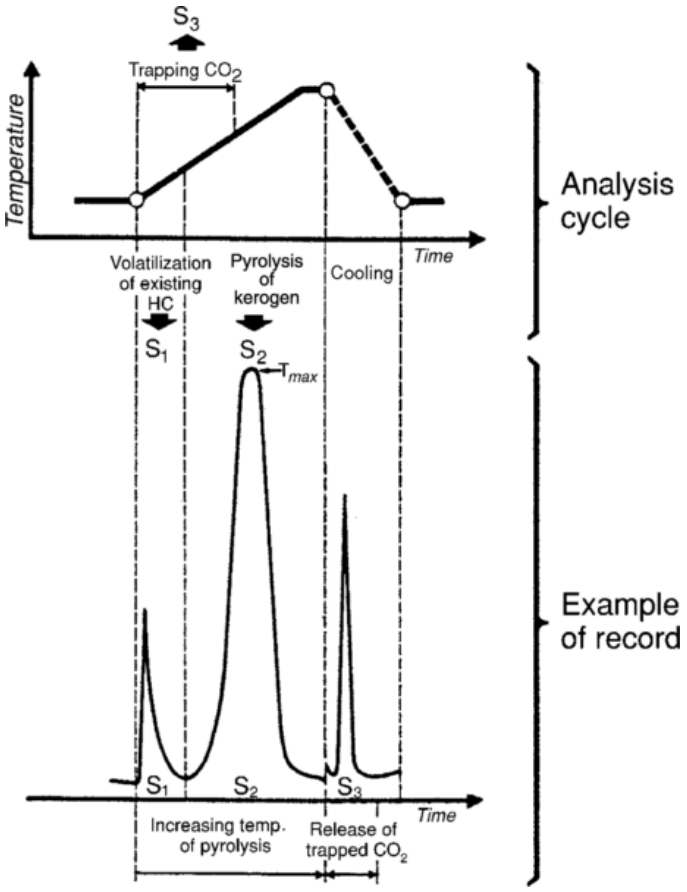

Figure 2.4: **Temperature profile (top) and schematic of pyrogram (bottom) produced by a source rock sample in Source Rock Analysis (SRA). S1 is a measured residual hydrocarbon in the sample before pyrolysis. S2 corresponds to the hydrocarbon generation potential of the sample and S3 is a measure of the liberated carbon dioxide from the sample during pyrolysis (Tissot and Welte, 1984).**

2.4.1 Analysis of pore fluids using Source Rock Analysis (SRA)

The pore fluid was characterized using SRA. **Figure 2.5** shows the pyrogram obtained from Woodford shale samples containing preserved *in-situ* reservoir fluids. S2 is defined in this study as the amount hydrocarbon volatilized between 350°C -500°C. In composition terms, this fraction corresponds to C20+ portion.

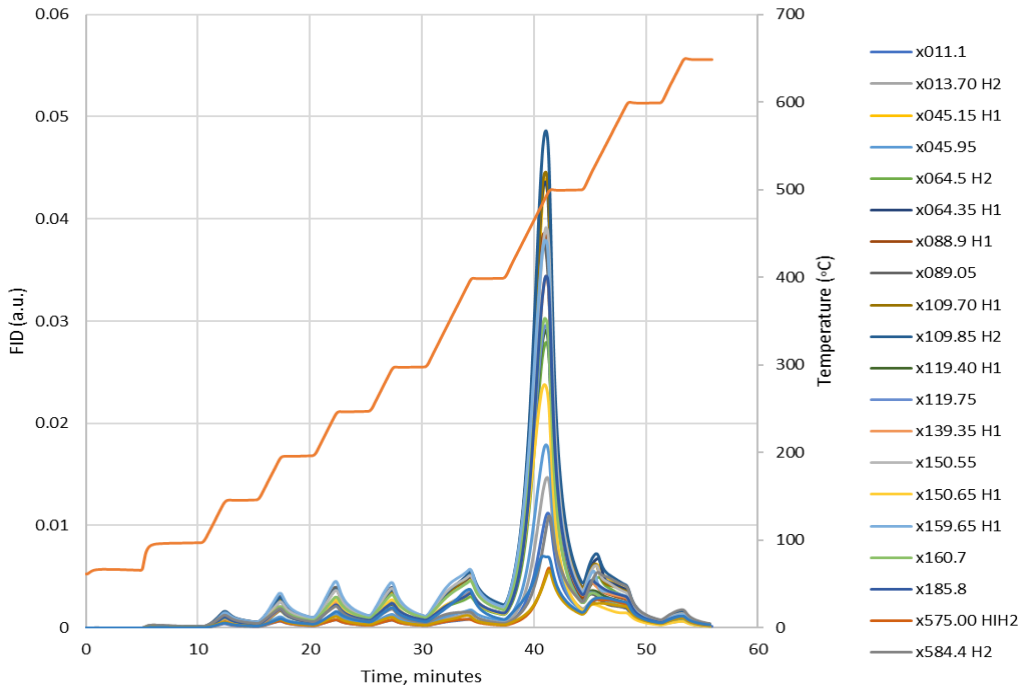

Figure 2.5: Pyrograms for Woodford shale samples containing preserved *in-situ* reservoir fluids. Most of the heavy hydrocarbon volatilizes between 350°C and 500°C. In composition terms, this fraction corresponds to C20+ portion.

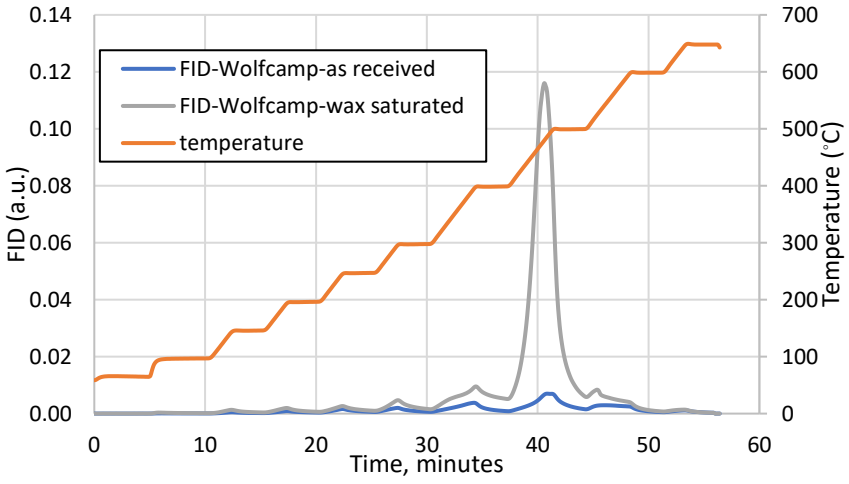

Figure 2.6: **Pyrogram of as-received and wax saturated Wolfcamp sample WC-xx491. The SRA signature of paraffin wax is very similar to that of *in-situ* hydrocarbon and hence paraffin wax can be considered as a surrogate for S2.**

The heating sequence for SRA followed in present study is a modified heating protocol in which temperature is raised by increments of 50°C for temperatures between 30°C and 300°C and raised by increments of 100°C between 300°C and 650°C. Using small, well-defined temperature increments allows the quantification of the hydrocarbon type based on number of carbon atoms.

The FID peak associated with temperatures between 400°C and 500°C is similar to the peak observed for Woodford shale samples containing preserved reservoir fluids (**Figure 2.6**). S2 before wax saturation was 1.08 mg HC/g of rock and S2 content after wax saturation was 21.7 mg HC/g of rock. The paraffin wax appears as an S2 signal. A similar signature of hydrocarbons is observed in the pyrograms of 'as-received' Bakken shale samples and is shown in **Appendix Section A.7**.

2.5 NMR measurements

The NMR measurements in this study were performed on an Oxford GeoSpec2 NMR spectrometer at a Larmor frequency of 2 MHz (**Figure 2.7**). The NMR data processing was done on the Green Imaging Technology® software. Longitudinal (T1), transverse (T2) and T1-T2 correlation spectra were collected in this study.

Figure 2.7: The Oxford GeoSpec2 NMR spectrometer used in present study operates at 2 MHz and has a minimum echo spacing of 57 μs.

In all the NMR measurements the readings are repeated over time and their data stacked in order to increase the signal-to-noise ratio (SNR). The minimum SNR used in this study is twenty-five, whereas the typical SNR encountered in the oilfield measurements rarely exceeds ten. The Signal-to-noise ratio (SNR) is defined as the peak height divided by the root mean square of noise (Hyberts et al., 2012).

The area under T2 or T1 curves corresponds to the number of hydrogen-bearing nuclei present in the fluid. Hydrogen index (HI) is the considered as the ratio concentration of hydrogen nuclei compared to deionized water. The NMR porosity is defined as:

$$NMR\ porosity\ (\phi_{NMR}) = \frac{Area\ under\ spectrum}{Number\ of\ scans * calibration\ factor * fluid\ volume} \quad \text{……(eq 2.2)}$$

Knowing the hydrogen index (HI) of a fluid, one can estimate the fluid porosity from NMR porosity using the relation:

$$fluid\ porosity\ (\phi_f) = \frac{\phi_{NMR}}{HI} \quad \text{……...…....(eq 2.3)}$$

We have assumed all the liquids in the study to have a temperature invariant hydrogen index of one, which is reasonable consideration (Kleinberg et al., 1996).

This study involves measurement of NMR spectra at ambient laboratory (35°C) and elevated temperature (110°C). The heating of the rock sample inside the NMR spectrometer was achieved by blowing hot dry air sourced from in-house air supply, around the glass vial enclosing the sample. The sample is heated for at least two hours prior to measurement to ensure thermal equilibrium within the sample. The sample is maintained at atmospheric pressure at all times throughout measurement. The sample holder is manufactured from glass and Teflon® , which do not generate NMR signals at such temperature (**Figure 2.8**).

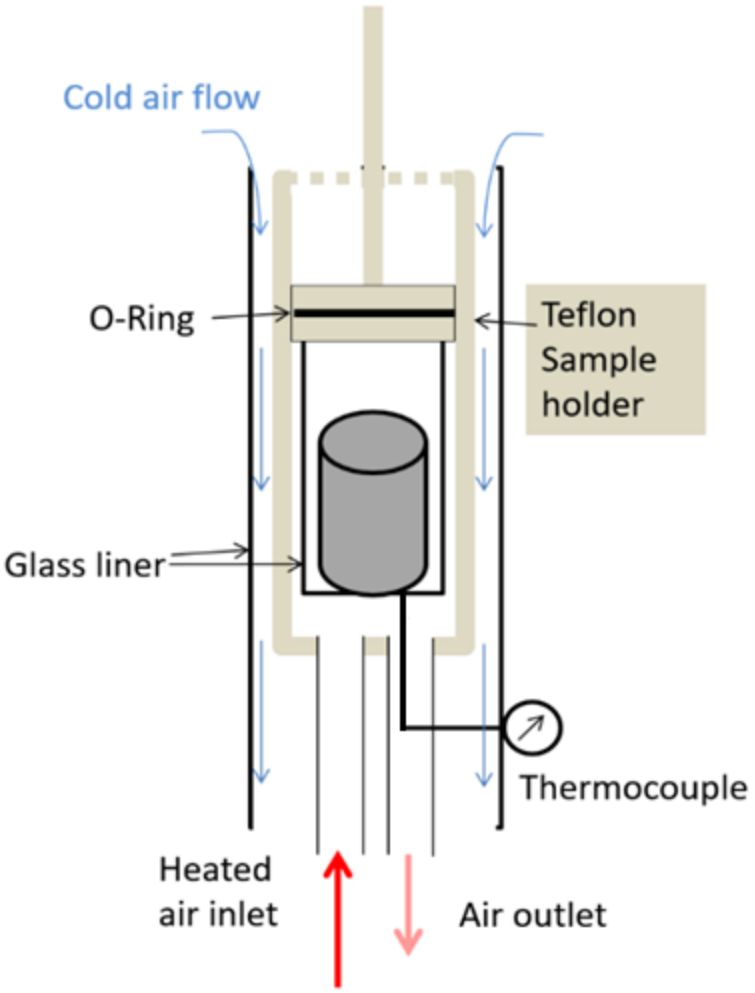

Figure 2.8: **Schematic of the sample holder within the NMR spectrometer. The apparatus is fabricated using glass and Teflon which do not have NMR signals. Heated air is in contact with the bottom and lateral surface of glass vial containing sample under study.**

2.5.1 Heating and Temperature measurement in NMR apparatus

The temperature was measured with an Omega® K-type thermocouple with an accuracy of ±0.5°C. To ensure that sample temperature matches the measured temperature, a temperature calibration experiment was carried out. The bottom thermocouple was inserted at heated air outlet (**Figure 2.9**) and touched the bottom surface of glass vial while the second thermocouple

was attached to the top surface of the rock sample. The recorded temperature was plotted as function of time as shown in **Figure 2.10.**

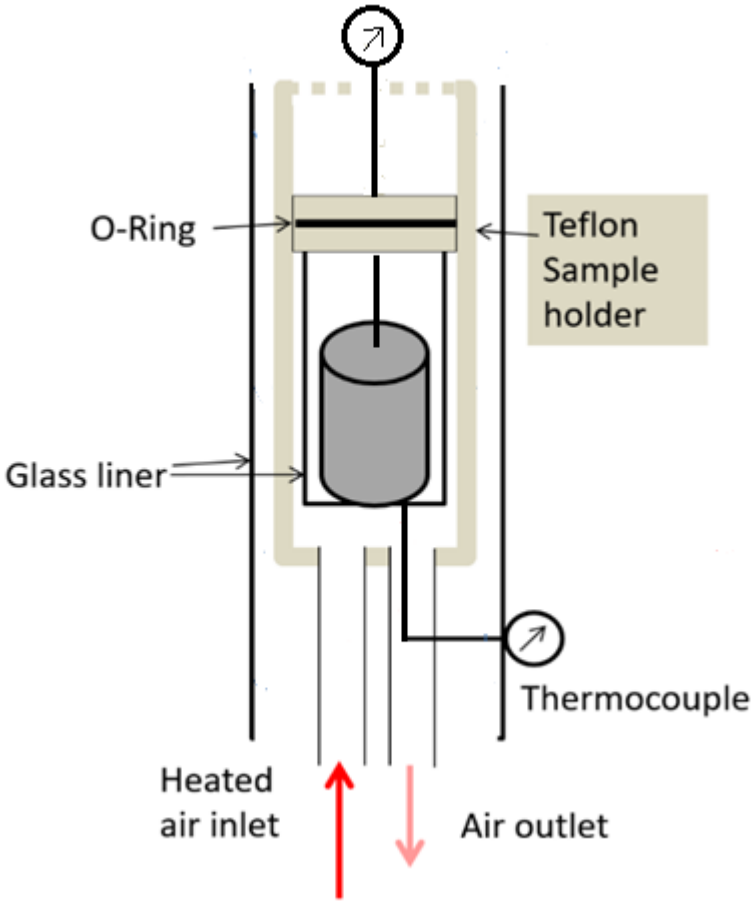

Figure 2.9: **Schematic of temperature calibration experiment. The top thermocouple is inserted into the glass vial through a hole and touches the top of sample. The bottom thermocouple is inserted through the heated air outlet and touches the bottom of the vial.**

The temperature recorded by the two thermocouples as a function of time is shown in **Figure 2.10.** As the hole for the top thermocouple is much wider than the thermocouple wire, some air naturally entered the heated region and cooled the top surfaces of rock during the experiment. As

a result, we observe a difference between the top and bottom surfaces of the rock which tends to stay constant with time. The difference in temperature is smaller than 5°C and thus negligible thermal gradient exists within the sample. It is expected that during a real NMR heating experiment when the hole is sealed by a Teflon shaft, there would be no cooling of top surface of sample due to influx of cool air and the temperature difference between top and bottom surface would decrease further.

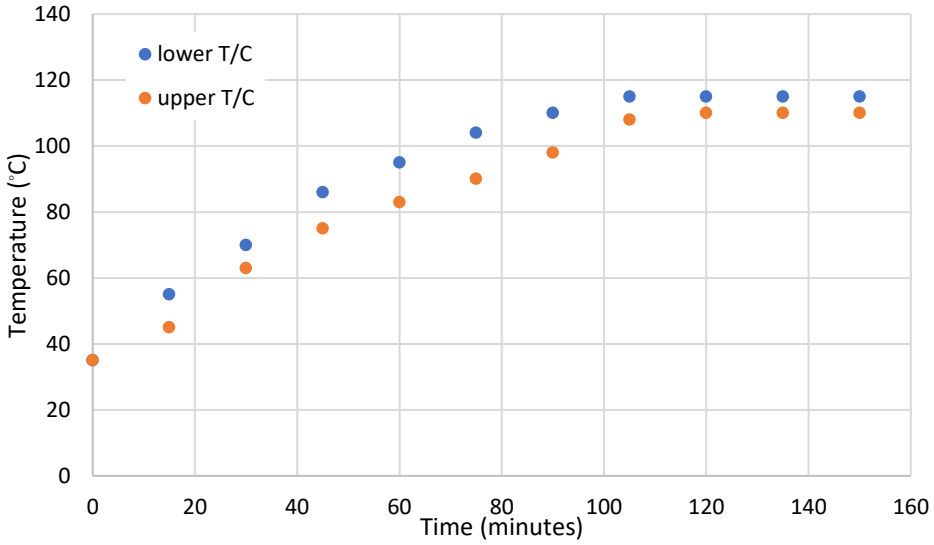

Figure 2.10: **Temperature measurement by upper and lower thermocouples (T/C) in the NMR sample holder during air heating. Two hours was chosen as the time required to reach thermal equilibrium at 110°C.**

2.5.2 Echo spacing considerations for NMR measurements on shale

It has been established that the echo spacing used in the NMR measurement impacts the measured porosity (e.g. Tinni, 2017). Longer echo spacing result loss of signal from fast relaxing components and thus reduced porosities, especially in shales/ **Figure 2.11** shows T2 spectra of rock measured with different echo spacings. Since shale rocks contain various volumes of fast relaxing components, the selection of optimal echo spacing becomes critical.

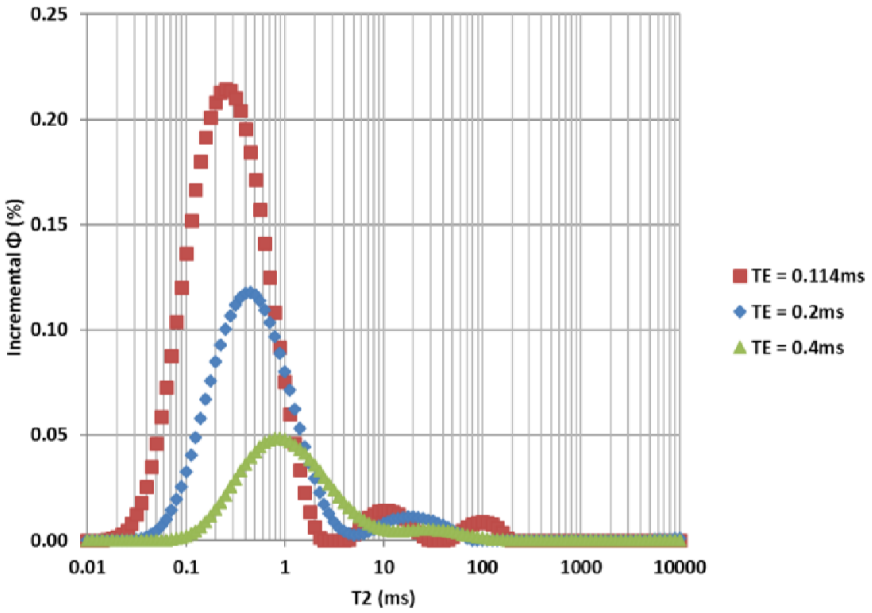

Figure 2.11: T2 spectra as function of inter echo spacing (TE) in shale. Note the reduction in apparent NMR porosity with increasing values of TE. (Tinni, 2017)

Ambient (35˚C) and elevated temperature (110˚C) NMR T2 and T1-T2 measurements conducted on twenty-six samples selected from a well in oil window of the Woodford shale. NMR T1 measurement using a sufficiently long polarization time would detect the entire porosity in a porous medium (Kleinberg, 1993). **Figure 2.12** shows the comparison of NMR T1 porosity (derived from NMR T1-T2 maps) and T2 porosity obtained on Woodford shales containing

preserved *in-situ* reservoir fluids, using an inter echo spacing (TE) of 0.114 ms. It is evident that T2 porosity is in close agreement with T1 porosity- the points mostly lie on the 1:1 line. This observation re-affirms our working assumption that echo spacing (TE=0.114 ms) is sufficiently short to capture the fast-relaxing components present in shale rocks.

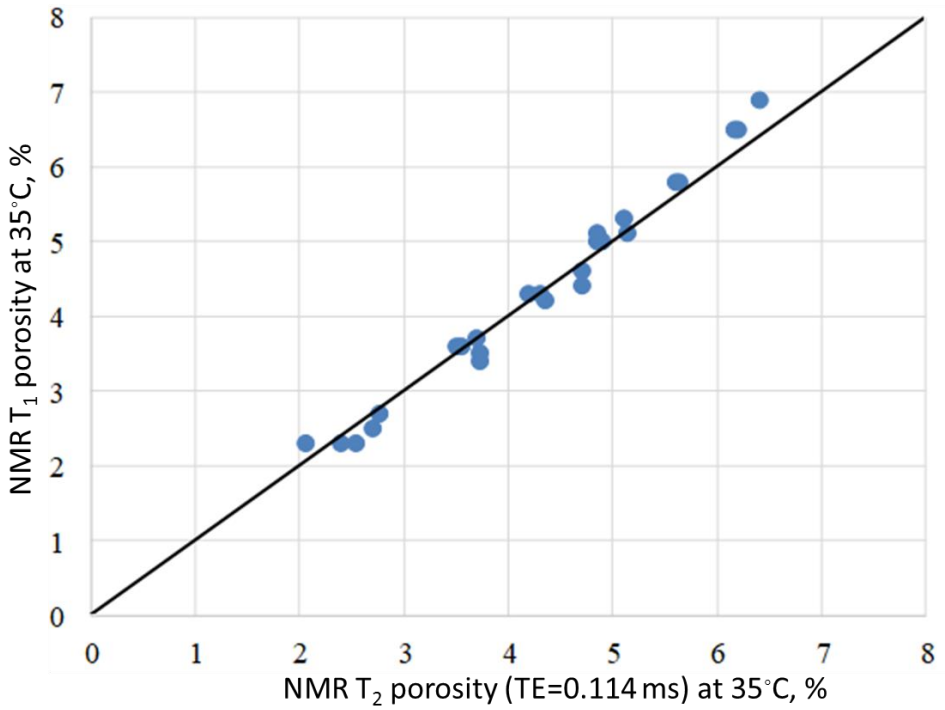

Figure 2.12: **In Woodford shale samples containing preserved reservoir fluids, data points lie closely on the 1:1 line when T_2 porosity captured using inter echo spacing (TE)=0.114 ms is compared against NMR T_1 porosity at ambient room temperature.**

2.6 Sample information

The samples in the study can be classified as follows:

a. Samples with no organic matter content: sintered silica glass, Berea sandstone and Tennessee sandstone.

b. Shale with low organic matter (OM) content: Utica (thermal maturity: condensate window), Barnett (gas window), Eagle Ford (gas window), Vaca Muerta (oil window). These samples were cleaned using Soxhlet extraction for four days using a toluene and methanol mixture solvent of 80:20 volume ratio.

c. Organic-rich shales: Wolfcamp (WC-x), Bakken. These samples were used in their native 'as-received' state.

d. Organic-rich shale with preserved state pore fluid: Woodford (WF-x).

In case of preserved samples, the fluid lost in evaporation was assumed to have density of pentane (n-C5).

The FTIR mineralogy, Total Organic Carbon (TOC) content and Source Rock Analysis derived parameters S1 and S2 are provided in **Table 1**.

Table 1: Properties of rock samples used in study (low OM content)

Sample Name	Sample ID	Qtz+Fd (wt %)	Total clay (wt %)	Total carbonate (wt %)	TOC (wt %)	S1 (mg HC/ g rock)	S2 (mg HC/ g rock)
Berea sandstone	BS	82	10	7	-	-	-
Tennessee Sandstone	TS	89	7	4	-	-	-
Utica-1	U1	1	2	90	0.1	0.3	0.5
Utica-2	U2	15	35	50	1.7	0.4	0.5

Utica-3	U3	22	68	9	0.6	0.3	0.9
Utica-4	U4	11	81	8	1.1	0.2	0.6
Vaca Muerta	VM	11	9	80	4.0	1.1	5.1
EF	EF	14	11	65	3.9	n.a.	n.a.
Barnett	Brn	30	41	21	1.6	0.29	0.78
Wolfcamp WC-xx419	WC-1	25	64	5	5.0	4.3	6.3
Wolfcamp WC-xx491	WC-2	23	58	15	3.1	2.1	1.1
Wolfcamp WC-xx550	WC-3	36	50	13	3.5	1.4	2.1
Bakken B1 xx439.65	B1	46	41	13	5.1	3.5	6.0
Bakken B2 xx654.8	B2	62	11	26	4.0	3.5	4.5
Bakken B3 xx657.7	B3	55	33	12	3.9	3.0	4.1
WF-1 (xx631 H3)	W-1	51	17	23	3.9	1.4	3.7
WF-2 (xx631 H2)	W-2	51	17	23	3.9	1.4	3.7
WF-3 (x608.9 H1)	W-3	47	24	29	3.5	0.9	2.4
WF-4 (x608.9 H2)	W-4	47	24	29	3.5	0.9	2.4
WF-5 (x584.4 H2)	W-5	67	11	5	5.1	2.0	4.9
WF-6 (x011.1)	W-6	80	13	2	2.0	0.7	3.6
WF-7 (x013.7)	W-7	n.a.	n.a.	n.a.	n.a.	n.a.	n.a.
WF-8 (x045.95)	W-8	58	37	3	6.2	2.9	12.1
WF-9 (x064.35)	W-9	66	20	7	6.3	2.8	12.6
WF-10 (x064.5)	W-10	64	20	7	6.3	n.a.	n.a.
WF-11 (x088.9)	W-11	65	19	7	5.5	3.2	10.9
WF-12 (x089.05)	W-12	n.a.	n.a.	n.a.	n.a.	n.a.	n.a.
WF-13 (x109.85)	W-13	58	30	6	6.5	3.0	12.6

WF-14 (x119.4)	W-14	56	25	17	5.0	1.8	8.3
WF-15 (x119.75)	W-15	56	25	17	n.a.	n.a.	n.a.
WF-16 (x159.65)	W-16	65	23	8	6.0	3.5	11.3
WF-17 (x139.35 H1)	W-17	56	23	15	5.6	1.9	9.4
WF-18 (x139.35 H2)	W-18	56	23	15	5.6	1.9	9.4
WF-19 (x160.7)	W-19	65	23	8	6.0	n.a.	n.a.
WF-20 (x185.45)	W-20	47	50	2	6.9	1.4	12.2
WF-21 (x150.55)	W-21	57	23	13	4.7	n.a.	n.a.
WF-22 (x150.65)	W-22	57	23	13	4.7	2.3	7.3
WF-23 (x185.8)	W-23	47	50	2	6.9	1.4	12.2

2.7: Sample preparation

2.7.1 Dry porous glass, Berea sandstone and dry shale

The samples were cleaned using solvent extraction, and dried for 48 hours under 25 mmHg vacuum at 120˚C prior to the heated NMR experiments. The samples are from Utica shale (condensate window) and Barnett and Eagle Ford (gas window). SRA analysis indicates that these samples contain negligible light and heavy hydrocarbon. Hence it is inferred that the fluid species detected by NMR is water. The NMR T2 spectra obtained are shown in the Appendix **Section A.1**. The $MnCl_2$ solution used as a paramagnetic dopant had a concentration of 75% v/v.

2.7.2 Shales partially saturated with oil and brine

Partial saturation was achieved by first immersing samples in hexadecane at 100°C in a vacuum oven. Following hexadecane immersion, the samples were saturated with brine at 5000 psi and then with hexadecane at 7000 psi. The saturation was achieved by using a Teledyne ISCO™ syringe pump attached to a HiP® pressure vessel as shown in **Figure 2.14**. The evaporative loss in the heating process is contributed to the loss of brine while heating. To correct for the lost fluid, the porosity associated with the lost mass was added to the porosity measured at elevated temperature. Saturation of all the rock samples with a single fluid (hexadecane or brine) was achieved using the same apparatus. The NMR T2 spectra obtained are shown in Appendix **Section A.2** and **Section A.3**.

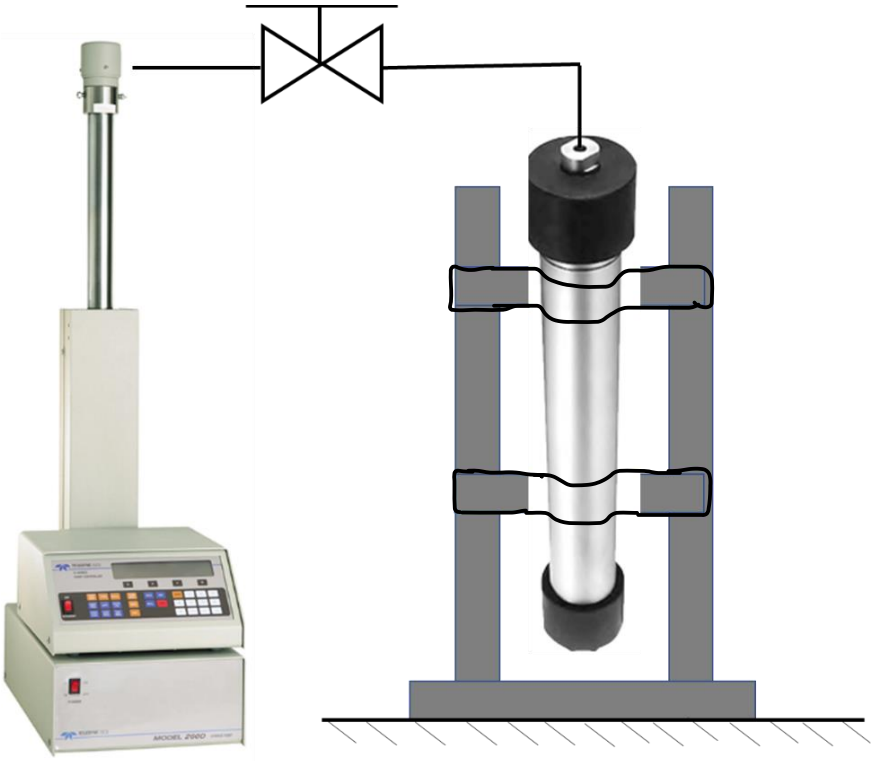

Figure 2.13: Schematic of the apparatus used for saturation in present study. The syringe pump (left) is used to pressurize the steel sample holder (right) using dodecane as pressurizing medium.

2.7.3 Wax saturated shales

Selected cleaned and dried shale samples were immersed in molten wax and kept in a VWR 1410 vacuum oven maintained at 150°C and 25 mmHg vacuum for 2 days to saturate with wax. Pore volume of shale samples prior to saturation was determined using high pressure helium pycnometry. The weight change of the sample after wax saturation was recorded; this is converted in a wax volume and saturation knowing the density. The NMR T2 spectra obtained are shown in Appendix **Section A.4**. The calculated wax saturations are shown in **Table 2**.

Table 2: Calculated wax saturation by weight of samples saturated with paraffin wax

Sample ID	Calculated wax saturation (%)
U1	61
EF	60
VM	44
WC-2	70

2.7.4 Shales containing preserved *in-situ* reservoir fluids

Ambient (35°C) and elevated temperature (110°C) NMR T2 and T1-T2 measurements were conducted on twenty-six samples selected from a well in oil window of Woodford shale. The

shales were received as preserved in wax. A film of volatile oil was observed on peeling off the wax. The vaporizing behavior suggested that fluid was most likely pentane. This fluid was most likely expelled from the rock with depressurization. As expected, there was an evaporative loss upon heating the shale samples. The weight of sample before and after heating was recorded and the lost weight considered to be of pentane (ρ =0.626 g/cc). To correct for the lost fluid, the porosity associated with the lost mass was added to the porosity measured at elevated temperature.

3: Results and Discussions

3.1 Dry porous glass and Berea sandstone

In reporting our study on the effect of temperature on NMR response of porous media, we begin with an analysis of results of heating NMR experiments on dry sintered glass and Berea sandstone.

Figure 3.1 Shows the T2 spectra at ambient and elevated temperature for a porous glass plug.

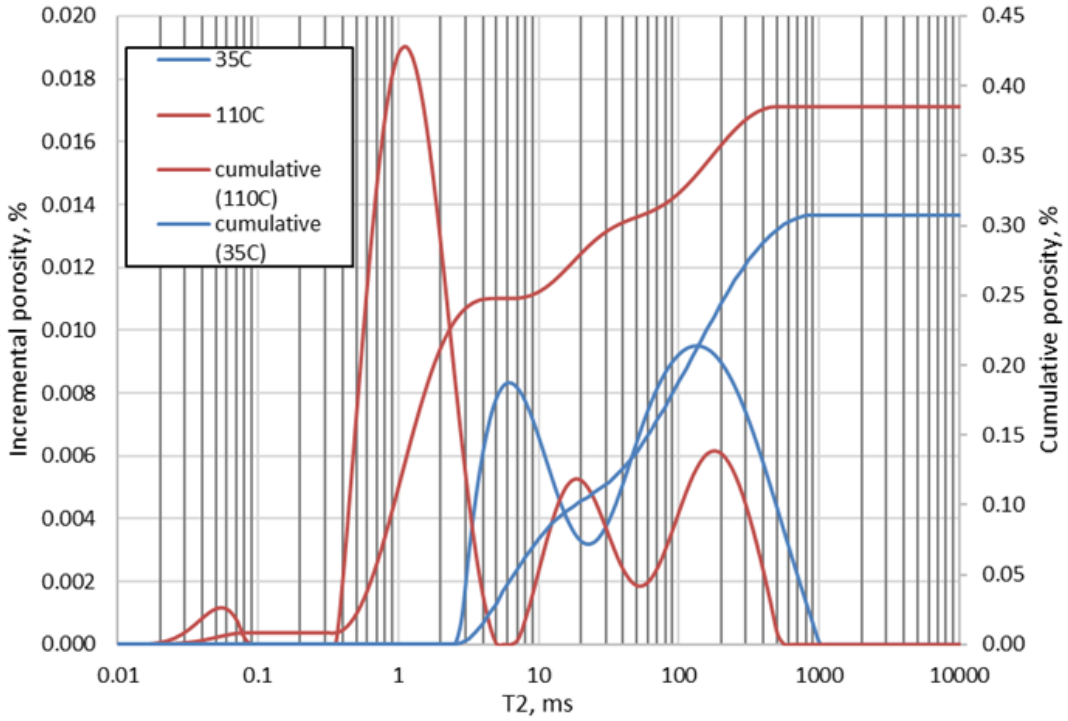

Figure 3.1: NMR T2 spectra of dry porous glass plug at ambient (blue) and elevated temperature (red).

As temperature increases from 35°C to 110°C, an increase in measured porosity is observed along with a marked change in the shape of the T2 spectrum. The two peaks near 5 ms and 100

ms shift towards longer times and a third peak, centered near 1 ms emerges. The only conceivable source of hydrogen nuclei in a dry porous glass plug could be water species on hydrophilic mineral surfaces that have been mobilized due to heating.

The amount of fluid detected by NMR in dry samples is minute. In order to gain confidence in the measurement of water on dry samples, the sample is saturated with concentrated $MnCl_2$ solution (75% v/v). Since manganese chloride is miscible in water, addition of paramagnetic dopant $MnCl_2$ solution 'kills' the water NMR signature. **Figure 3.2** shows the T2 spectra of dry and concentrated $MnCl_2$solution saturated Berea sandstone sample at room temperature. Instead of a complete absence of NMR signal, we do observe a signal which indicates the 2 MHz NMR captures some fast-relaxing water which is hosted on grain surface of the sandstone sample.

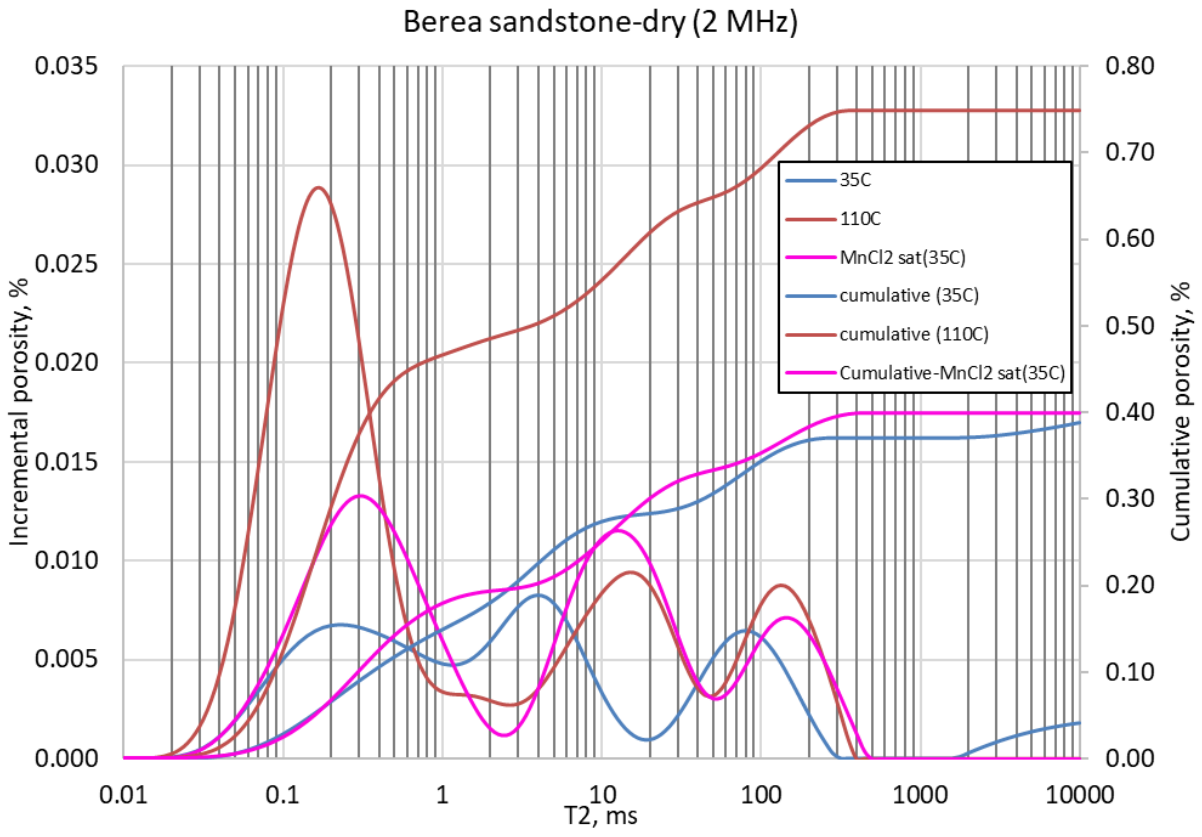

Figure 3.2: 2 MHz NMR T2 spectra of Berea sandstone dry (blue) saturated with 75 wt % Manganese Chloride solution (pink) at ambient and elevated temperature. The T2 spectrum at elevated temperature is shown by red.

The Berea sandstone sample shows a behavior similar to the porous glass plug described in previous section. The T2 spectra shift towards longer T2 times with the emergence of a third peak at very low T2 (~0.5 ms). The net NMR porosity increases with temperature in all cases. This behavior suggests that dry rocks do contain water species which are rather strongly adsorbed to mineral surfaces but become mobilize on heating. These species appear to be immoveable.

3.2 Conventional rocks and sintered glass plug saturated with hexadecane

Figure 3.3 shows the comparison of 2 MHz NMR porosities measured at ambient and elevated temperature on sandstone and limestone rock samples saturated either with oil or brine. The dataset includes the information obtained from literature (Godefroy, 2001 and Latour et al., 1992) as well as measurements obtained in present study-which includes sintered glass plug, Berea sandstone and Tennessee sandstone saturated with n-hexadecane at 5000 psi. These samples represent conventional rocks. T2 spectra of conventional rocks and porous glass are shown in the Appendix **Section A.1**.

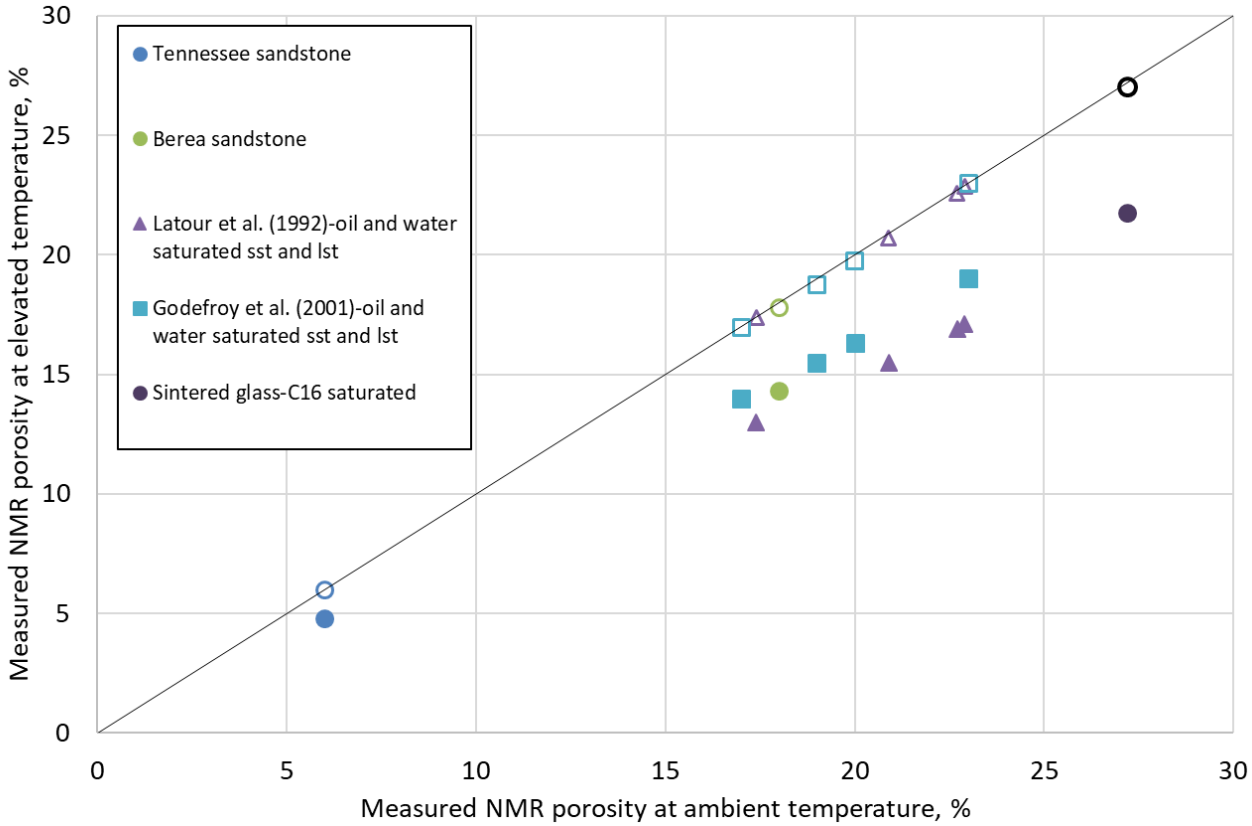

Figure 3.3: **Comparison of 2 MHz NMR porosity at ambient and elevated temperature for a range of conventional rocks. Measured data are represented by solid symbols and corresponding Curie corrected porosity is shown by hollow symbols. Note that Curie corrected porosity falls on 1:1 line showing that Curie correction works well for conventional rocks.**

Also included is the data on sintered glass at dry and hexadecane saturated states. From a fluid storage perspective, the sintered glass sample provides a 'base case' of the pore system in a rock. There is no micro-porosity, a homogenous quartz matrix, zero organic matter content and zero clay content.

The samples used here encompass the saturation states possible in conventional rocks like sandstone and limestone. All the points of the dataset systematically lie beneath the 1:1 lie and once corrected (represented by hollow symbols) by the inverse temperature approach, lie on the 1:1 line. This observation demonstrates that the inverse temperature correction works satisfactorily for conventional rocks when saturated with oil and brine.

The characteristics of pore systems in shales are shown in Sections 1.1 through Section 1.6. The pore system of shale differs from that of conventional rocks. Key differences include:

a. pore sizes orders of magnitude smaller conventional rocks,

b. presence of more than one type of wettability component,

c. porosity hosted by organic matter and clays, and

d. presence of pore-lining and/or pore-hosting heavy hydrocarbon.

3.3 Shale

Figure 3.4 and **Figure 3.5** show a comparison of measured 2 MHz NMR porosity (TE=0.114 ms) of shales at 35°C and 110°C.

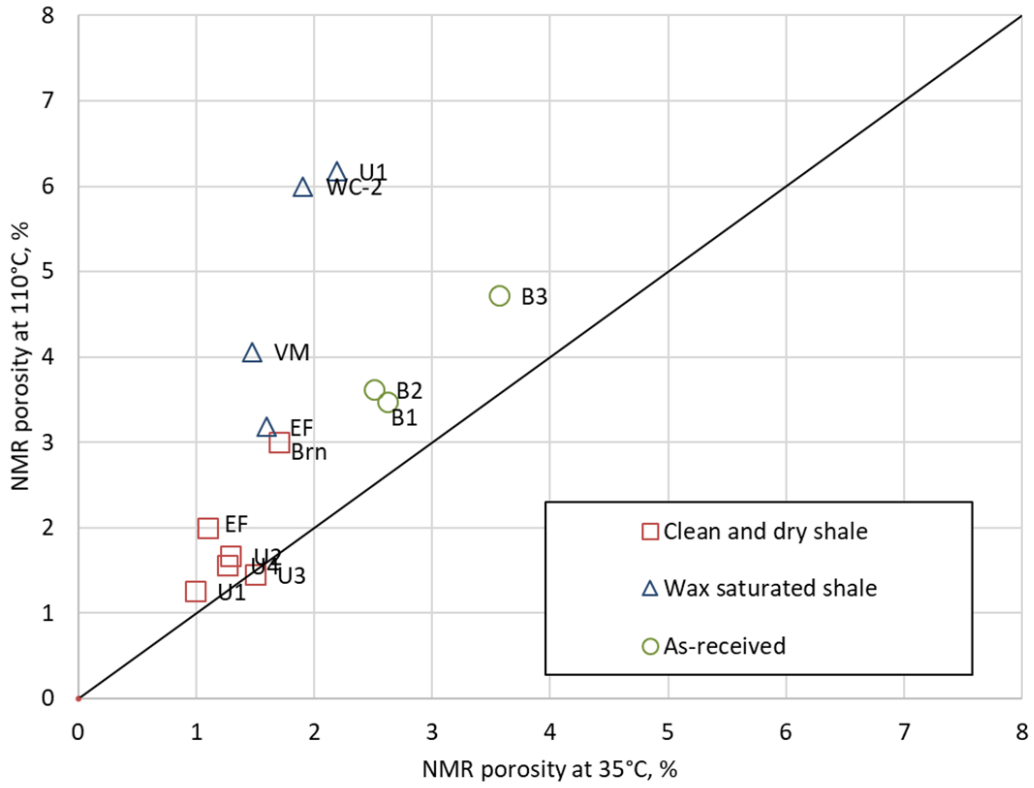

Figure 3.4: **Comparison of 2MHz NMR porosity of shales measured at 35°C and 110°C in measured in saturation states: square represents cleaned and dried shale samples, triangles represent wax saturated shales and circles represent 'as received'.**

The observation from **Figure 3.4** is that all samples show an increase in porosity with increase in temperature. All data points lie above the 1:1 line. This is a marked departure from the NMR behavior of conventional rocks like sandstone (see Figure 3.4). The shale samples include cleaned and dried, as received, and wax saturated. The cleaned and dried shale samples contain

negligible heavy hydrocarbon; the increase in porosity at elevated temperature is due to influx of additional hydrogen nuclei caused by mobilization of adsorbed water from hydrophilic surfaces of the rock. NMR porosity of shales saturated with hydrocarbon is shown in **Figure 3.5.** Mostly the samples lie on or above the 1:1 line.

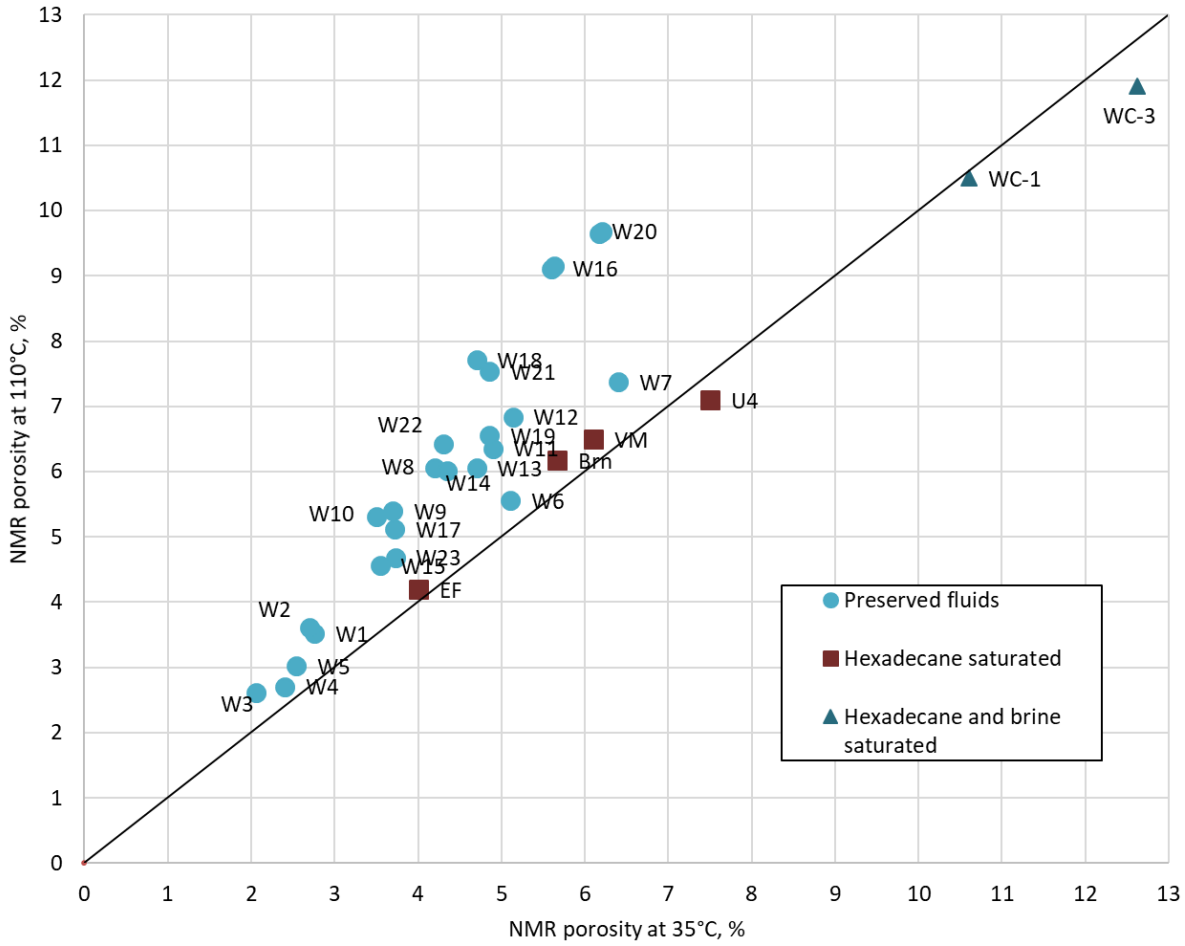

Figure 3.5: **Comparison of 2MHz NMR porosity of saturated shales measured at 35˚C and 110˚C; circles represent samples containing preserved *in-situ* reservoir fluids (Woodford shale), squares represent shales saturated with hexadecane, and triangles represent shales saturated with brine and hexadecane.**

To study the effect of temperature on the NMR response of shale samples saturated with heavy hydrocarbon, NMR T2 spectra were obtained for a suite of as-received Bakken shale samples a Wolfcamp shale sample saturated with paraffin wax. The results are shown in **Figure 3.6**.

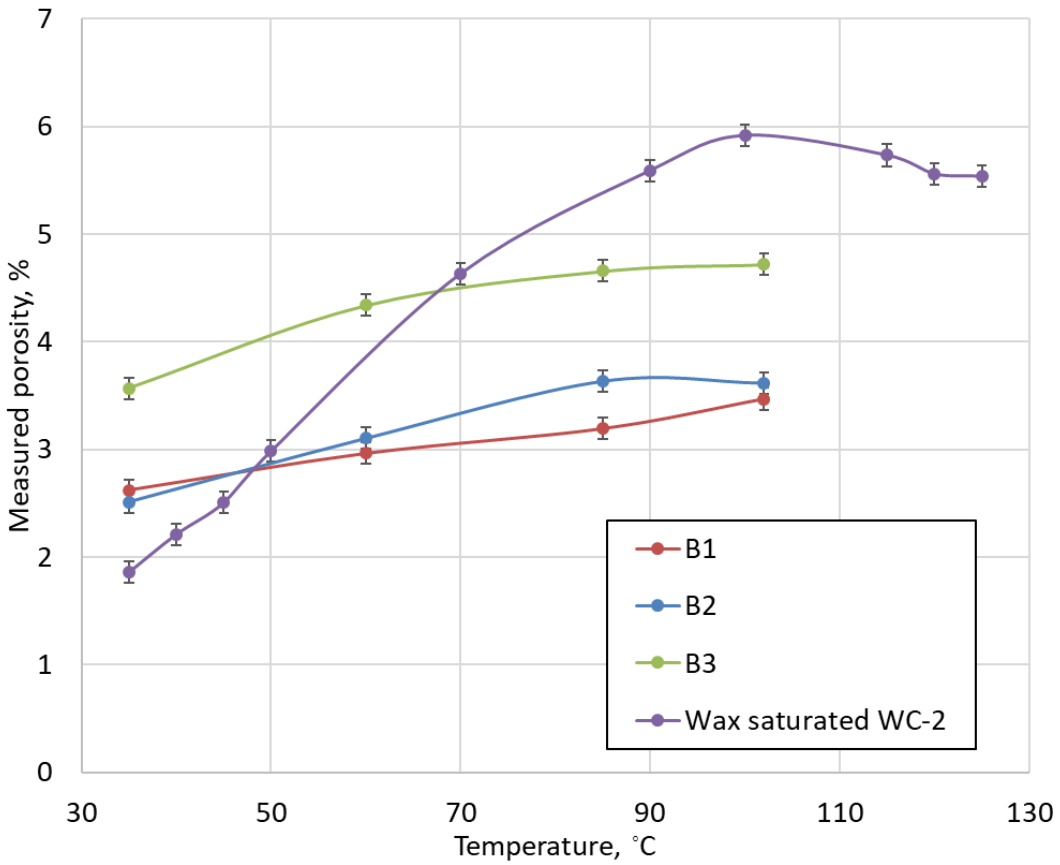

Figure 3.6: **Measured NMR porosity of a wax saturated Wolfcamp sample and as-received Bakken shale samples as function of temperature. The variation of porosity in these samples may be treated as linearly dependent on temperature between 35˚C and 105˚C.**

The peak near 100˚C suggests that all wax has melted and is visible to NMR. This observation suggests that the confined wax appearance temperature in shale is close to 100˚C. As temperature rises further, there is decrease in net magnetization of sample due to Curie effect. Till 100˚C, the increase in number of nuclei due to melting outweighed the decrease in magnetization due to the

Curie effect of temperature. We also note that between the temperatures 35°C and 110°C, the porosity depends, to a good approximation, linearly on temperature (**Figure 3.6**). Above 110°C, as no more nuclei are introduced in the system the overall magnetization decreases with increase in temperature. This decrease with temperature agrees well with the decrease predicted by Curie correction. (**Figure 3.7**). The T2 spectra are shown in section A4.4.

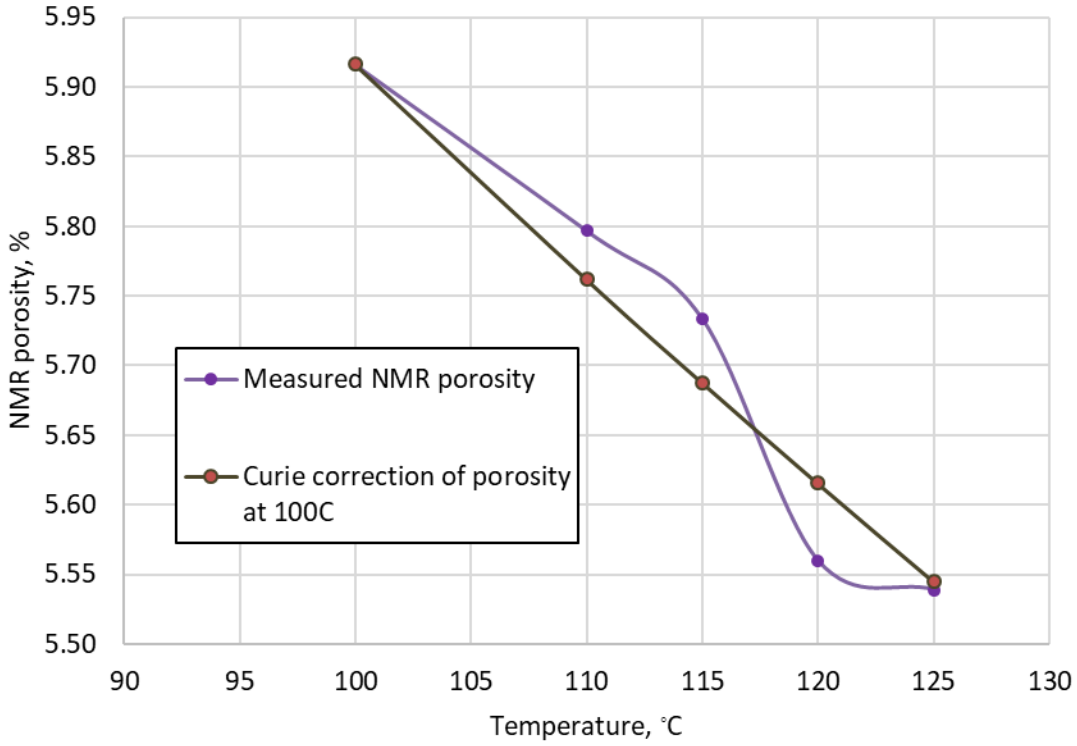

Figure 3.7: **NMR porosity for wax saturated sample WC-xx491 at temperature above 100°C, there is close agreement between measured NMR porosity and porosity predicted by Curie correction. This observation indicates that no additional hydrogen atoms are entering beyond 100°C and the magnetization of fixed number of nuclei decreases predictably with temperature increase.**

We note that in general, the NMR porosity of shale samples increases with increase in temperature, a marked difference from the NMR behavior of conventional rocks like sandstone and limestone. **Figure 3.8** shows the variation of NMR porosity of samples as a function of temperature.

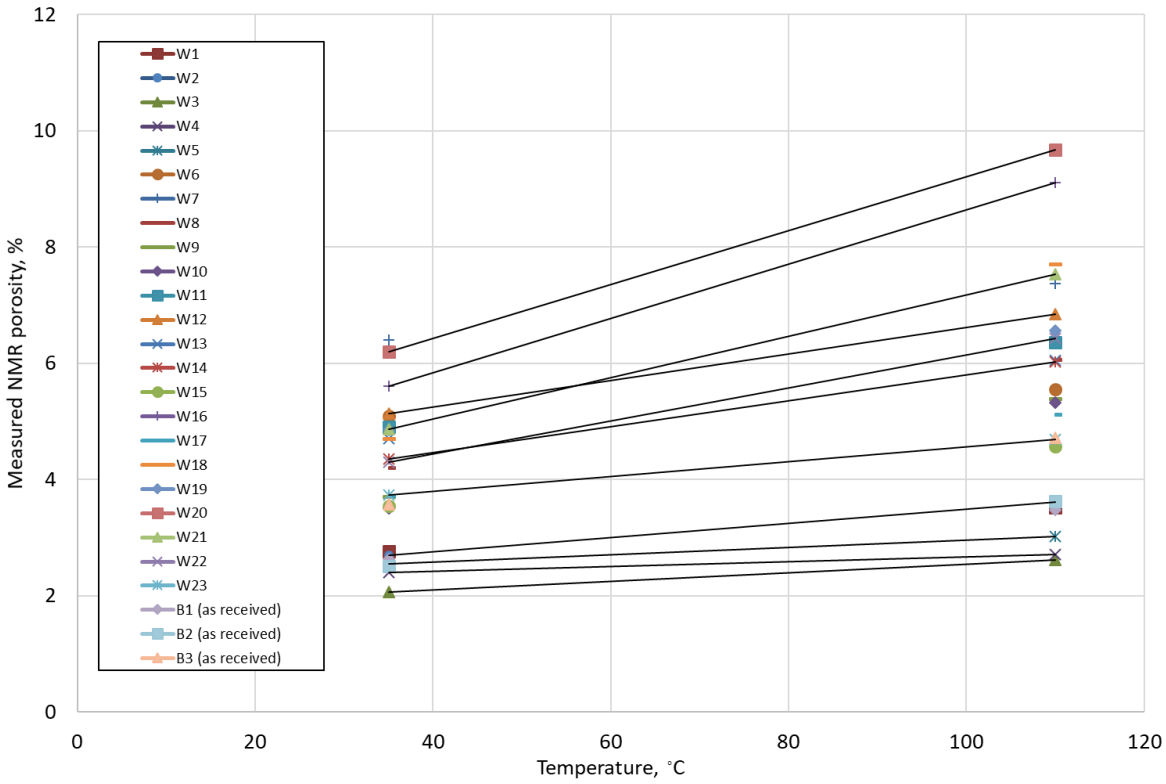

Figure 3.8: **Measured NMR porosity of shale samples containing preserved fluids and in as-received state. In all cases, the porosity increases with temperature.**

The dependence of change in NMR porosity on the amount of heavy hydrocarbon present is shown in **Figure 3.9**. As demonstrated previously, paraffin wax can be considered a part of S2 component in a pyrogram. The increase in NMR porosity at elevated temperature has a very strong dependence on the amount of heavy hydrocarbon present in rock.

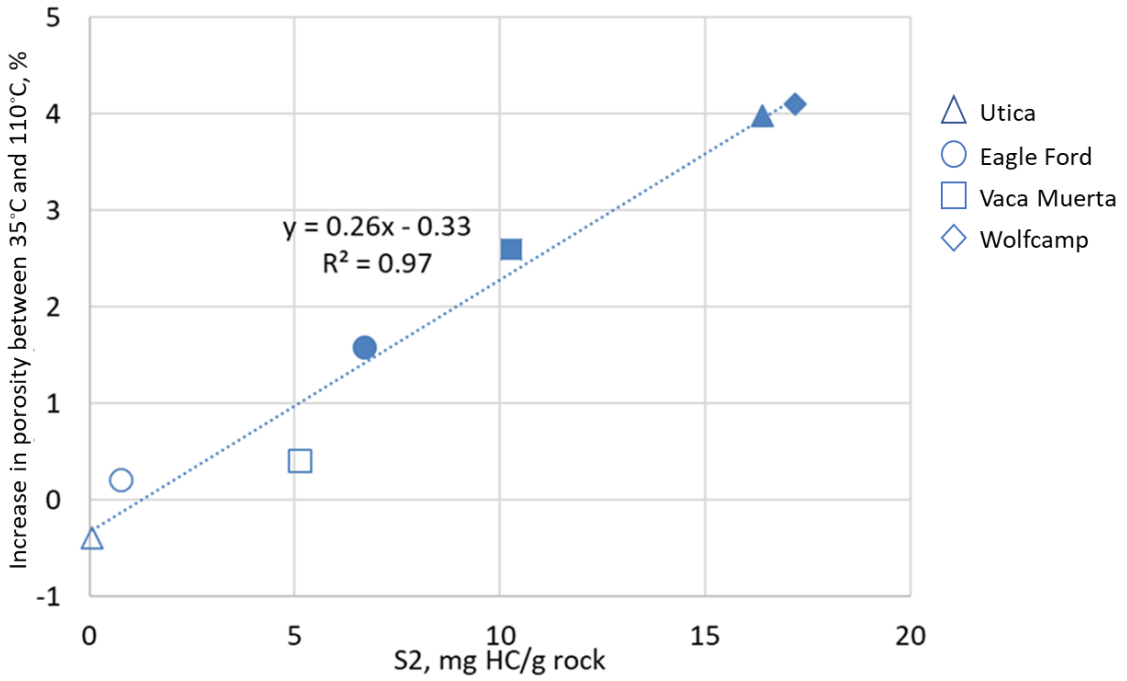

Figure 3.9: **Measured change in NMR porosity as function of S2, where the S2 corresponds to paraffin wax content. A strong dependence on heavy hydrocarbon is observed. Hollow points represent cleaned state samples and solid points represent wax saturated samples.**

3.2 Temperature correction for NMR porosity measurement in shales

The tests described in this study cover dry shales and shales saturated with different kinds of fluid: oil (hexadecane), heavy hydrocarbon (wax), partially with oil and brine, and preserved *in-situ* reservoir liquid.

It is shown that the approach used for predicting NMR porosity in conventional rocks fails when applied to shales. Instead of porosity decreasing as predicted by the inverse temperature relation, shales display an increase with temperature or stay constant. The present study shows

experimentally that heavy hydrocarbon and adsorbed water can contribute to NMR porosity at elevated temperature.

For conventional rocks like sandstone and limestone saturated with fluids like oil or brine, temperature dependence of measured NMR porosity can be expressed as:

$$\phi_{HT} = \phi_{RT}\left(\frac{T_R}{T_H}\right) \qquad \text{……..……..…(eq 3.1)}$$

Where ϕ_{RT} and ϕ_{HT} denote porosity at room temperature and high temperature in Kelvin, respectively. T_R and T_H represent ambient and elevated temperatures in Kelvin, respectively. This is the application of the Curie correction. The correction only depends on the two temperatures under consideration. As shown experimentally, the temperature dependent NMR behavior of shales is markedly different from conventional rocks. As temperature increases, the measured NMR porosity either increases or stays constant. It has been shown through previous examples (**Figure 3.4 and 3.5**) that both adsorbed water as well as heavy hydrocarbon can contribute to NMR porosity at elevated temperature.

At ambient room temperature signal from these nuclei is not detected but is embedded in the initial NMR porosity. We also note that in case of melting of heavy hydrocarbon, the dependence of porosity on temperature up to 110°C can be modelled, to a good approximation, as linear. Hence, in order to modify the temperature correction for shales we introduce two additional terms in equation 3.2. The modified equation to predict NMR porosity at elevated temperature for shales can be expressed as:

$$\phi_{HT} = \phi_{RT}\left(\frac{T_R}{T_H}\right) + C$$

$$\text{where } C = \phi_{RT}\left(1 - \frac{T_R}{T_H}\right) + (0.26 \text{ X } S_2)\left(\frac{T_H - 308}{348}\right) \quad \text{……...eq 3.2}$$

ϕ_{RT} and ϕ_{HT} represent NMR porosity measured at ambient (room) and elevated (high) temperature, respectively. T_R and T_H represent ambient and elevated temperature in Kelvin. S_2 is a surrogate for heavy hydrocarbon present in rock, and is expressed in

milligrams of hydrocarbon present in one gram of rock sample. This equation is valid in temperatures ranging from room temperature to 110°C.

The first term accounts for the decrease in magnetization of the starting number of nuclei due to the increase in temperature. The second term represents the addition of nuclei from residual fluids present in rock. This term depends on the magnitude of initial NMR porosity at room temperature and accounts for mobilization of residual water on mineral hosted surfaces at elevated temperatures. The last term accounts for the addition of nuclei from the melting of heavy hydrocarbon present in rock. The model may be visualized as shown in **Figure 3.10**. S_2 is defined as the amount of heavy hydrocarbon in mg HC/g of rock which volatilizes between 350°C and 500°C. It increases linearly with temperature between 35°C and 110°C.

Equation 3.2 reduces to

$$\phi_{HT} = \phi_{RT} + (0.26 \text{ X } S_2)\left(\frac{T_H - 308}{348}\right) \quad \text{…….eq 3.3}$$

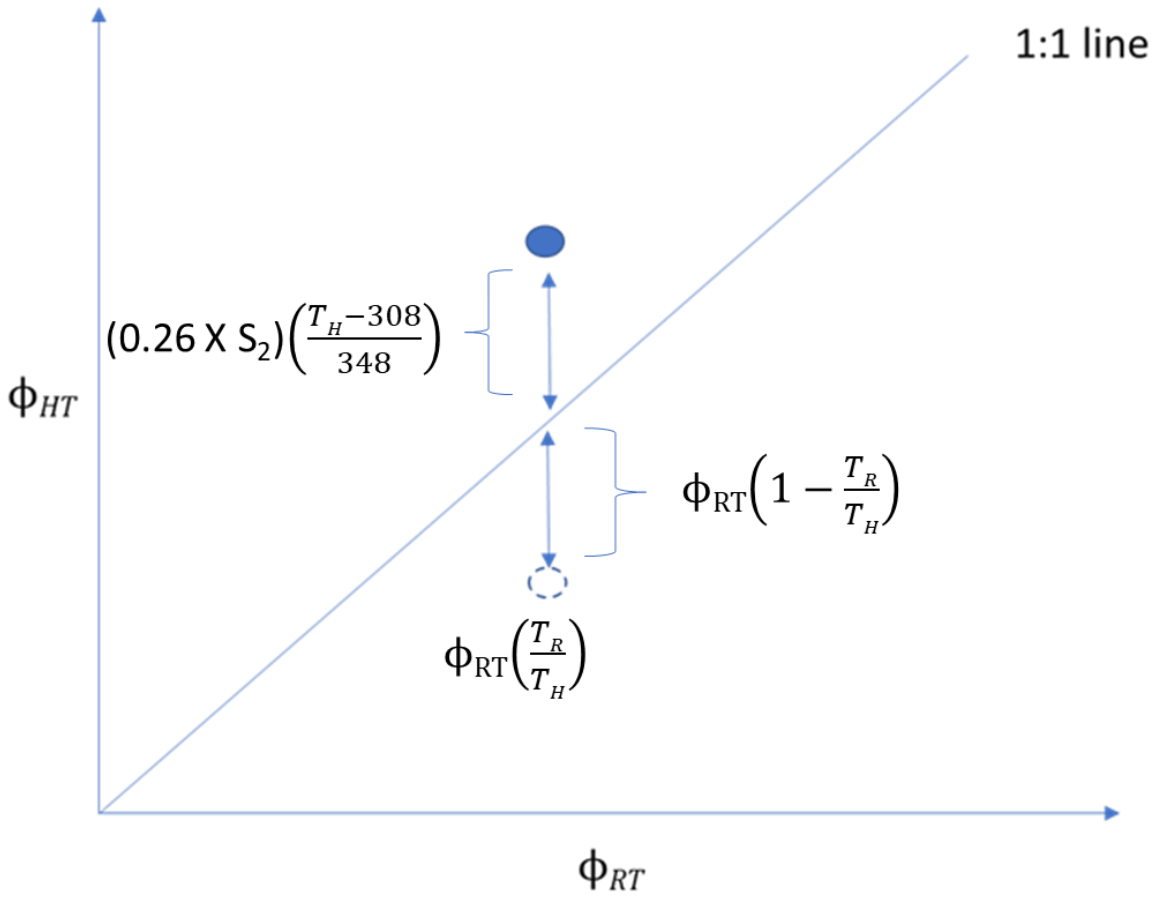

Figure 3.10: Model for NMR porosity correction for shales. ϕ_{RT} and ϕ_{HT} represent NMR porosity measured at ambient (room) and elevated (high) temperature, respectively. T_R and T_H represent ambient and elevated temperature in Kelvin. Dotted circle shows conventional rock response and solid circle shows shale response.

To test the validity of equation 3.3, it is applied to predict the elevated temperature porosity of a dataset consisting of shale samples containing preserved *in-situ* reservoir liquids (suite of Woodford shale samples), shales re-saturated with hexadecane, and shales re-saturated with both brine and hexadecane. The comparison of predicted and measured NMR porosity at 110°C is shown in **Figure 3.11**.

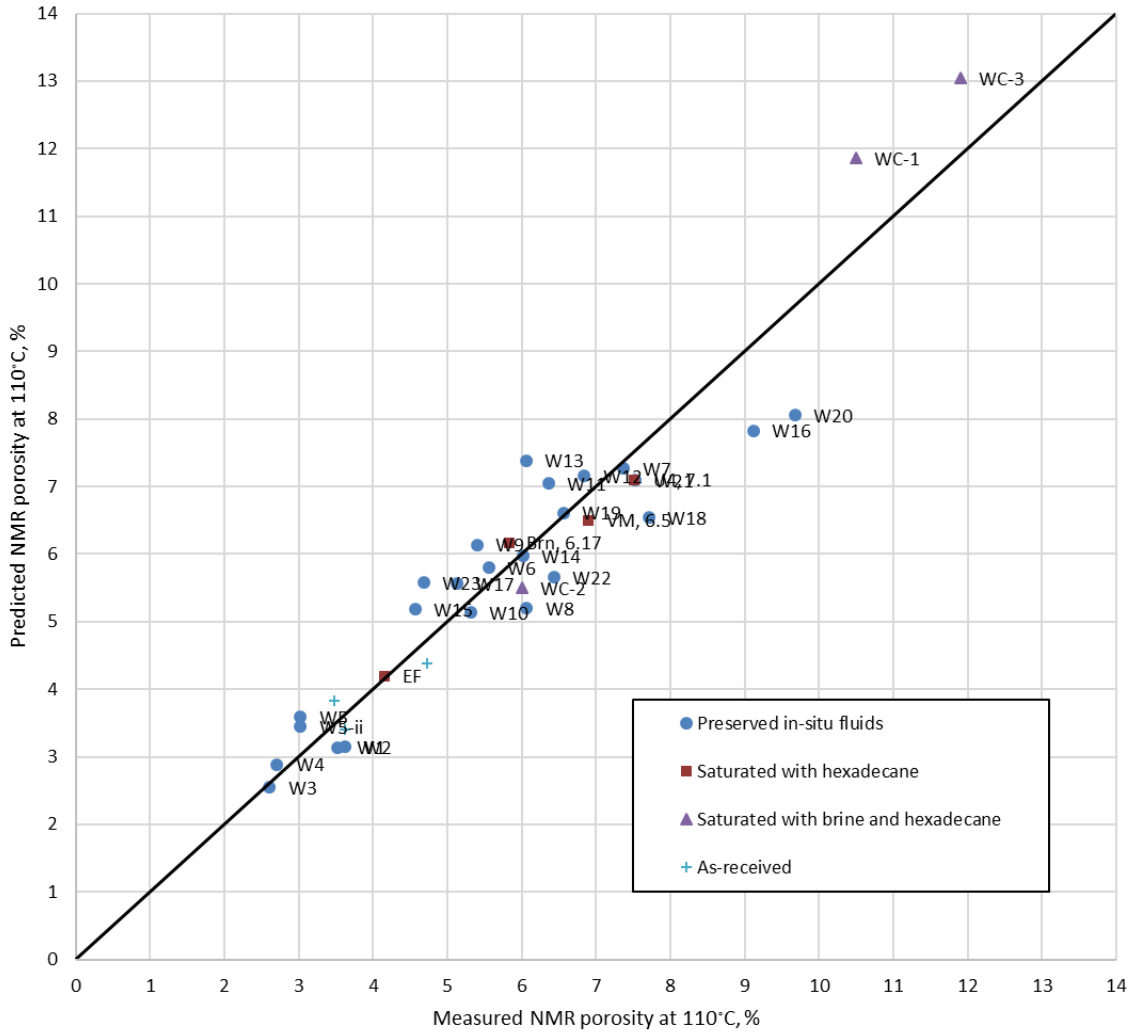

Figure 3.11: Comparison of predicted and measured NMR porosity at elevated temperature (110 ˚C) using the proposed temperature correction (equation 3.3).

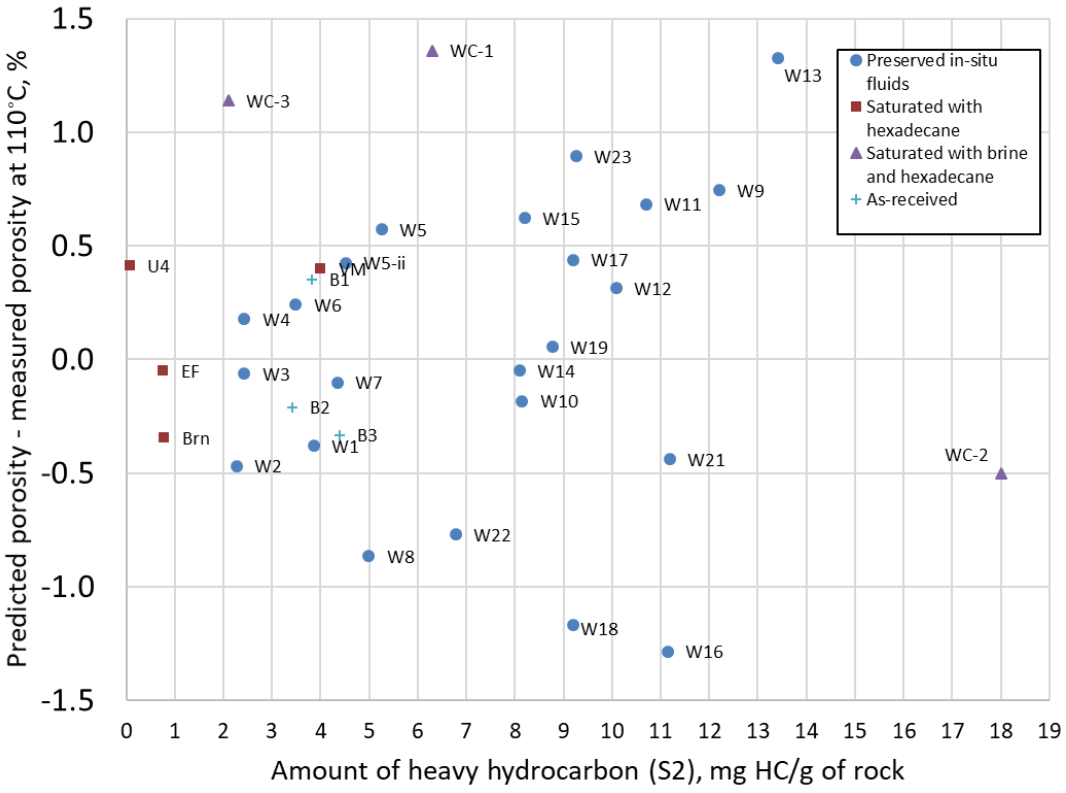

Figure 3.12: **Difference between predicted and measured 2 MHz NMR porosity at elevated temperature (110°C) over a range of S2 values found in unconventional resource shales. The data set consists of shales in various saturation states. More than two-thirds of the samples show a difference of less than 0.5 %**.

Figure 3.12 shows the difference between predicted values and measured values at 110°C. More than two-thirds of the samples show a difference of less than 0.5 %.

Application of equation 3.3 requires an a-priori knowledge of the heavy hydrocarbon content and lithology, i.e. whether the rock is shale or conventional sandstone/limestone.

3.5 Interpreting porosity-temperature data for shale

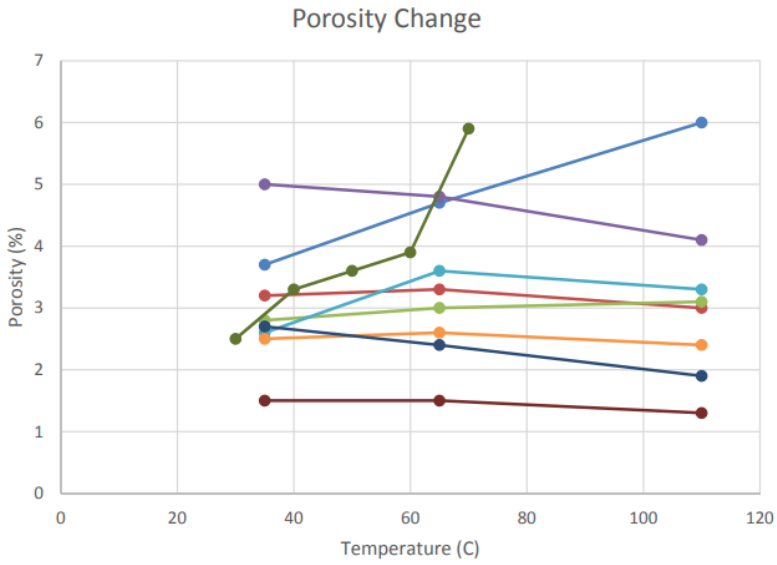

Figure 3.13: **Effect of temperature on NMR T2 porosity of 'as-received' shale samples (Veselinovic et al., 2017).**

With the proposed model of NMR porosity at elevated temperature, I now attempt to explain the behavior of shale rocks in Veselinovic et al.'s (2017) dataset of measured 2 MHz NMR porosities of as-received shales at 35˚C and 110˚C (**Figure 3.13**). Samples indicated by brown and dark blue line likely contain negligible heavy hydrocarbon and water species, and therefore, show a predictable decrease of porosity with increase in temperature. The samples which show an increase in porosity going from 35˚C to 65˚C behave that way due to mobilization of water and/or heavy hydrocarbon. After a certain temperature beyond 65˚C, no additional nuclei enter the system due to heating, and from thereon, the measured porosity decreases with temperature. The two samples indicated by green and light blue line are most likely contain significant amounts of heavy hydrocarbon, whose mobilization with temperature explains the monotonic increase in measured NMR porosity.

3.6 Combined effect of temperature and echo spacing

NMR logging tools use inter echo spacings (TE) much longer than 0.114 ms – ranging from 0.2 ms to 0.6 ms. **Figure 3.14** shows the measured NMR porosities at 110˚C for sample EF saturated with hexadecane. The measurements are made using a range of inter echo spacing (TE) which encompasses both laboratory and field-based values.

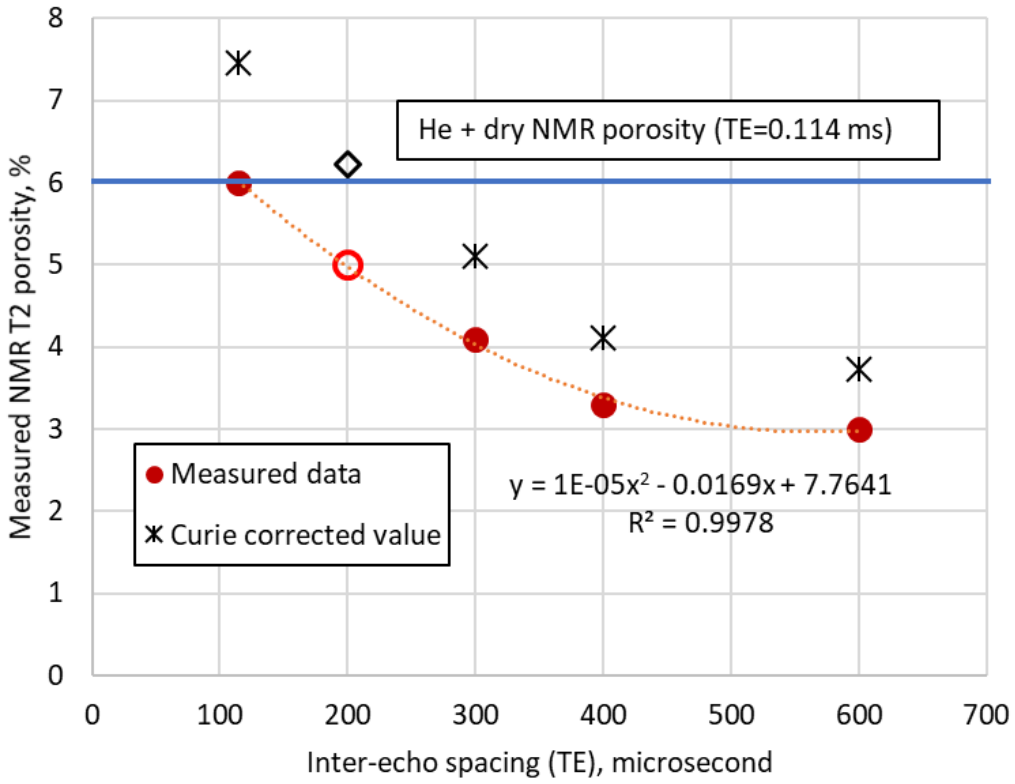

Figure 3.14: Dependence of measured NMR T_2 porosity on inter echo spacing (TE) of NMR tools. Sample is Eagle Ford shale plug saturated with hexadecane at 5000 psi. Red points show data at 110˚C and black points represent the temperature corrected NMR porosity using Curie correction. The blue line indicates the sum of helium porosity and NMR porosity on cleaned and dried plug. Hollow points show the estimated porosity values at TE=0.2 ms which is the minimum TE in current generation NMR logging tools.

We observe a decrease in measured NMR porosity with increasing inter echo spacing, as expected in shales (Tinni et al., 2017). At TE =0.114 ms, the NMR porosity at 110°C is equal to the sum of high-pressure helium porosity on plug and dried NMR porosity – considered as the total porosity in petrophysical workflows. Therefore, the application temperature correction in present generic form would lead to overestimation of NMR porosity.

At present the smallest inter-echo spacing (TE) used by NMR tools in oilfield is 0.2 ms. We observe from **Figure 3.14** that an increase in TE from 0.114 ms to 0.2 ms results in reduction of measured NMR porosity by 1 % (hollow red circle). However, application of Curie correction (shown to be invalid for shales) results in an overestimated value (indicated by black, hollow diamond) which fortuitously closely agrees with the total porosity obtained from the sum of high-pressure helium porosity on plug and dried NMR porosity. This observation may explain the agreement of NMR porosity obtained by tools with TE longer than 0.114 ms. with core-derived porosity obtained in the laboratory.

4: Summary and conclusions

The objective of study was to understand low field (2 MHz) NMR behavior of shales at ambient (35°C) and elevated temperature (110°C) and atmospheric pressure. To this end, NMR measurements were made on shales and other porous media having a variety of saturation states: dry and saturated with different reservoir liquids – oil, brine and heavy hydrocarbon (replicated in this study by paraffin wax). All measurements were made using an inter-echo spacing (TE) of 0.114 millisecond and frequency of 2.2 MHz. Rock samples under study include sintered silica glass, Berea and Tennessee sandstones, and shales in different configurations as described previously in experiments section. Based on present study, we draw the following conclusions:

1. Temperature correction of NMR porosity applied to conventional rocks (e.g. sandstone and limestone) does not fit observations made on shales. Contrary to an observed decrease in measured NMR porosity in conventional rocks with increase in temperature, shales shown an increase of measured NMR porosity with temperature.

2. The deviation in the behavior is attributed to the complex microstructure of shales. The mobilization of heavy hydrocarbon and absorbed water on mineral surfaces at elevated temperature are thought to contribute to NMR porosity.

3. A revised equation to predict NMR porosity of shales at elevated temperature is proposed. The revised equation has two additional temperature dependent terms which represent addition of NMR signal from mobilized heavy hydrocarbon and adsorbed liquids:

$$\phi_{HT} = \phi_{RT}\left(\frac{T_R}{T_H}\right) + C$$

$$\text{where } C = \phi_{RT}\left(1 - \frac{T_R}{T_H}\right) + (0.26 \text{ X } S_2)\left(\frac{T_H - 308}{348}\right)$$

which reduces to $\phi_{HT} = \phi_{RT} + (0.26 \text{ X } S_2)\left(\frac{T_H - 308}{348}\right)$

ϕ_{RT} and ϕ_{HT} represent NMR porosity measured at ambient (room) and elevated (high) temperature, respectively. T_R and T_H represent ambient and elevated temperature in Kelvin. S_2 is a surrogate for heavy hydrocarbon (C20+) present in rock, and is expressed in milligrams of hydrocarbon present in one gram of rock sample. This equation is valid at temperatures ranging from 35°C to 110°C.

4. The revised equation was used to predict the elevated temperature porosity of data set of 31 samples which included shales containing preserved in-situ reservoir liquids (twenty-four samples), shales saturated with n-hexadecane (four samples) and shales saturated partially by brine at 5000 psi and n-hexadecane at 7000 psi (three samples). In two-thirds of samples studied, the difference between measured and predicted NMR porosity at 110°C is less than 0.5 %.

5. Current generation NMR logging tools in the field use TE ≥ 0.2 ms which results in underestimation of porosity in shales. Application of current form of correction (Curie correction) to shale porosity at elevated temperature, increases the porosity to a value which incidentally matches well with values derived from industry-prevalent laboratory workflows.

5: References

1. Anand, V., Hirasaki, G., and Fleury, M., 2008, NMR Diffusional Coupling: Effects of Temperature and Clay Distribution. *Petrophysics*, vol. 49, number 4, 362-372.

2. Ballard, B. 2007. Quantitative Mineralogy of Reservoir Rocks Using Fourier Transform Infrared Spectroscopy. SPE 113023, presented at the Annual Technical Conference and Exhibition, Anaheim, California, 11-14 November 2007.

3. Barakat, A.J., Pel, L., and Adan, O.C.G., 2018. One-Dimensional NMR Imaging of High-Temperature First-Drying in Monoliths, *Appl Magn Reson* (2018) 49:739-753.

4. Chen, S., Zhang, G., Kwak, H., Edwards, C.M., Ren, J., and Chen, J., 2004.Laboratory Investigation of NMR Crude Oils and Mud Filtrates Properties in Ambient and Reservoir Conditions. SPE-90553-MS, presented at the SPE ATCE held in Houston, Texas, 26-29 September

5. Coates, G.R., Xiao, L., and Prammer, M.G., 1999. *NMR Logging Principles and Applications*. Halliburton Energy Services.

6. Coman, R., and Tietjen, H., 2017, Temperature correction in NMR Logging While Drilling. SPE-185334, presented at SPE Oil and Gas Conference held in Mumbai, India, April 2017.

7. Cowan, B.P., 1997. *Nuclear Magnetic Resonance and Relaxation*. Cambridge University Press.

8. Curtis, M.E., Sondergeld, C.H. and Rai, C.S., 2013. Investigation of the microstructure of shales in the oil window. URTeC – 1581844, presented at the Unconventional Resources Technology Conference held in Denver, Colorado, 12-14 August 2013.

9. Dang, S.T., Sondergeld, C.H. and Rai, C.S., 2017. Interpretation of NMR Response to Hydrocarbons as a Function of Fluid Composition and Temperature, SCA-201-015. Presented at the International Symposium of the Society of Core Analysts held in Vienna, Austria, 27-30 August 2017.

10. Gannaway, G., 2014. NMR Investigation of Pore Structure in Gas Shales, SPE-173474-STU, presented at the SPE Annual Technical Conference and Exhibition held in Amsterdam, The Netherlands, 27-29 October 2014.

11. Godefroy, S., Fleury, M., Deflandre, F. and Korb, J.P., 2001. Temperature effect on NMR surface relaxation. SPE-71700, presented at presented at the Annual Technical Conference and Exhibition held in New Orleans, Louisiana, 30 September-3 October 2001.

12. Griffiths, P.R. and De Haseth, J.A., 2007. *Fourier Transform Infrared Spectrometry, 2nd edition*, Wiley Publications.

13. Gupta, I., Rai, C., Tinni, A. and Sondergeld, C., 2017. Impact of Different Cleaning Methods on Petrophysical measurements. *Petrophysics*, Vol. 58 (6): 613-621.

14. Hyberts, S. G., Robson, S. A., & Wagner, G. (2012). Exploring signal-to-noise ratio and sensitivity in non-uniformly sampled multi-dimensional NMR spectra. *Journal of biomolecular NMR*, *55*(2), 167–178. doi:10.1007/s10858-012-9698-2

15. Karastathis, A., 2007. Petrophysical Measurements on a Tight Gas Shale. Master's Thesis, University of Oklahoma, Norman, Oklahoma.

16. Kausik, R., Fellah, K., Rylander, E., Singer, P.M., Lewis, R.E., and Sinclair, S.M., 2016. NMR Relaxometry in Shale and Implications for Logging, *Petrophysics*, Vol. 57, No. 4, p 339-350.

17. Kausik,R., Fellah, K., Feng, L., Freed, D., and Simpson, G., 2018. Temperature Dependence of 2D NMR T1-T2 Maps of Shale. Presented at the SPWLA 59th Annual Logging Symposium held in London, UK, June2-6, 2018.

18. Kleinberg, R.L., Straley, C., Kenyon, W.E., Akkurt, R., and Farooqui, S.A., 1993. Nuclear Magnetic Resonance of Rocks: T_1 vs. T_2. SPE-26470, presented at the Annual Technical Conference and Exhibition, Houston, Texas, 3-6 October 1993.

19. Kleinberg, R.L. and Vinegar, H.J., 1996. NMR Properties of reservoir fluids. The Log Analyst, November-December 1996.

20. Lai, J., Wang, G., and Fan X., 2018. Three-dimensional quantitative fracture analysis of tight gas sandstones using industrial computed tomography. Scientific Reports Volume 8, number 1.

21. Latour, L.L., Kleinberg, R.L. and Sezginer, A., 1992. Nuclear magnetic resonance properties of rock at elevated temperatures. *Journal of Colloid and Interface Science*, Volume 150, number 2.

22. Lessenger, M., Merkel, D., Medina, R., Ramakrishna, S., Chen, S., Balliet, R., and Knackstedt, M.,2015.. Subsurface Fluid Characterization Using Downhole and Core NMR T1-T2 Maps Combined with Pore-Scale Imaging Techniques. SPWLA Journal.

23. Martinez, A., 2000. Nuclear Magnetic Resonance Relaxation Measurements in Shales. Master's thesis, Texas Tech University, Lubbock, Texas (May 2000).

24. Odusina, E., Sondergeld, C. H. and Rai, C.S., 2011. An NMR Study on Shale Wettability. Presented at the Canadian Unconventional Resources Conference, Calgary, Alberta, Canada, 15–17 November. SPE147371-MS. http://dx.doi.org/10.2118/147371-MS.

25. Ramakrishnan, T.S., Fordham, E.J., Venkataramanan, L., Flaum, M. and Schwartz, L.M., 1999. New Interpretation Methodology based on Forward models for Magnetic Resonance in Carbonates. Paper MMM, presented at SPWLA 40th Annual Logging Symposium, May 30-June 3, 1999.

26. Romero-Sarmiento, M. and Fleury, M., 2016. Characterization of shales using T1–T2 NMR maps. Journal of Petroleum Science and Engineering, 137 (2016), 55–62.

27. Rylander, E., Singer, P., Jiang, T., Lewis, R., McLin, R. and Sinclair, S., 2013. NMR T_2 Distributions in the Eagle Ford Shale: Reflections on pore size. SPE-164554, presented at the Unconventional Resources Technology Conference held in The Woodlands, Texas, 10-12 April 2013.

28. Simpson, G. A., Fishman, N. S., and Hari-Roy, S., 2018.. New Nuclear Magnetic Resonance Log T2 Cut-Off Interpret Parameters for the Unconventional Tight Oil of the Bakken Petroleum System Using 2-D NMR Core Laboratory Measurements on Native State and Post-Cleaned Core Samples. Society of Petrophysicists and Well-Log Analysts.

29. Singer, P.M., Rylander, E., Jiang, T., McLin, R., Lewis, R.E. and Sinclair, S.M., 2013. 1D and 2D NMR Core-Log Integration in Organic Shale. SCA 2013-018, presented at the Society of Core Analysts Symposium held in Napa Valley, California, 2013.

30. Sondergeld, C. H., and Rai, C. S., 1993. A New Exploration Tool: Quantitative Core Characterization. *Pure and Applied Geophysics* 141: 249-268.

31. Sondergeld, C., Tinni, A., Rai, C., and Besov, A., 2016. NMR Considerations in Shale Evaluation. Society of Petrophysicists and Well-Log Analysts. Presented at the SPWLA 57th Annual Logging Symposium held in Reykjavik, Iceland June 25-29, 2016.

32. Straley, C., 1995. Investigation of The Structure of Porous Media. PhD dissertation, The University of Delaware. UMI: 9540564.

33. Straley, C., 2002. A Mechanism for the Temperature dependence of the relaxation rates in carbonates. SCA 2002-27, presented at the Society of Core Analysists Symposium held in Monterey, California, 2002.

34. Sulucarnain, I., Sondergeld, C. H. and Rai, C.S., 2012. An NMR Study of Shale Wettability and Effective Surface Relaxivity. Presented at the Canadian Unconventional Resources Conference, Calgary, Alberta, Canada, 30 October–1 November. SPE-162236-MS.

35. Tinni, A., Sondergeld, C. and Rai, C., 2014. NMR T_1-T_2 Response of Moveable and non-Moveable Fluids in Conventional and Unconventional Rocks. SCA 2014-A105. Presented at the International Symposium of the Society of Core Analysts held in Avignon, France, 8-11 September 2014.

36. Tinni, A., Sondergeld, C. and Rai, C., 2017. Investigation of 2 MHz NMR Measurements Sensitivity to Moveable, Bound and Structural Water in Shales. Presented at the SPWLA 58th Annual Logging Symposium held in Oklahoma City, Oklahoma, June 17-21, 2017.

37. Tissot, B.P. and Welte, D.H., 1984. *Petroleum Formation and Occurrence, 2nd edition*. Springer-Verlag.

38. Veselinovic, D., Green, D. and Mike, D., 2017. NMR at different temperatures to evaluate shales. URTeC – 2671166, presented at the Unconventional Resources Technology Conference held in Austin, Texas, 24-26 July,2017.

39. Winkler, M., Freeman, J.J., Quint, E., and Caputi, M. ,2006. Evaluating Tight Gas Reservoirs with NMR – The Perception, The Reality and How to Make it Work. Presented at the SPWLA 47th Annual Logging Symposium, Veracruz, Mexico, 4-7 June, SPWLA-2006-BB.

40. Yang, Z. and Hirasaki, G., 2008. NMR Measurement of bitumen at different temperatures, *Journal of Magnetic Resonance* vol. 192 (2008), 280–293.

41. Ying, R., Saulnier, L., and Rondeau-Mouro, C., 2011. Films of Arabinoxylans and beta-Glucans Extracted from Cereal Grains: Molecular Motions by TD-NMR. *Carbohydrate Polymers*, 86(2011), 812-822

6: Appendix

Section A.1: NMR T2 spectra Tennessee sandstone and porous glass plug

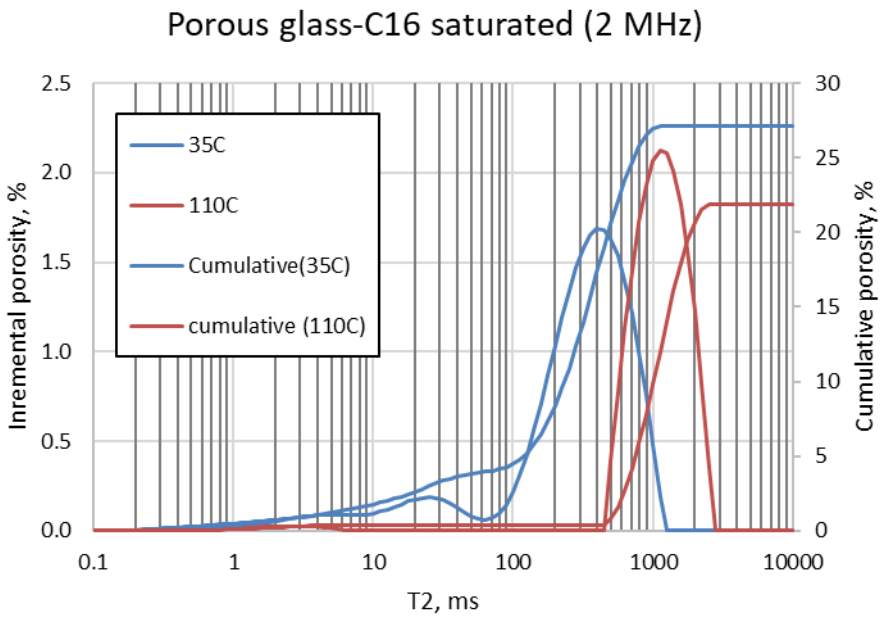

Figure A1.1: 2 MHz NMR T2 spectra of sintered glass plug saturated with n-hexadecane

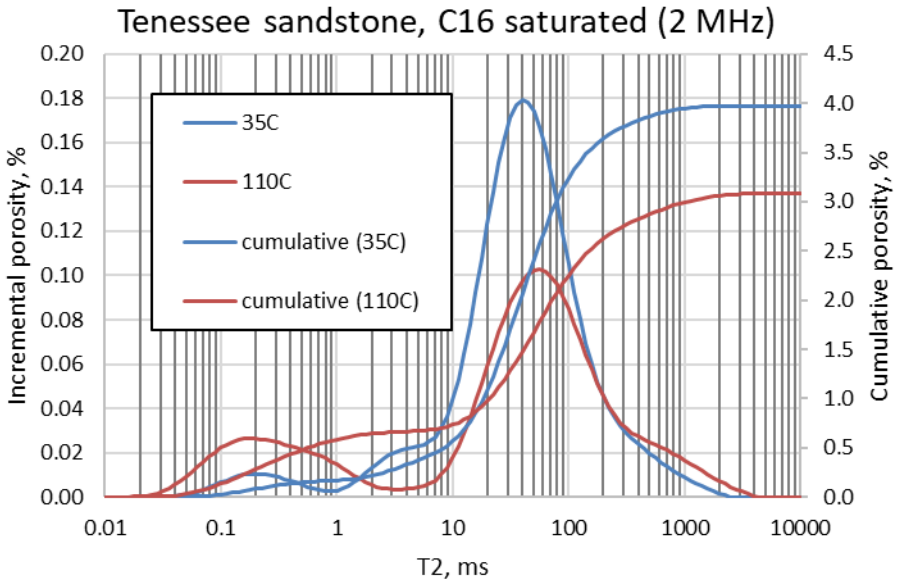

Figure A1.2: 2 MHz NMR T2 spectra of Tennessee sandstone saturated with n-hexadecane

Section A.2: Dry shales

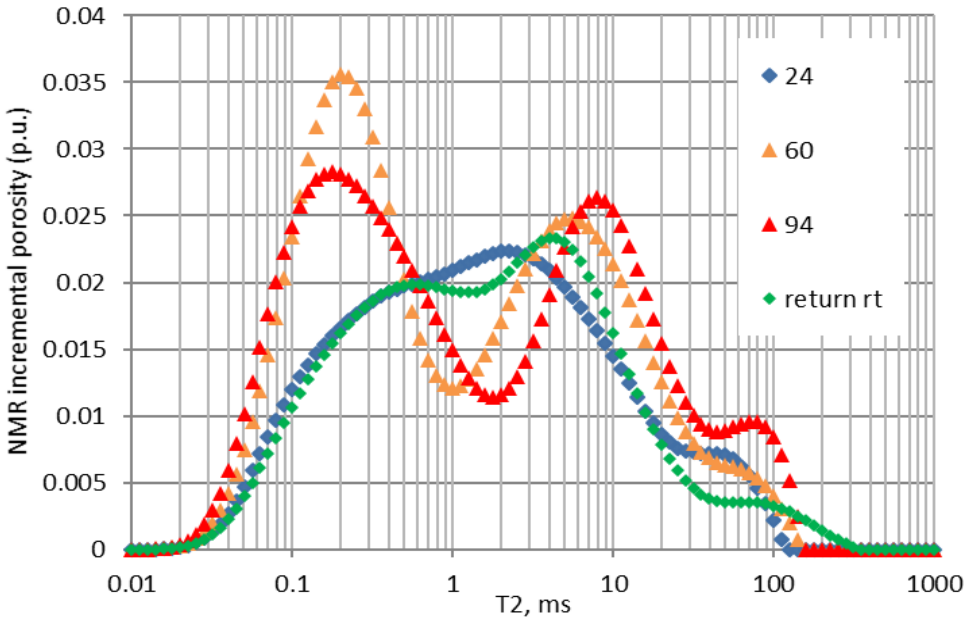

Figure A2.1: 2 MHz NMR incremental T2 spectra of Utica shale sample U1.

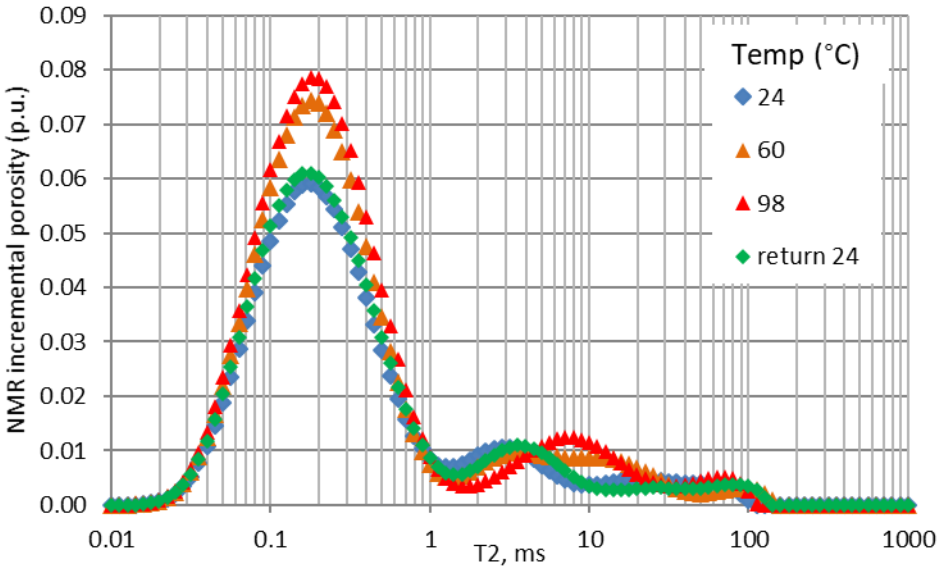

Figure A2.2: 2 MHz NMR incremental T2 spectra of Utica shale sample U2

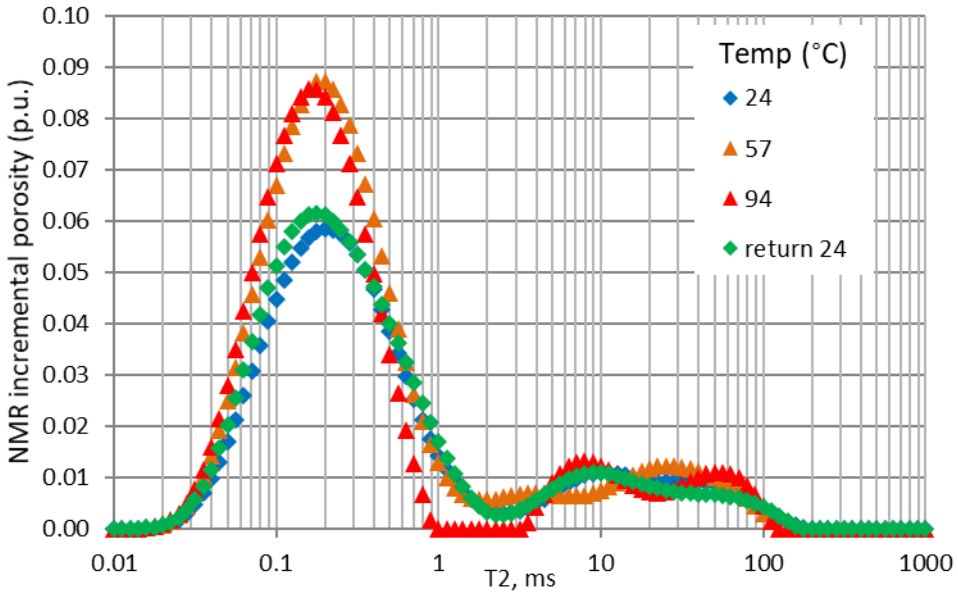

Figure A2.3: 2 MHz NMR incremental T2 spectra of Utica shale sample U3.

Section A.3: cleaned shale re-saturated with n-hexadecane at 5000 psi.

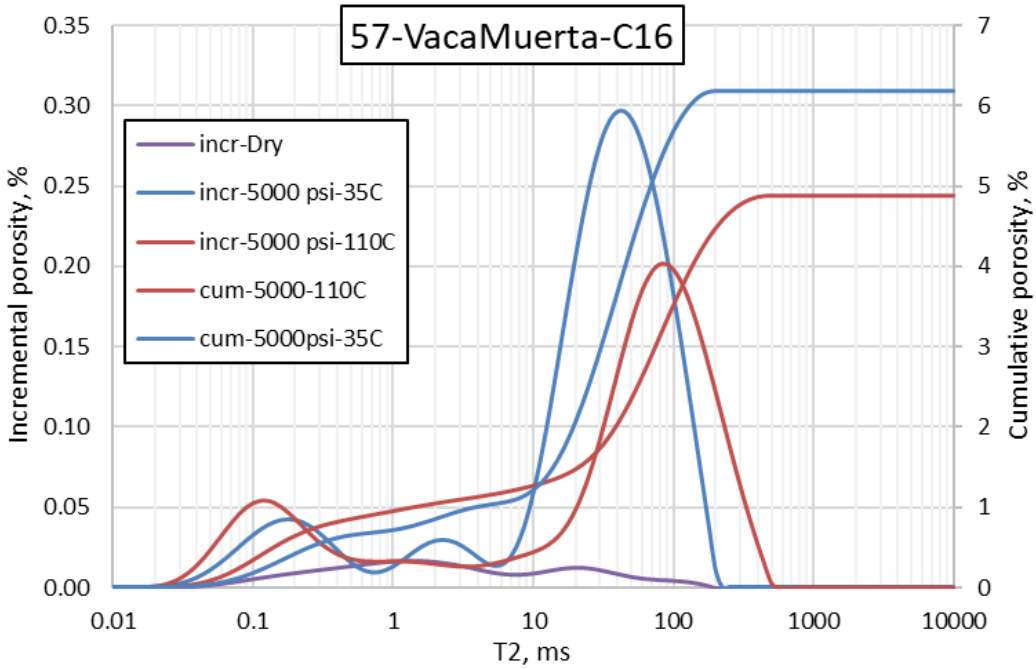

Figure A3.1: 2 MHz NMR incremental T2 spectra of Vaca Muerta shale saturated with hexadecane.

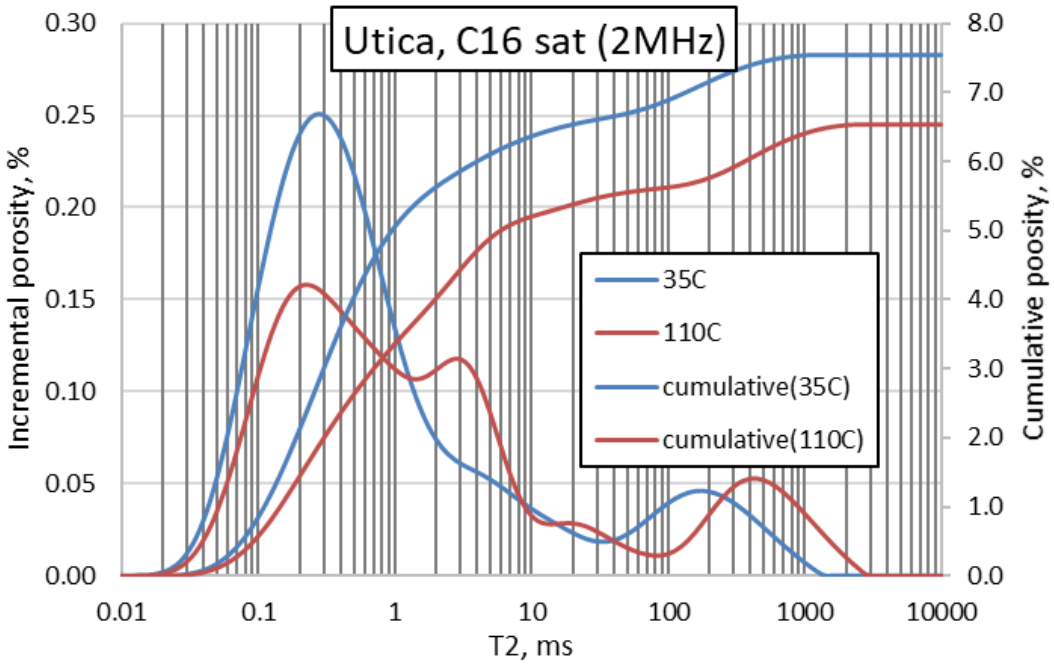

Figure A3.2: 2 MHz NMR incremental T2 spectra of Utica shale saturated with hexadecane.

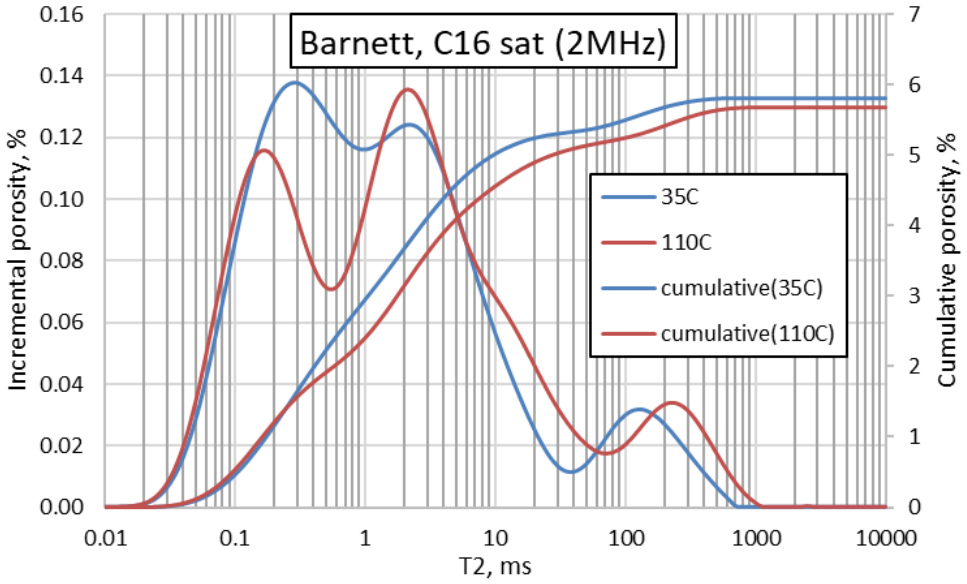

Figure A3.3: 2 MHz NMR incremental T2 spectra of Barnett shale saturated with hexadecane.

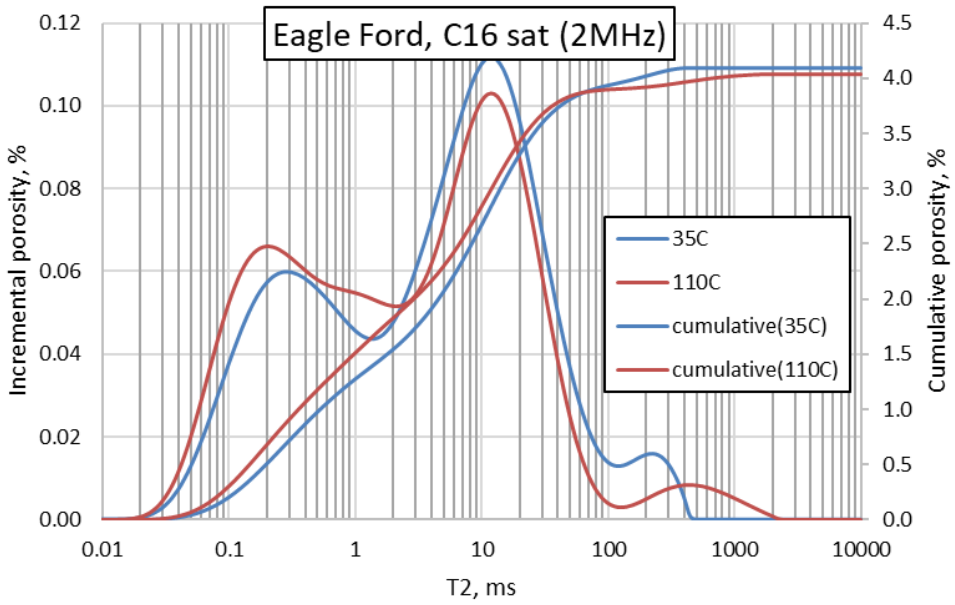

Figure A3.4: 2 MHz NMR incremental T2 spectra of Eagle Ford shale saturated with hexadecane.

Section A.4: NMR incremental T2 spectra of shales saturated with paraffin wax

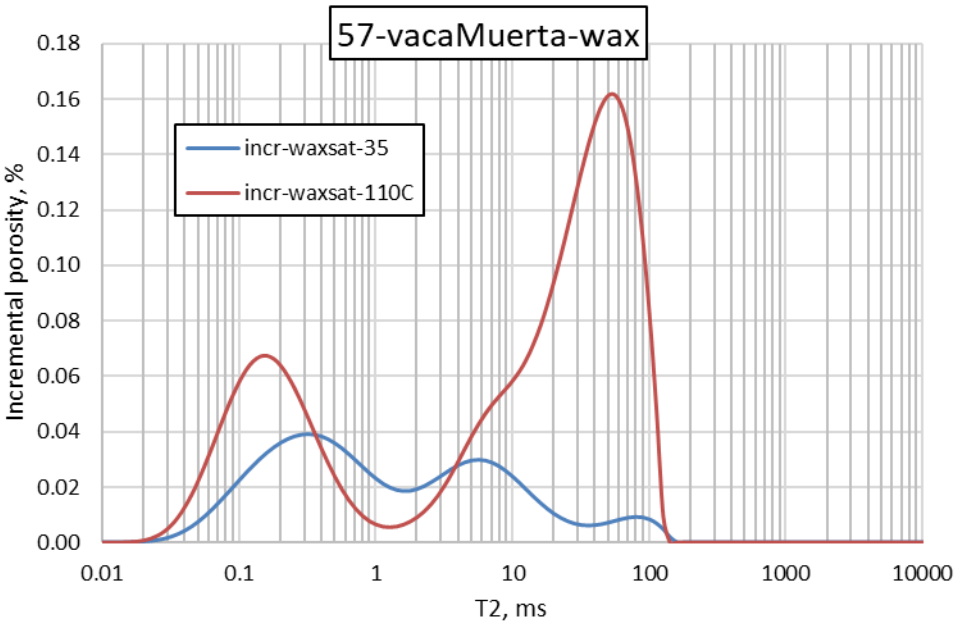

Figure A4.1: 2 MHz NMR incremental T2 spectra of Vaca Muerta shale saturated with paraffin wax.

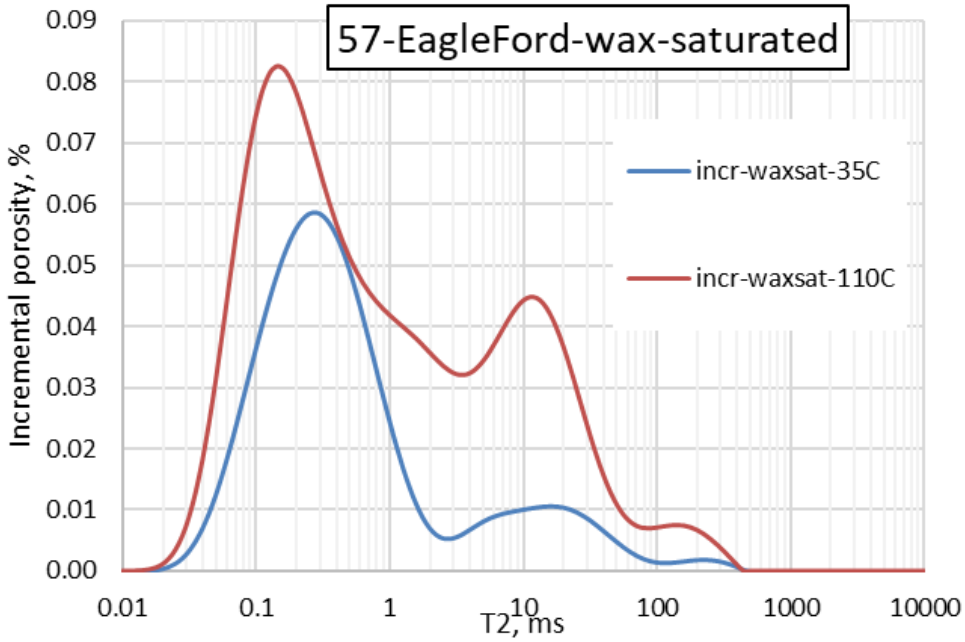

Figure A4.2: 2 MHz NMR incremental T2 spectra of Eagle Ford shale saturated with paraffin wax.

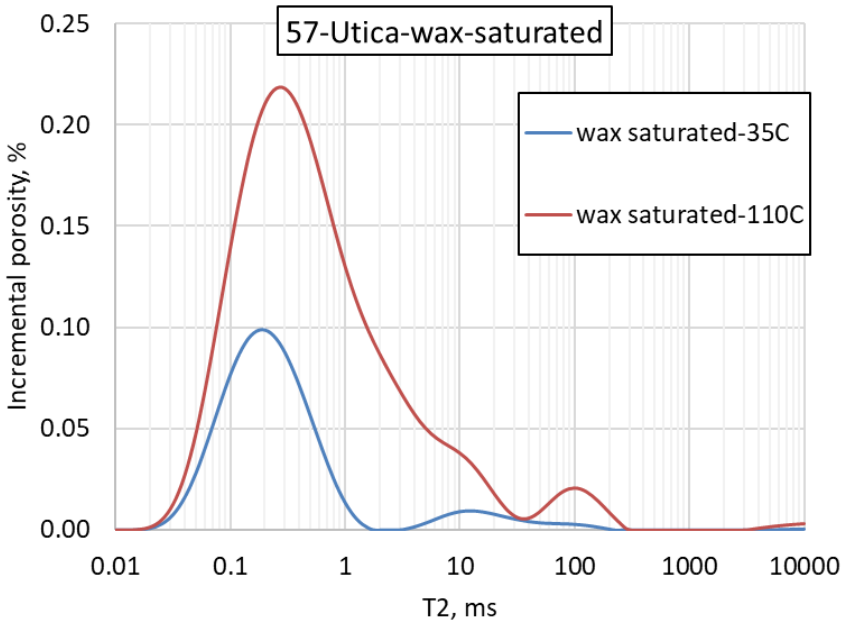

Figure A4.3: 2 MHz NMR incremental T2 spectra of Utica shale saturated with paraffin wax.

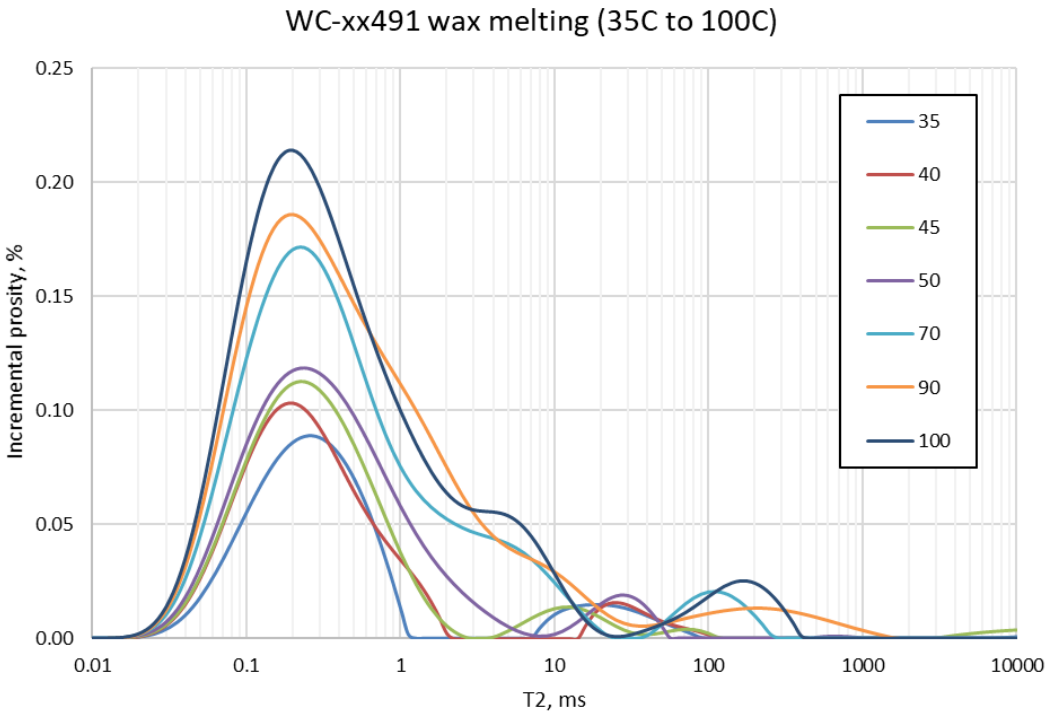

Figure A4.4: 2 MHz NMR incremental T2 spectra of Woodford shale WC-2 saturated with paraffin wax as function of temperature ranging from 35˚C to 100˚C.

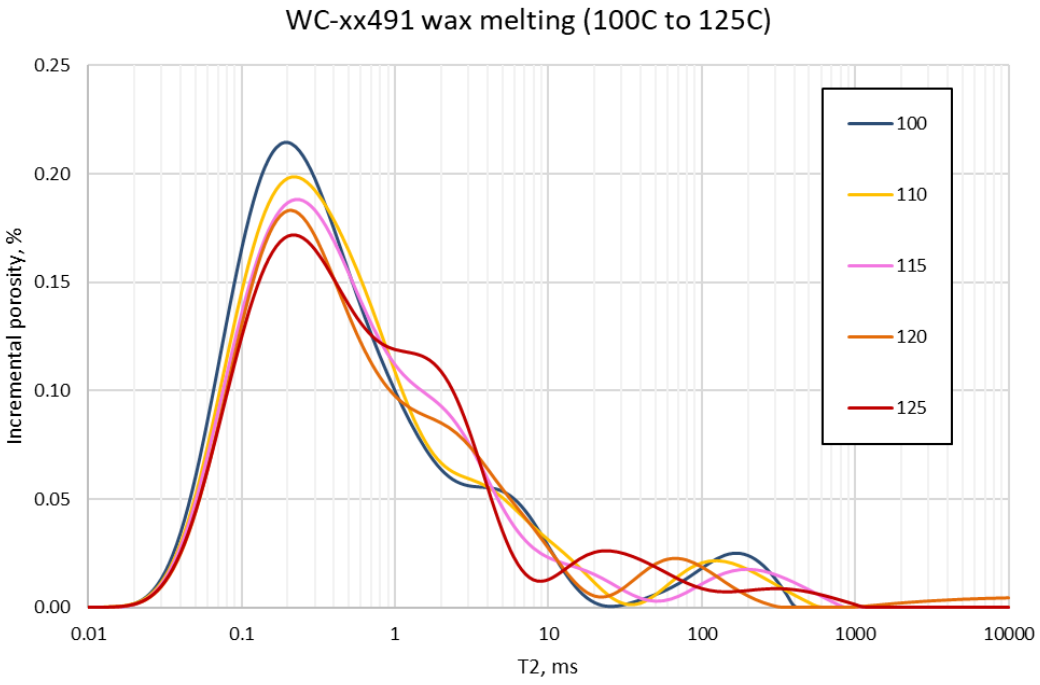

Figure A4.5: 2 MHz NMR incremental T2 spectra of Woodford shale WC-2 saturated with paraffin wax as function of temperature ranging from 100˚C to 125˚C.

Section A.5: NMR T2 spectra of Woodford shale (oil window) samples containing preserved in-situ reservoir fluids

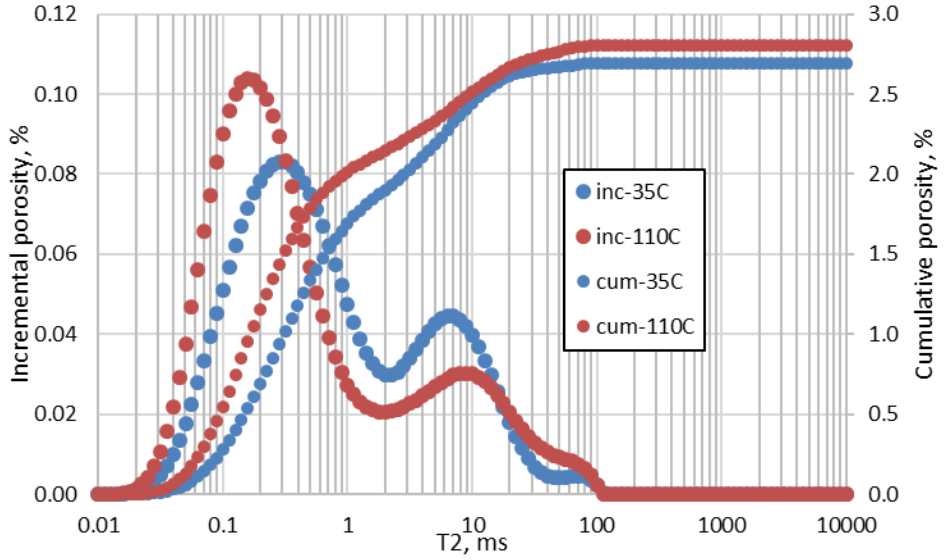

Figure A5.1: 2 MHz NMR T2 spectra of Woodford shale WF-xx631 H2 at 35˚C to 110˚C.

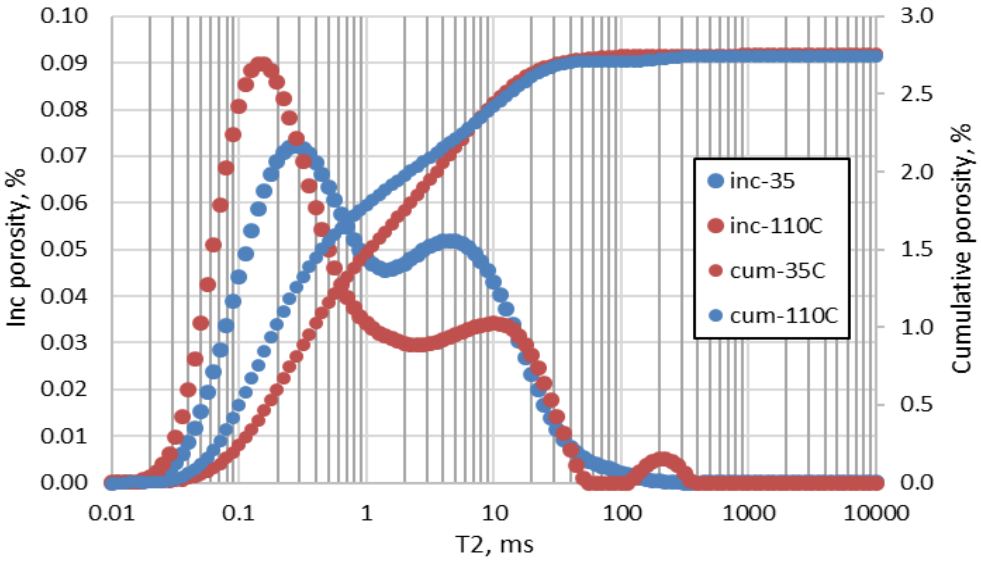

Figure A5.2: 2 MHz NMR T2 spectra of Woodford shale WF-xx631 H3 at 35˚C to 110˚C.

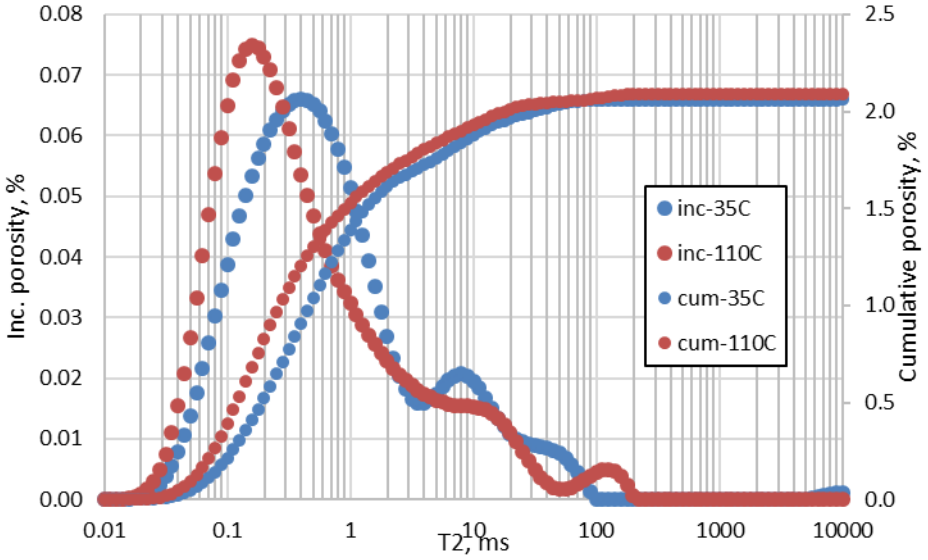

Figure A5.3: 2 MHz NMR T2 spectra of Woodford shale WF-xx608.9 H1 at 35°C to 110°C.

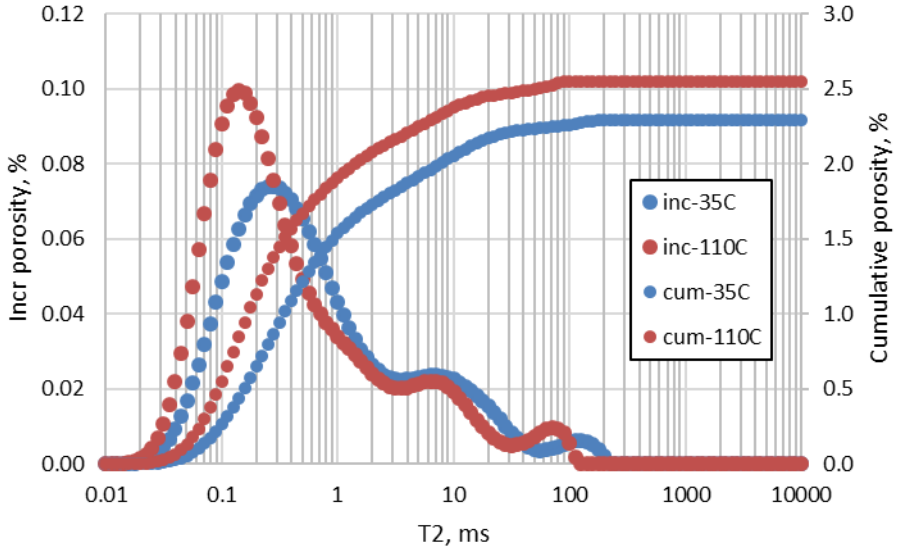

Figure A5.4: 2 MHz NMR T2 spectra of Woodford shale WF-xx608.9 H2 at 35°C to 110°C.

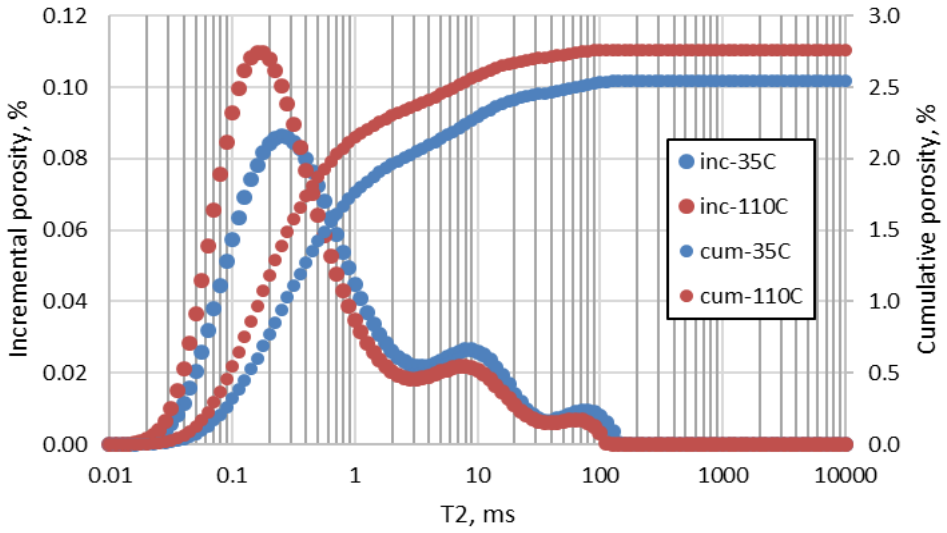

Figure A5.5: 2 MHz NMR T2 spectra of Woodford shale WF-xx584.4 H2 at 35˚C to 110˚C.

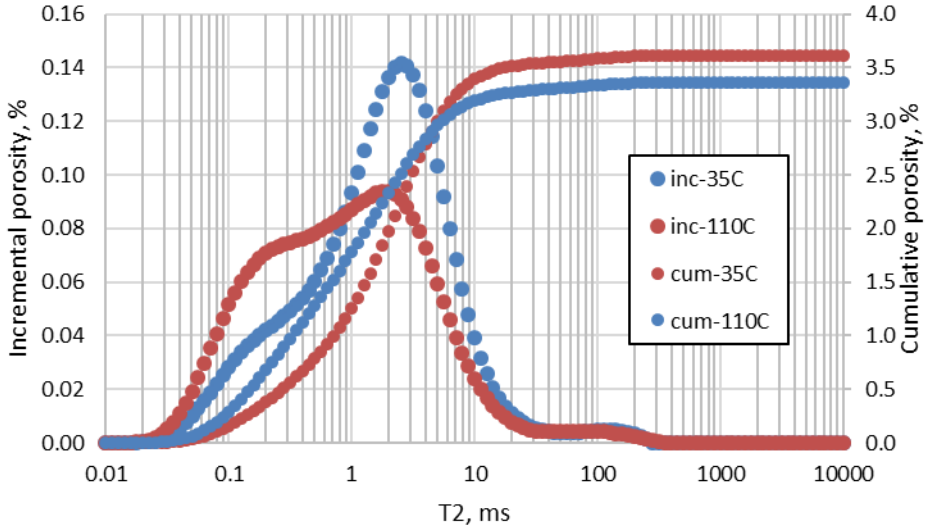

Figure A5.6: 2 MHz NMR T2 spectra of Woodford shale WF-xx13.7 at 35˚C to 110˚C.

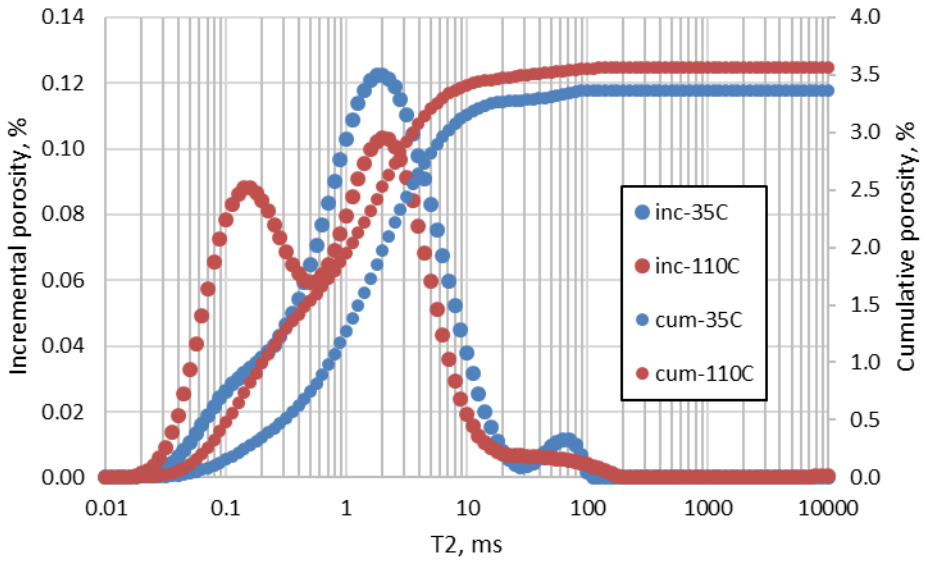

Figure A5.7: 2 MHz NMR T2 spectra of Woodford shale WF-xx11.1 at 35˚C to 110˚C.

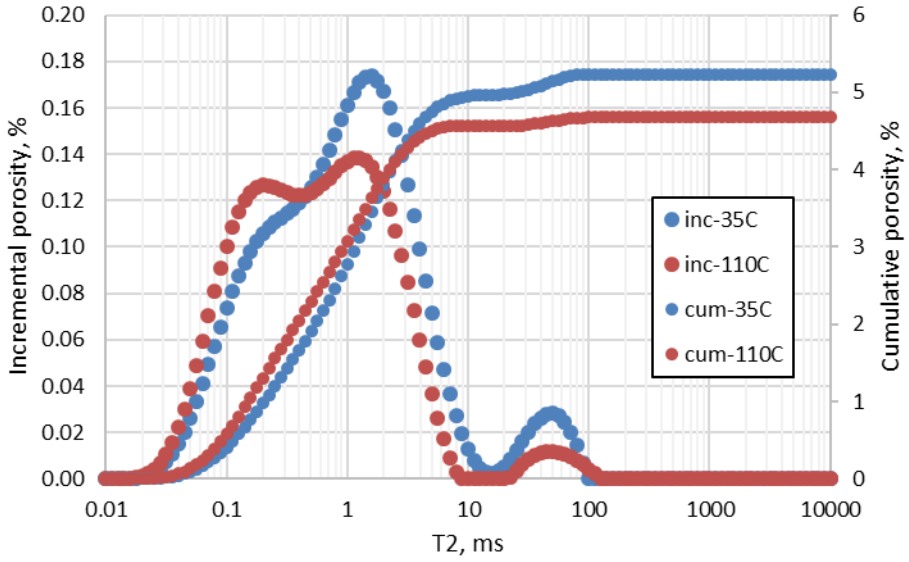

Figure A5.8: 2 MHz NMR T2 spectra of Woodford shale WF-xx45.15 at 35˚C to 110˚C.

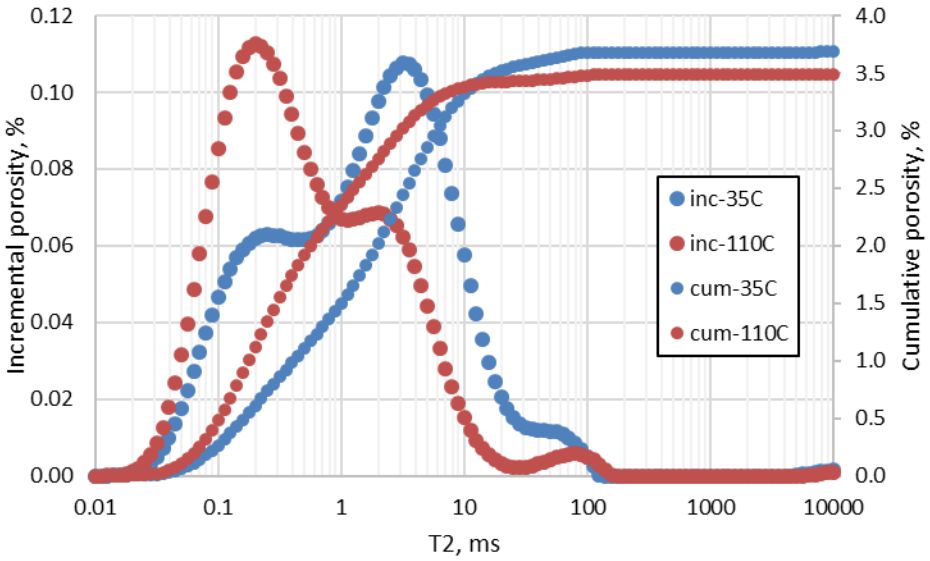

Figure A5.9: 2 MHz NMR T2 spectra of Woodford shale WF-xx64.35 at 35˚C to 110˚C.

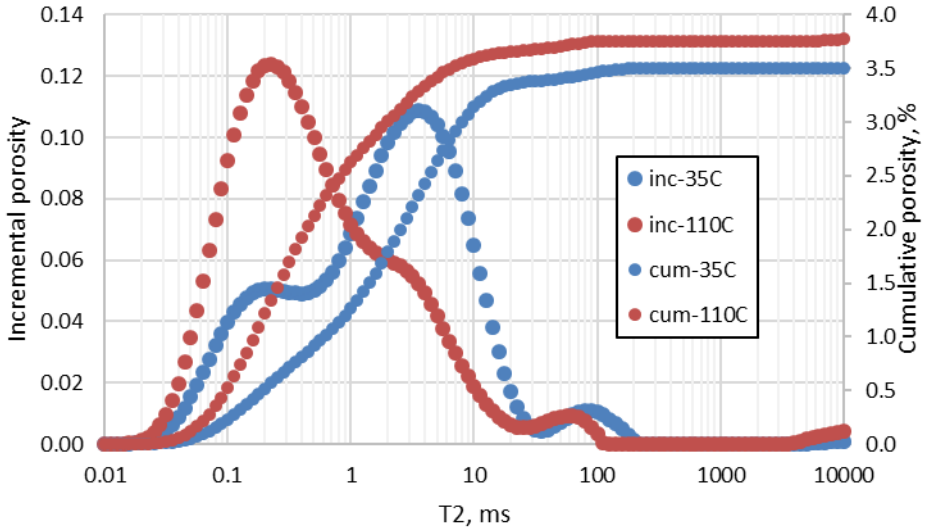

Figure A5.10: 2 MHz NMR T2 spectra of Woodford shale WF-xx64.5 at 35˚C to 110˚C.

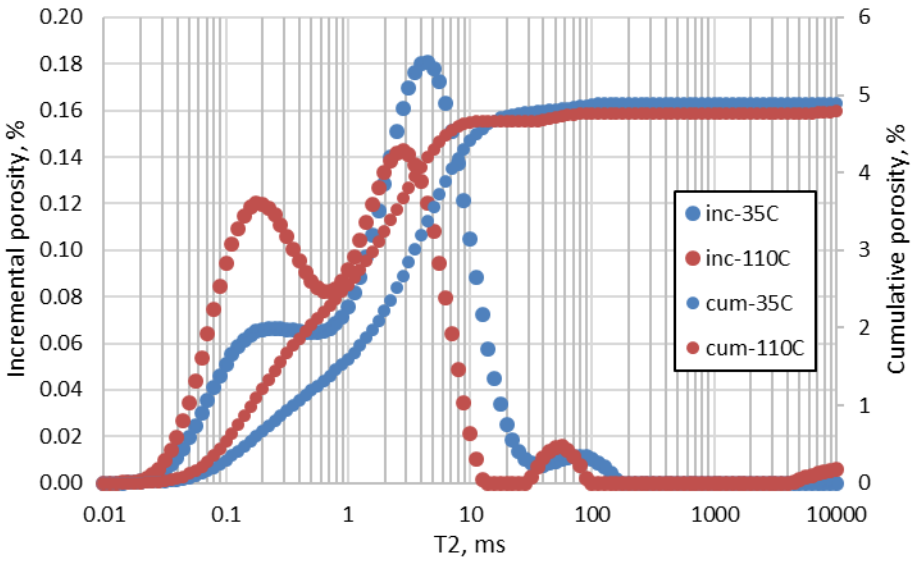

Figure A5.11: 2 MHz NMR T2 spectra of Woodford shale WF-xx88.9 at 35°C to 110°C.

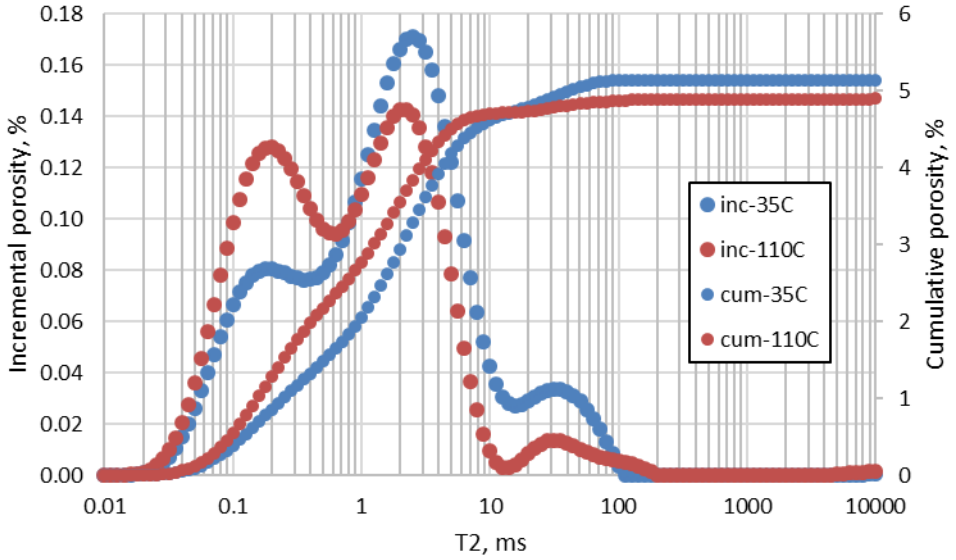

Figure A5.12: 2 MHz NMR T2 spectra of Woodford shale WF-xx89.05 at 35°C to 110°C.

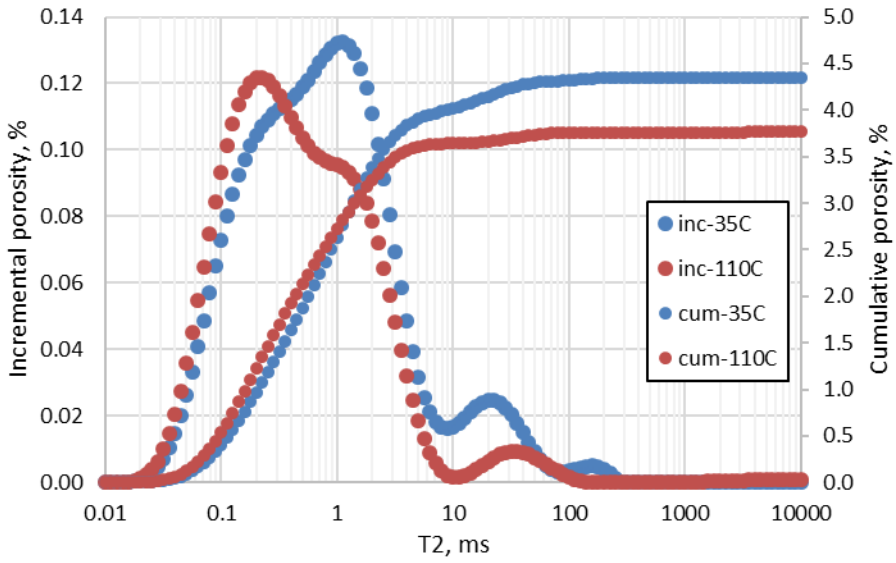

Figure A5.13: 2 MHz NMR T2 spectra of Woodford shale WF-xx19.4 at 35˚C to 110˚C.

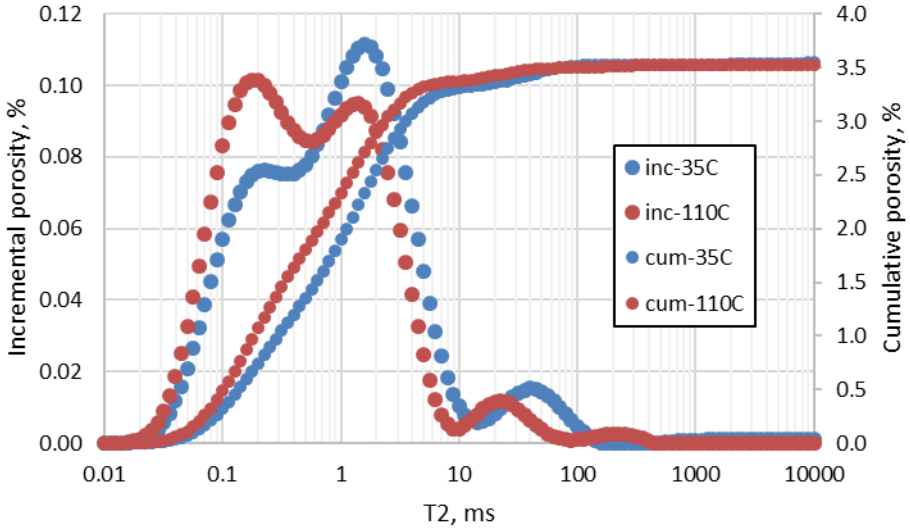

Figure A5.14: 2 MHz NMR T2 spectra of Woodford shale WF-xx19.75 at 35˚C to 110˚C.

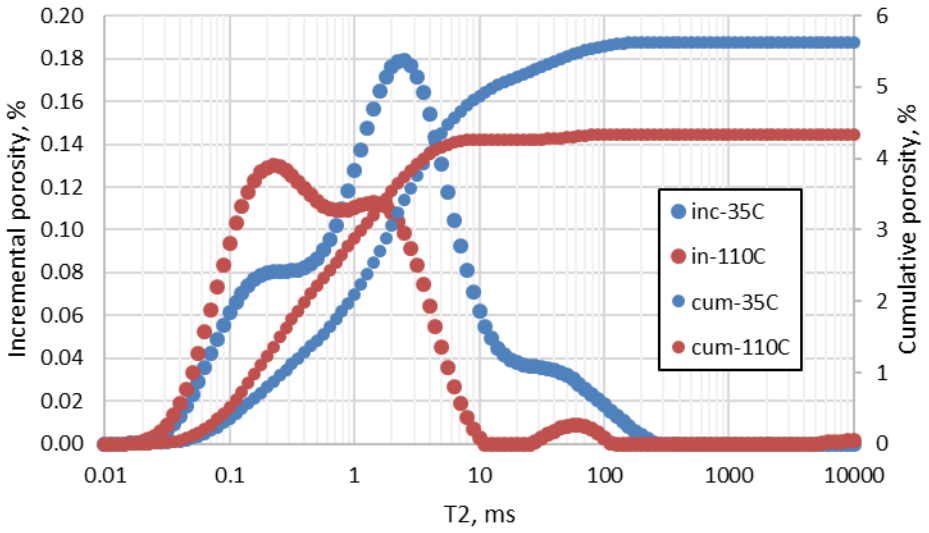

Figure A5.15: 2 MHz NMR T2 spectra of Woodford shale WF-xx59.65 at 35˚C to 110˚C.

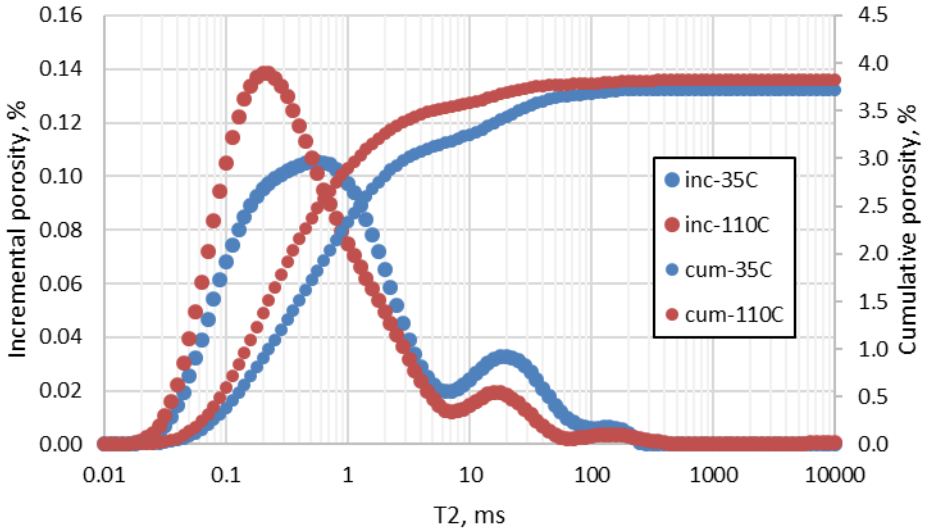

Figure A5.16: 2 MHz NMR T2 spectra of Woodford shale WF-xx39.35 H1 at 35˚C to 110˚C.

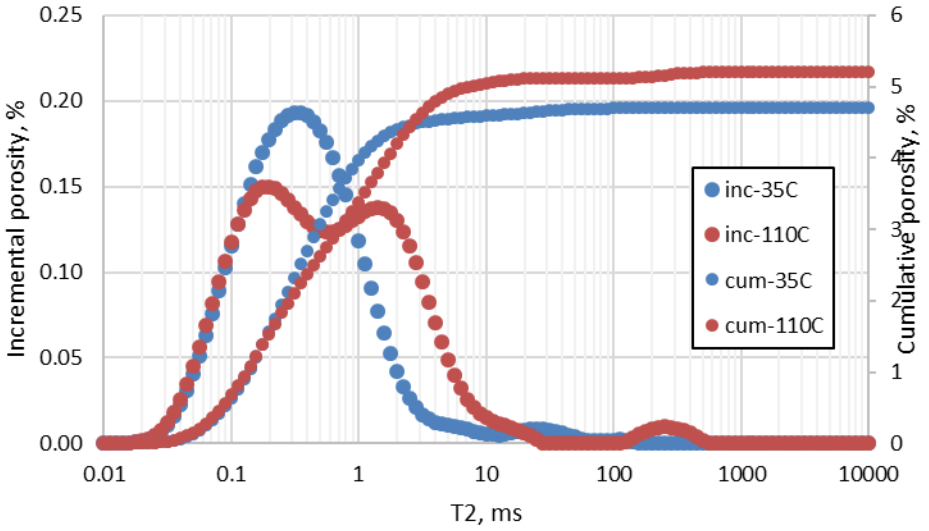

Figure A5.17: 2 MHz NMR T2 spectra of Woodford shale WF-xx39.35 H2 at 35˚C to 110˚C.

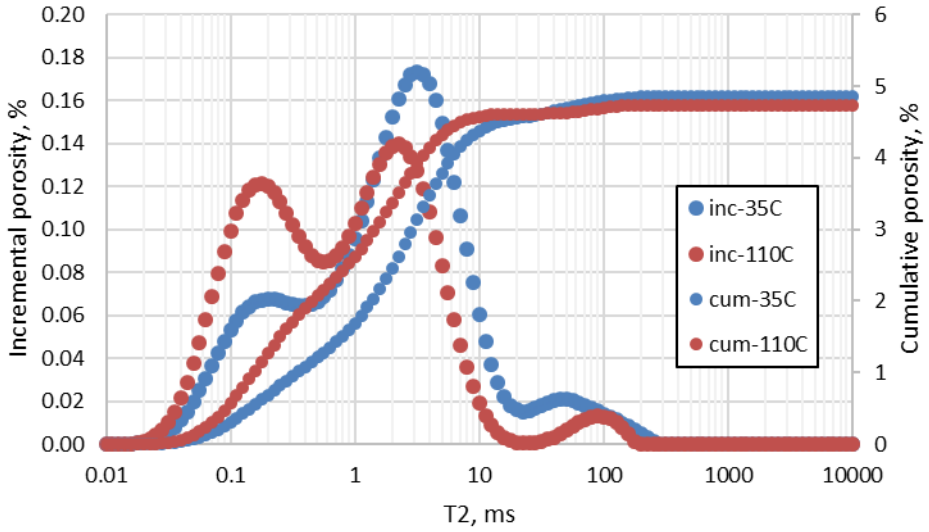

Figure A5.18: 2 MHz NMR T2 spectra of Woodford shale WF-xx60.7 at 35˚C to 110˚C.

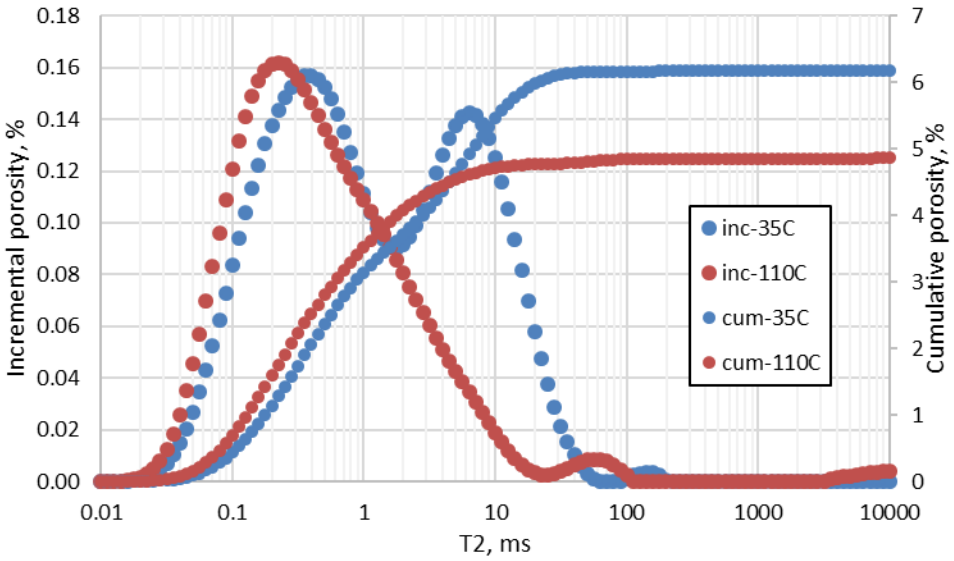

Figure A5.19: 2 MHz NMR T2 spectra of Woodford shale WF-xx85.45 at 35˚C to 110˚C.

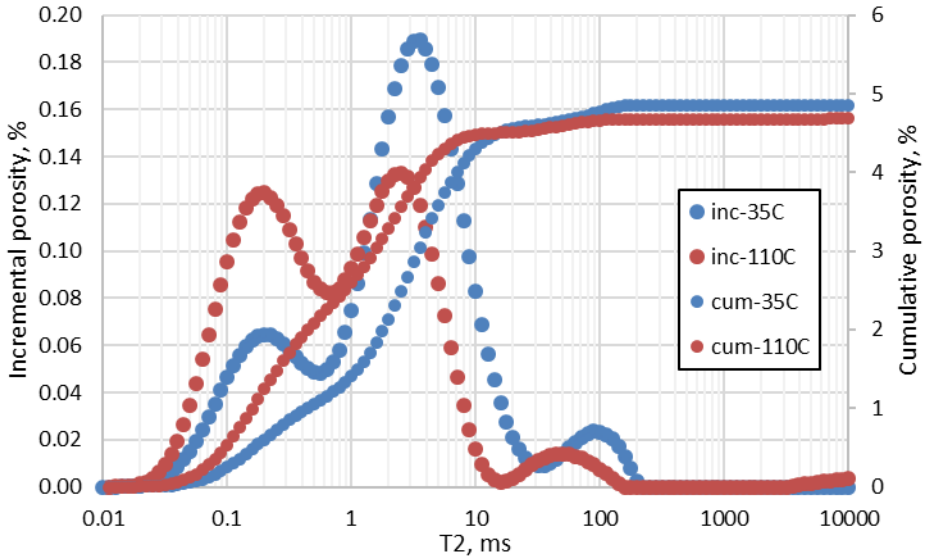

Figure A5.20: 2 MHz NMR T2 spectra of Woodford shale WF-xx50.55at 35˚C to 110˚C.

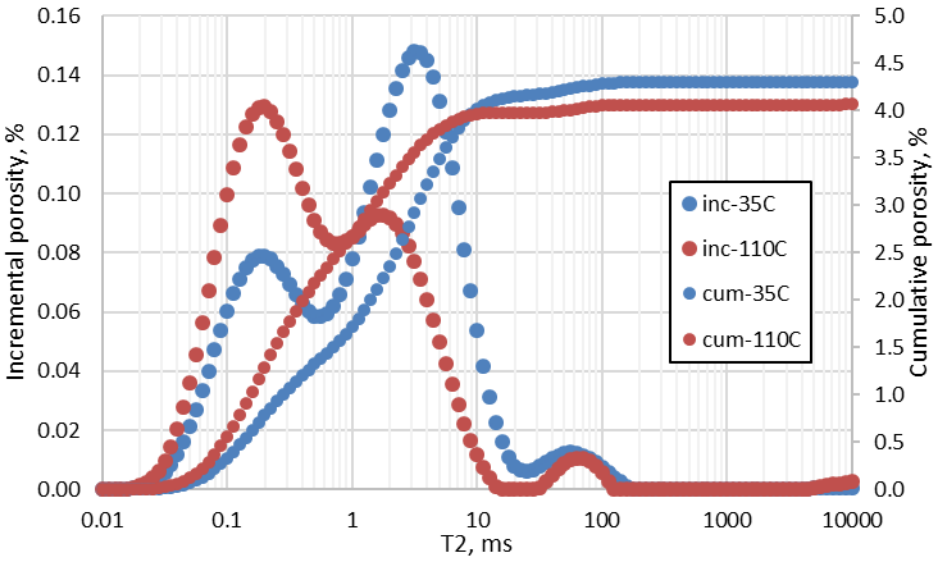

Figure A5.21: 2 MHz NMR T2 spectra of Woodford shale WF-xx50.65 at 35˚C to 110˚C.

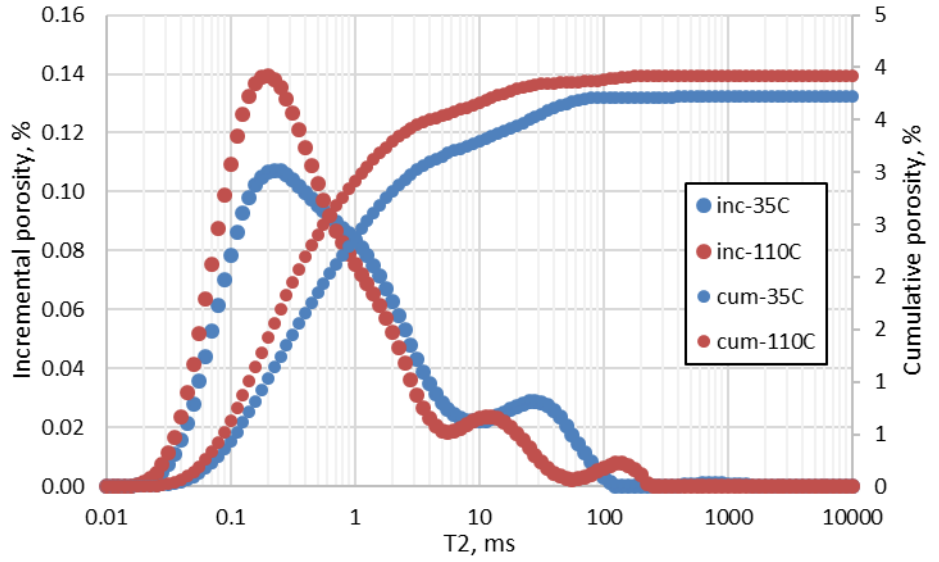

Figure A5.22: 2 MHz NMR T2 spectra of Woodford shale WF-xx85.8 at 35˚C to 110˚C.

Section A.6: T2 spectra of shale samples saturated partially with brine (5000 psi) and hexadecane (7000 psi)

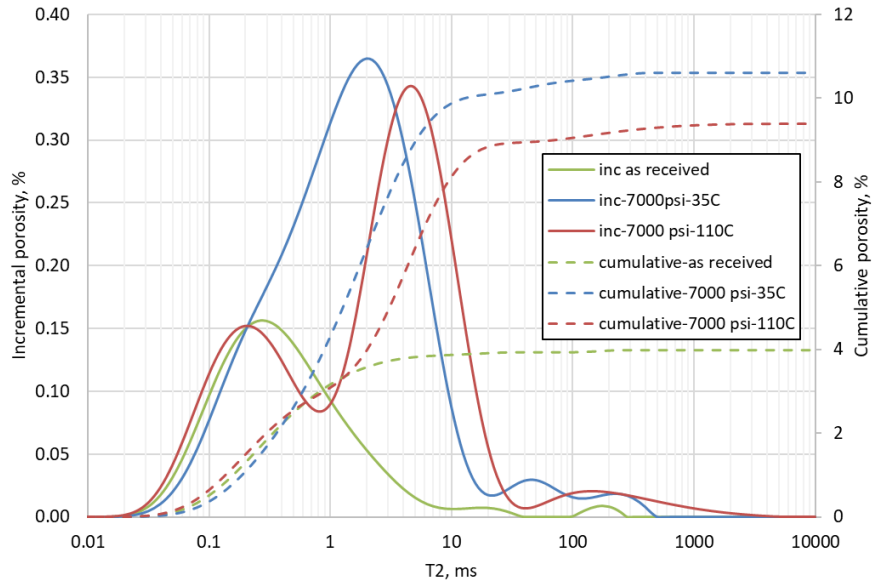

Figure A6.1: 2 MHz NMR T2 spectra of Wolfcamp shale WC-xx419 at 35°C and 110°C.

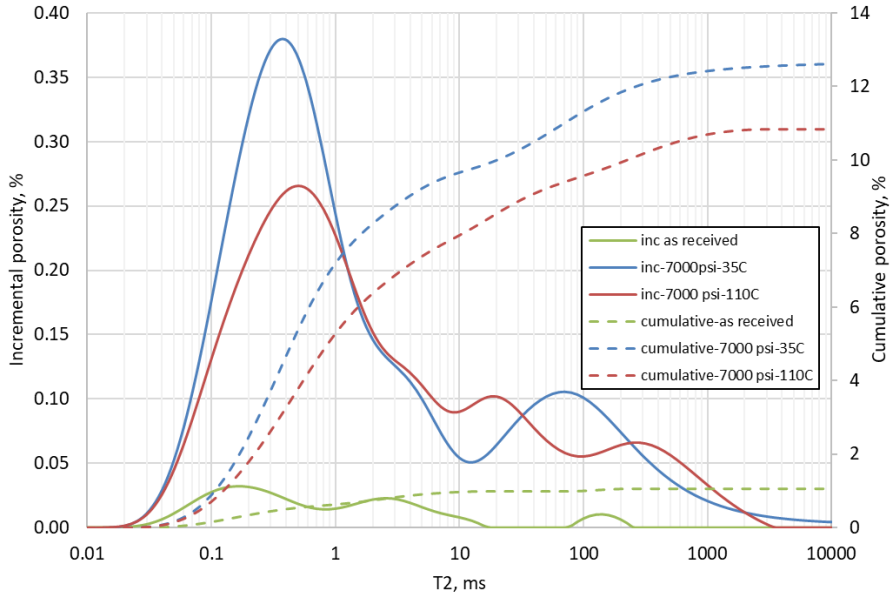

Figure A6.2: 2 MHz NMR T2 spectra of Wolfcamp shale WC-xx550 at 35°C and 110°C.

Section A.7: Pyrograms of ‘as-received’ Bakken shale samples

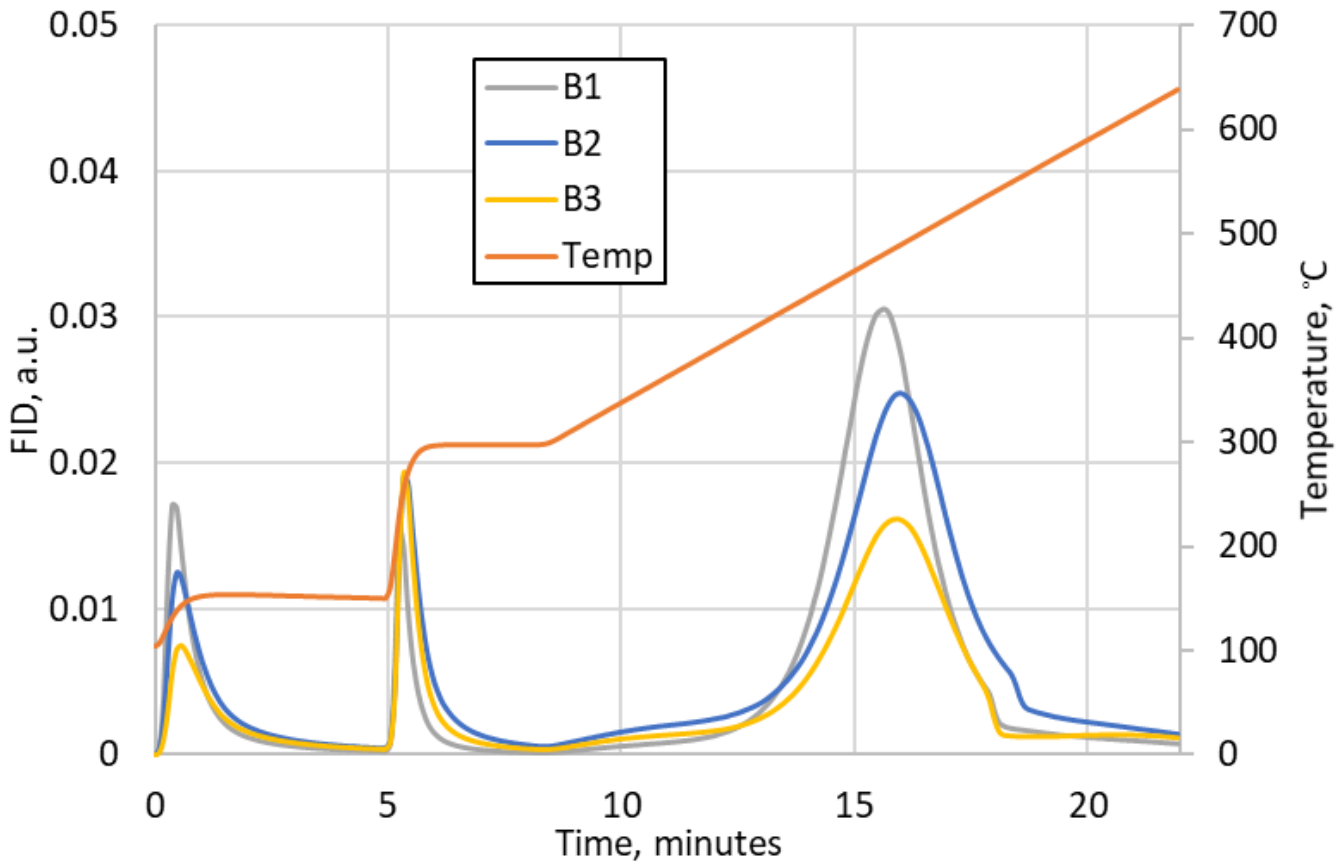

Section A.8: 2 MHz NMR T1-T2 maps of 'as-received' Bakken shale samples at 35°C (from top to bottom: Sample B1, B2, B3). Presence of high T1/T2 ratio regions indicates presence of heavy hydrocarbon (C20+).